3

Aviation-Produced Aerosols and Cloudiness

DAVID W. FAHEY AND ULRICH SCHUMANN

Lead Authors:
S. Ackerman, P. Artaxo, O. Boucher, M.Y. Danilin, B. Kärcher, P. Minnis, T. Nakajima, O.B. Toon

Contributors:
J.K. Ayers, T.K. Berntsen, P.S. Connell, F.J. Dentener, D.R. Doelling, A. Döpelheuer, E.L. Fleming, K. Gierens, C.H. Jackman, H. Jäger, E.J. Jensen, G.S. Kent, I. Köhler, R. Meerkötter, J.E. Penner, G. Pitari, M.J. Prather, J. Ström, Y. Tsushima, C.J. Weaver, D.K. Weisenstein

Review Editor:
K.-N. Liou

CONTENTS

EXECUTIVE SUMMARY

- Current aircraft engines emit aerosol particles and gaseous aerosol precursors into the upper troposphere and lower stratosphere that may affect air chemistry and climate. Aircraft engines also directly emit soot and metal particles. Liquid aerosol precursors include water vapor, oxidized sulfur in various forms, chemi-ions (charged molecules), nitrogen oxides, and unburned hydrocarbons.

- Large numbers (about 10^{17}/kg fuel) of small (radius 1 to 10 nm) volatile particles are formed in the exhaust plumes of cruising aircraft, as shown by *in situ* observations and model calculations. These new particles initially form from sulfuric acid, chemi-ions, and water vapor; they grow in size by coagulation and uptake of water vapor and other condensable gases. The conversion fraction of fuel sulfur to sulfuric acid in the young plume is inferred to be likely in the range of 0.4 to about 20%.

- Subsonic aircraft emissions near the tropopause at northern mid-latitudes are a significant source of soot mass and sulfate aerosol surface area density and number concentration, according to existing measurements and model results. Aircraft generate far less aerosol than that emitted and produced at the Earth's surface or by strong volcanic eruptions. Aircraft emissions injected directly at 9- to 12-km altitudes are more important than similar surface emissions because of longer atmospheric residence times in the upper troposphere. The impact of present aircraft emissions on the formation of polar stratospheric clouds is much smaller than what is expected for a projected fleet of supersonic aircraft.

- Regional enhancements in concentrations of aircraft-produced aerosol have been observed near air traffic corridors. Global changes in sulfate aerosol properties at subsonic air traffic altitudes were small over the past few decades. The contribution of aircraft emissions to changes or possible trends in these regions is difficult to determine because of the large variability of natural sources.

- Contrails are visible line clouds that form behind aircraft flying in sufficiently cold air as a result of water vapor emissions. Contrail formation can be accurately predicted for given atmospheric temperature and humidity conditions. In the exhaust, water droplets form on soot and sulfuric acid particles, then freeze to form contrail particles. Models suggest that contrails would also form without soot and sulfur emissions by activation and freezing of background particles. Increasing fuel sulfur content results in more and smaller ice particles. In the future, aircraft with more fuel-efficient engines will produce lower exhaust temperatures for the same concentration of emitted water vapor, hence will tend to cause contrails at higher ambient temperatures and over a larger altitude range.

- Persistent contrails often develop into more extensive contrail cirrus in ice-supersaturated air masses. Ice particles in such persistent contrails grow by uptake of water vapor from the surrounding air. The area of the Earth covered by persistent contrails is controlled by the global extent of ice-supersaturated air masses and the number of aircraft flights in those air masses. Present contrail cover will increase further as air traffic increases. The properties of persistent contrails depend on the aerosol formed in exhaust plumes. Regions of ice-supersaturation vary with time and location and are estimated to cover an average of 10 to 20% of the Earth's surface at mid-latitudes. Ice-supersaturation in these regions is often too small to allow cirrus to form naturally, so aircraft act as a trigger to form cirrus clouds.

- The mean coverage of line-shaped contrails is currently greatest over the United States of America, Europe, and the North Atlantic; it amounts to 0.5% on average over central Europe during the daytime. The mean global linear contrail coverage represents the minimum change in cirrus cloud coverage from air traffic; its present value is estimated to be 0.1% (possibly 0.02 to 0.2%).

- Aviation-induced aerosol present in exhaust plumes and accumulated in the background atmosphere may indirectly affect cirrus cloud cover or other cloud properties throughout the atmosphere. Observations and models are not yet sufficient to quantify the aerosol impact on cirrus cloud properties.

- Satellite and surface-based observations of seasonal and decadal changes in cirrus cover and frequency in main air traffic regions suggest a possible relationship between air traffic and cirrus formation. Cirrus changes in main air traffic regions suggest global cirrus cover increases of up to 0.2% of the Earth's surface since the beginning of jet aviation, in addition to the 0.1% cover by line-shaped contrails. Observed cirrus cover changes have not been conclusively attributed to aircraft emissions or to other causes.

- Contrails cause a positive mean radiative forcing at the top of the atmosphere. They reduce both the solar radiation

reaching the surface and the amount of longwave radiation leaving the Earth to space. Contrails reduce the daily temperature range at the surface and cause a heating of the troposphere, especially over warm and bright surfaces. The radiative effects of contrails depend mainly on their coverage and optical depth.

- For an estimated mean global linear-contrail cover of 0.1% of the Earth's surface and contrail optical depth of 0.3, radiative forcing is computed to be 0.02 W m^{-2}, with a maximum value of 0.7 W m^{-2} over parts of Europe and the United States of America. Radiative forcing by linear contrails is uncertain by a factor of about 3 to 4 (range from 0.005 to 0.06 W m^{-2}), reflecting uncertainties in contrail cover (x 2) and contrail mean optical depth (x 3).

- In the current atmosphere, the direct radiative forcing of accumulated aircraft-induced aerosol is smaller than that of contrails. The optical depth of aircraft-induced aerosol is less than 0.0004 in the zonal mean and is much smaller than that of stratospheric aerosol from large volcanic eruptions or mean tropospheric aerosol abundances.

- Indirect radiative forcing is caused by aviation-induced cirrus that is produced in addition to line-shaped contrail cirrus. This forcing is likely positive and may be larger than that from line-shaped contrails. Radiative forcing from additional cirrus may be as large as 0.04 W m^{-2} in 1992. Indirect forcing from other cloud effects has not yet been determined and may be either positive or negative.

- In the future, contrail cloudiness and radiative forcing are expected to increase more strongly than global aviation fuel consumption because air traffic is expected to increase mainly in the upper troposphere, where contrails form preferentially, and because aircraft will be equipped with more fuel-efficient engines. More efficient engines will cause contrails to occur more frequently and over a larger altitude range for the same amount of air traffic. For the threefold increase in fuel consumption calculated for a 2050 scenario (Fa1), a fivefold increase in contrail cover and a sixfold increase in radiative forcing are expected. The contrail cover would increase even more strongly if the number of cruising aircraft increases more than their fuel consumption. For other 2050 scenarios (Fc1 and Fe1), the expected cirrus cover increases by factors of 3 and 9, respectively, compared to 1992. Higher cruise altitudes will increase contrail cover in the subtropics; lower cruise altitudes will increase contrail cover in polar regions. Future climate changes may cause further changes in expected aircraft-induced cirrus cover.

- The future aerosol impact of aviation will increase with fuel consumption. The trends depend on future fuel-sulfur content, engine soot emissions, and the efficiency with which fuel sulfur is transformed into aerosol behind the aircraft.

- Aerosol microphysical and chemical processes are similar in subsonic and supersonic aircraft plumes. Aerosol properties will differ because soot emission levels, aerosol formation potential, and plume dilution properties vary with engine type and atmospheric conditions at cruise altitudes. Significant increases in stratospheric aerosol are expected for the operation of a large fleet of supersonic aircraft, at least for non-volcanic periods.

3.1. Introduction

Recent advances in our understanding of heterogeneous chemistry in the lower stratosphere and the role of aerosols and clouds in climate forcing have increased the need to understand the influence of these aircraft emissions on atmospheric composition. Aerosol particles from aviation—comprising soot, metals, sulfuric acid, water vapor, and possibly nitric acid and unburned hydrocarbons—may influence the state of the atmosphere in many ways. These particles may provide surfaces for heterogeneous chemical reactions, both in the exhaust plume and on regional and global scales; represent a sink for condensable atmospheric gases; absorb or scatter radiation directly; and change cloud properties that may affect radiation indirectly. Persistent contrails can directly cause additional cirrus clouds to form. In addition, aerosol particles may enhance sedimentation and precipitation of atmospheric water vapor, hence affecting the hydrological cycle and the budget of other gases and particles. Changes in cloud formation properties and cloud cover may also affect actinic fluxes in the atmosphere and ultraviolet-B (UV-B) radiation at the surface.

This chapter addresses the following questions related to aviation-induced aerosol particles:

- What are the processes that produce aerosols and contrails in the plume of a jet aircraft engine?
- What is the relationship of the aircraft aerosol source to background aerosol abundances and trends in the atmosphere?
- Why do persistent contrails form, and what are their properties?
- What is the relationship of aircraft-induced aerosol and contrails to cirrus cloudiness and trends?
- What are the radiative properties of aviation-induced aerosol, contrails, and cirrus clouds, and how do they affect the Earth-atmosphere system?
- What changes in the effects of aviation-induced aerosol might occur in response to future changes in climatological conditions or aircraft operating parameters?

Section 3.2 describes the theoretical and experimental basis of the emission and formation of aerosol in aircraft plumes. Section 3.3 describes findings and calculations of regional and global aerosol distributions and their trends, quantifies the change in aerosol mass and surface density from present aviation emissions at global scales, and compares aircraft sources with volcanic and other natural or anthropogenic sources. Section 3.4 reviews recent results on contrails and cirrus clouds, provides estimates for regional and global contrail coverage, and describes measured contrail particle properties. Section 3.5 presents recent evidence that may relate changes in cirrus cloudiness and related climate parameters to aircraft emissions. Section 3.6 describes changes in radiative fluxes from contrails as a function of various cloud parameters using three one-dimensional radiation transport models, and presents a computation of global radiative forcing from contrails. Finally, Section 3.7 identifies climatological and aircraft operational parameters that may influence the future importance of aviation-induced aerosol and cloudiness and estimates future contrail cover for a fixed climate.

The material in this chapter relies on Chapters 7 and 9 to describe emissions present at the engine exit plane and total emissions from global air traffic; Chapters 2 and 4 to discuss the chemical implications of changes in aerosol properties; and Chapters 5 and 6 to describe changes in UV-B radiation and climate from aerosols.

3.2. Aerosol Emission and Formation in Aircraft Plumes

Aircraft jet engines directly emit aerosol particles and condensable gases such as water vapor (H_2O), sulfuric acid (H_2SO_4), and organic compounds, which lead to the formation of new, liquid (volatile) particles in the early plume by gas-to-particle conversion (nucleation) processes. Other gas-phase species and charged molecular clusters (chemi-ions, or CIs) are also generated at emission, including nitric acid (HNO_3) and nitrous acid (HNO_2). Emission and formation of H_2SO_4 depend on fuel sulfur content, or sulfur emission index [EI(S)], and the conversion fraction of fuel sulfur to H_2SO_4. Formation of HNO_3 and HNO_2 depends on reactions of nitrogen oxides (NO_x = NO + NO_2) with hydroxyl radicals (OH). Particle formation depends on mixing of exhaust gases with ambient air, plume cooling rate, plume chemistry, and ambient aerosol properties. Soot particles formed during fuel combustion and emitted metallic particles constitute the solid (nonvolatile) particle fraction present in exhaust plumes. Under certain thermodynamic conditions, emitted water vapor condenses and freezes to form water-ice particles, thereby producing a condensation trail (contrail). These line clouds evaporate rapidly if the ambient humidity is low but may change the size and chemical composition of the remaining liquid aerosol particles. If the humidity is above ice saturation, contrails persist and grow through further deposition of ambient water.

An invisible aerosol trail is always left behind cruising aircraft. Aerosol and contrail formation processes in an aging plume determine the number, surface area, and mass of particles that are formed per mass of fuel consumed. Exhaust particle properties change in the presence of a contrail. Exhaust particle morphology and surface properties and aircraft-induced perturbations of background aerosol surface areas (Section 3.3) are of central importance for ozone changes caused by heterogeneous chemical reactions (Chapters 2 and 4). Particle number and freezing probability are key for the formation of ice (cirrus) clouds after passage of an aircraft in a region where otherwise no clouds would form (Section 3.4). Finally, aviation-produced aerosol can directly or indirectly influence the radiation budget of the atmosphere (Section 3.6 and Chapter 6). For recent reviews see Schumann (1996a), Fabian and Kärcher (1997), Friedl (1997), and Brasseur *et al.* (1998).

The following subsections provide a description of volatile aerosol precursors and the formation of volatile aerosol particles,

a characterization of emitted soot and metal particles, a review of contrail and ice formation, and a discussion of the mutual interactions between these particle types. Comments on reducing the impact of aerosols are given in Section 3.7.4.

3.2.1. Volatile Aerosol Precursors

3.2.1.1. Water Vapor

Water vapor is present in aircraft exhaust in known amounts because the emission index is specified by the stoichiometry of near-complete fuel combustion (Chapter 7). Water vapor concentrations of a few percent at the engine exhaust nozzle far exceed the concentrations of other aerosol precursor gases. Ambient water vapor also participates in aerosol processes, with concentrations that vary widely depending on flight altitude and meteorological processes. Because of its abundance and thermodynamic properties, water vapor participates in nearly all aerosol formation and nucleation processes (e.g., Pruppacher and Klett, 1997).

3.2.1.2. Sulfur Species

Aviation fuels (kerosene) contain sulfur in trace amounts. In the current world market, the sulfur content—hence the EI(S)—of aviation fuels is near 0.4 g S/kg fuel or 400 parts per million by mass (ppm; 1 ppm = 0.0001%), with an upper limit specification of 3 g S/kg (Chapter 7). Of importance for the formation of plume aerosol is the partitioning of sulfur at the engine exhaust nozzle into sulfur dioxide (SO_2) and fully oxidized sulfur S(VI) compounds, sulfur trioxide and sulfuric acid ($S(VI) = SO_3 + H_2SO_4$). Most fuel sulfur is expected to be emitted as SO_2 based on combustion kinetics and some observations (Miake-Lye *et al.*, 1993, 1998; Arnold *et al.*, 1994; Schumann *et al.*, 1998). However, a fraction of the SO_2 can be converted into S(VI) by gas phase chemical reactions with OH, oxygen atoms (O), and H_2O inside the engine. The fractional conversion depends on details of combustion conditions, turbine flow properties, blade cooling effects (Chapter 7), and mixing (Chapter 2). Further oxidation can occur in the plume, where the rate-limiting step is thought to be oxidation of SO_2 by OH to form SO_3 (Stockwell and Calvert, 1983) or liquid-phase reactions of SO_2 with H_2O_2, O_3, metals (Jacob and Hofmann, 1983), or HNO_3 (Fairbrother *et al.*, 1997). Once SO_3 is formed, the gas-phase reaction with emitted H_2O to form H_2SO_4 is fast (< 0.1 s) under plume conditions (Reiner and Arnold, 1993; Kolb *et al.*, 1994; Lovejoy *et al.*, 1996). Gaseous H_2SO_4 and $HSO_4^-(H_2SO_4)_n$ (mostly with n = 1,2) ion clusters have been observed in jet exhaust (Frenzel and Arnold, 1994; Arnold *et al.*, 1998a,b).

The chemical lifetime of exhaust OH in the early jet regime is determined by reactions with emitted NO_x and by OH self-reactions, the latter leading to the formation of hydrogen peroxide (H_2O_2) (Kärcher *et al.*, 1996a; Hanisco *et al.*, 1997). Measurements indicate OH exit concentrations below 1 ppmv (Tremmel *et al.*, 1998). For an OH concentration of 0.5 to 1 ppmv at the engine's nozzle exit plane and without SO_3 emissions, the OH-induced pathway alone yields about 0.3 to 1% S-to-H_2SO_4 conversion in the plume (Miake-Lye *et al.*, 1993; Danilin *et al.*, 1994; Kärcher *et al.*, 1996a). Model calculations indicate overall S(VI) conversion fractions in the range of 2 to 10% for various supersonic and subsonic jet engines (Brown *et al.*, 1996a; Lukachko *et al.*, 1998; Chapter 7), consistent with some earlier SO_3 measurements behind gas turbines (e.g., CIAP, 1975; Hunter, 1982).

3.2.1.3. Chemi-ions

A large number of chemi-ions (CIs) are expected to be present in aircraft exhaust because ion production via high-temperature chemical reactions is known to occur in the combustion of carbon-containing (not necessarily sulfur-containing) fuels (e.g., Burtscher, 1992). In the jet regime, some recent models indicate that CIs effectively promote formation and growth of electrically charged droplets containing H_2SO_4 and H_2O (Yu and Turco, 1997). In addition, CIs may contribute to the activation of exhaust soot. Positive ions include H_3O^+ and organic molecules like CHO^+, $C_3H_3^+$, and larger molecules (Calcote, 1983), whereas the free electrons rapidly attach to other molecules to form negative ions with sulfate and nitrate cores. Measurements of positive CIs in exhaust plumes are not available, and only very few *in situ* measurements of negative CIs are available to date.

Arnold *et al.* (1998a) measured a total negative CI concentration of 3×10^7 cm^{-3} (about 3×10^{15}/kg fuel) at plume ages of around 10 ms in the exhaust of a jet engine on the ground, consistent with approximately 10^9 cm^{-3} at a plume age of 1 ms (Yu *et al.*, 1998).

That concentration represents a lower bound from diffusion losses of these particles within sampling devices prior to detection and the limited detection range of the employed mass spectrometer. The fact that these measurements yielded only a fraction of CIs in the plume has been partially confirmed by in-flight measurements (Arnold *et al.*, 1998b) showing smaller total CI count rates for high-sulfur fuel compared with low-sulfur fuel. Therefore, current CI data are consistent with a CI emission index of about 2–4 x 10^{17}/kg, corresponding to a concentration of about 2×10^9 cm^{-3} at the engine exit. This value has been estimated numerically based on coupled ion-ion recombination kinetics and plume mixing (Yu and Turco, 1997; Kärcher *et al.*, 1998b; Yu *et al.*,1998). Although not directly comparable, CIs have been observed in hydrocarbon flames at concentrations of about 10^8 to 10^{11} cm^{-3} (Keil *et al.*, 1984), supporting the estimated concentration of negative CIs.

3.2.1.4 Nitrogen Species

The primary nitrogen emission from aircraft is in the form of NO_x (Chapter 2). In reactions of NO_x with OH in the plume, gaseous HNO_2 and HNO_3 are formed. Despite larger reaction

rates, less HNO_3 is formed than HNO_2 because the ratio of NO_2 to NO at the engine exit is small (< 0.2) (e.g., Schulte *et al.*, 1997) (see Chapter 7). HNO_3 can also form in the plume even in the absence of NO_2 emissions (Kärcher *et al.*, 1996a). *In situ* measurements in young plumes revealed both HNO_2 and HNO_3 concentrations above background levels (Arnold *et al.*, 1992, 1994; Tremmel *et al.*, 1998). HNO_3 can be more abundant in plumes than H_2SO_4, especially for low EI(S) values. These acids (especially HNO_3) are important because they can be taken up by water-soluble exhaust particles and form stable condensed phases such as nitric acid trihydrate (NAT = $HNO_3 \bullet 3H_2O$) and liquid ternary ($H_2O/H_2SO_4/HNO_3$) solutions under cold and humid plume conditions (Arnold *et al.*, 1992; Kärcher, 1996).

3.2.1.5. Hydrocarbons

Aircraft engines emit non-methane hydrocarbons (NMHCs) as a result of incomplete fuel combustion. These species include alkenes (mostly ethene), aldehydes (mostly formaldehyde), alkines (mostly ethine), and a few aromates. A few (8 to 10) species were found to account for up to 80% of NMHC emissions (Spicer *et al.*, 1992, 1994). High levels of carbonyl compound emissions (on the order of 0.2 ppmv) also have been observed in a combustor (Wahl *et al.*, 1997). Some in-flight data indicate that NMHCs with up to 8 carbon atoms have EIs in the range 0.05 to 0.2 g C/kg fuel and represent approximately 70% of total NMHC emissions (Slemr *et al.*, 1998). However, the current database on NMHC emissions and on partitioning between individual compounds is small and perhaps not representative for all engine types. Some emitted NMHCs might act as aerosol-forming agents in nascent plumes and may be adsorbed or dissolved in plume particles, thereby possibly contributing to the total amount of volatile aerosol found in plumes (Kärcher *et al.*, 1998b). In addition, the presence of trace NMHCs amounts may facilitate nucleation (e.g., Katz *et al.*, 1977) and alter the hygroscopic behavior and growth rates of particles (Saxena *et al.*, 1995; Cruz and Pandis, 1997). Engines also may emit volatile particles containing engine oils or other lubricants, but this effect has not been quantified.

Aircraft also occasionally introduce hydrocarbons by jettisoning fuel at low altitudes in the troposphere. Most of the fuel evaporates while it falls to the ground (Quackenbush *et al.*, 1994), which leads to a small increase of hydrocarbons in this region. Because of the small amounts of fuel released in this way, no essential impacts on atmospheric aerosols are expected.

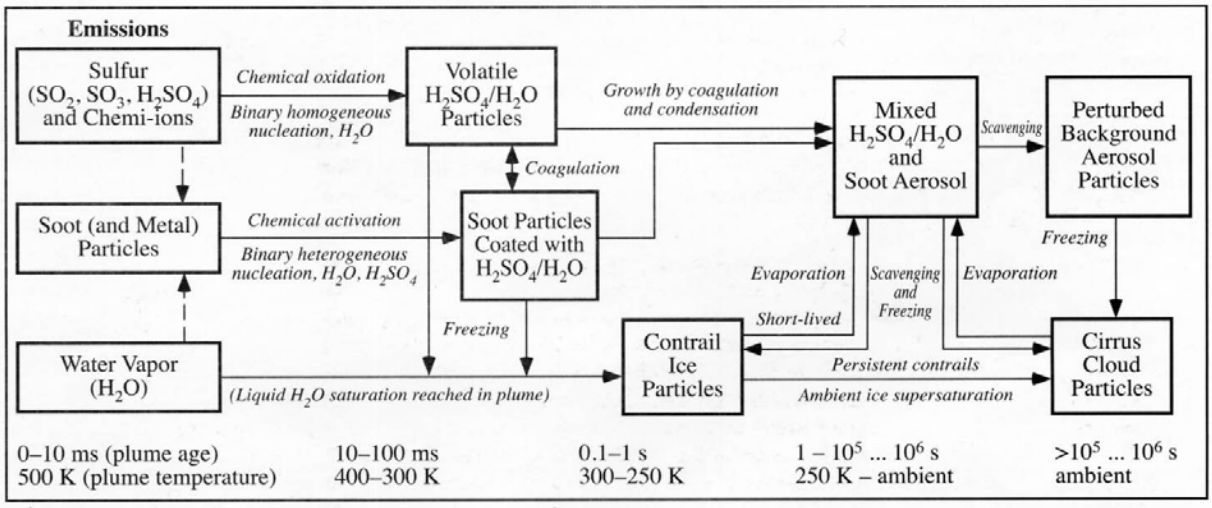

Figure 3-1: Aerosol and contrail formation processes in an aircraft plume and wake as a function of plume age and temperature. Reactive sulfur gases, water vapor, chemi-ions (charged molecules), soot aerosol, and metal particles are emitted from the nozzle exit planes at high temperatures. H_2SO_4 increases as a result of gas-phase oxidation processes. Soot particles become chemically activated by adsorption and binary heterogeneous nucleation of SO_3 and H_2SO_4 in the presence of H_2O, leading to the formation of a partial liquid H_2SO_4/H_2O coating. Upon further cooling, volatile liquid H_2SO_4/H_2O droplets are formed by binary homogeneous nucleation, whereby chemi-ions act as preferred nucleation centers. These particles grow in size by condensation and coagulation processes. Coagulation between volatile particles and soot enhances the coating and forms a mixed H_2SO_4/H_2O-soot aerosol, which is eventually scavenged by background aerosol particles at longer times. If liquid H_2O saturation is reached in the plume, a contrail forms. Ice particles are created in the contrail mainly by freezing of exhaust particles. Scavenging of exhaust particles and further deposition of H_2O leads to an increase of the ice mass. The contrail persists in ice-supersaturated air and may develop into a cirrus cloud. Short-lived and persistent contrails return residual particles into the atmosphere upon evaporation. Scavenging time scales are highly variable and depend on exhaust and background aerosol size distributions and abundances, as well as on wake mixing rates (see Section 3.3).

3.2.2. *Volatile Particles*

3.2.2.1. Basic Processes

Volatile particles form in the exhaust plume of an aircraft as a result of nucleation processes associated with the emission of aerosol precursors (Hofmann and Rosen, 1978). Typical aerosol parameters in a young plume are included in Table 3-1 for reference. The newly formed particles grow by condensation (uptake of gaseous species) and coagulation (particles collide and attach) in the expanding plume. Coagulation processes involving charged particles originating from CI emissions are more effective because charge forces enhance collision rates. These processes are schematically presented in Figure 3-1. Key processes at young plume ages are determined mainly from the results of simulation models because of the lack of suitable plume measurements.

Previous models (Miake-Lye *et al.*, 1994; Kärcher *et al.*, 1995; Zhao and Turco, 1995; Brown *et al.*, 1996b; Taleb *et al.*, 1997; Gleitsmann and Zellner, 1998a,b) show that particles form when the condensing species, primarily H_2SO_4/H_2O, reach concentrations critical for binary homogeneous nucleation in the expanding and cooling exhaust gas. Because concentrations fall below nucleation thresholds as the plume further dilutes, the amount of H_2SO_4 in the early stages of the plume (< 1 s) controls the formation of new volatile particles. More recent models emphasize the role of CI emissions in volatile particle formation and growth (Yu and Turco, 1997, 1998a,b; Kärcher, 1998a; Kärcher *et al.*, 1998a).

Table 3-1: *Summary of number mean radius, number density, and surface area density for sulfate and soot particles in aircraft plumes and in the background atmosphere, and for ice particles in contrails and cirrus. Flight levels of subsonic (supersonic) aircraft are in the 10–12 km (16–20 km) range. Also included are estimates of zonal mean perturbations to sulfate and soot properties caused by the 1992 aircraft fleet.*

	Radius (μm)	**Number Density (cm^{-3})**	**Surface Area Density ($\mu m^2\ cm^{-3}$)**
Sulfate			
Plume (1 s)[a]	0.002	$(1–2) \times 10^7$	500–1000
Background (10–12 km)[b]	0.01–0.1	50–1000	1–6 (10–40)
Background (20 km, non-volcanic)[c]	0.07	5–10	0.5–1
Background (20 km, volcanic)[d]	0.2–0.5	10–100	10–40
Soot			
Plume (1 s)[e]	0.01–0.03	$5 \times 10^4 – 5 \times 10^5$	50–5000
Background (10–20 km)[f]	0.05–0.1	0.01–0.1	$3 \times 10^{-5} – 3 \times 10^{-2}$
Ice			
Young Contrail (0.1–0.5 s)[g]	0.3–1	$10^4–10^5$	$10^4–10^5$
Persistent Contrail (10 min to 1 h)[h]	1–15	10–500	$10^3–10^4$
Young Cirrus[i]	5–10	1	$10^2–10^4$
1992 Aircraft Perturbation[j]			
Sulfate Aerosol (10–12 km, 50–60°N)	0.01	90–900	0.1–1.1
Soot (10–12 km, 50–60°N)	0.02	3–30	0.02–0.2

[a] Detectable only by ultrafine particle counters (particles smaller than 2-3 nm radius are not detected). Calculations by Yu and Turco (1997) for average FSC consistent with observed data.

[b] Properties highly variable; size distributions often bimodal. Ranges include small (> 10 nm) particles. Large particle mode (~100 nm) often similar to stratospheric aerosol particles (Hofmann, 1993; Yue *et al.*, 1994; Schröder and Ström, 1997; Solomon *et al.*, 1997; Hofmann *et al.*, 1998). High range of values inferred from satellite extinction data and represents mixtures of aerosols and subvisible clouds.

[c,d] Yue *et al.*, 1994; Kent *et al.*, 1995; Borrmann *et al.*, 1997; Thomason *et al.*, 1997b.

[e] Hagen *et al.*, 1992; Rickey, 1995; Petzold *et al.*, 1999.

[f] Only largest soot particles with longest atmospheric lifetimes are measured by wire impactors (Sheridan *et al.*, 1994; Blake and Kato, 1995; Pueschel *et al.*, 1997). Uncertainties in total surface area introduced by fractal geometry of particles.

[g] Kärcher *et al.*, 1996b, 1998a; Petzold *et al.*, 1997.

[h] Values representative of contrail core for low ice-supersaturation (Heymsfield *et al.*, 1998a; Schröder *et al.*, 1998b) (see also Sections 3.4.4 and 3.6.3). Far larger particles are observed for large ice-supersaturation (Knollenberg, 1972; Gayet *et al.*, 1996).

[i] Ström *et al.*, 1997; Schröder *et al.*, 1998b. Larger values are observed in warm cirrus clouds (Heymsfield, 1993; see also Sections 3.4.4 and 3.6.3).

[j] Results of fuel tracer simulations discussed in Section 3.3.4. Values shown represent upper bounds to zonal mean perturbations caused by emissions of the 1992 aircraft fleet. Results are representative of flight levels at northern mid-latitudes and are calculated using the range of values of computed tracer concentrations from all models and assuming a fuel sulfur content of 0.4 g/kg fuel, a 5% conversion of sulfur to sulfate aerosol, an EI(soot) of 0.04 g/kg fuel, and a mean particle size of 10(20) nm for sulfate (soot) particles.

Figure 3-2 shows the size distributions of exhaust particles at a plume age of 1 s, as inferred from models and a few measurements. In the radius range below 10 nm, volatile particles containing H_2SO_4 and H_2O dominate the overall distribution. Model analyses of near-field particle measurements strongly suggest that the volatile particle size distribution exhibits a bimodal structure (Yu and Turco, 1997), with smaller particles formed by the aggregation of homogeneously nucleated clusters of hydrated H_2SO_4 molecules (neutral mode) and larger particles formed by rapid scavenging of charged molecular clusters by CIs (ion-mode). Only particles from the ion mode are expected to grow beyond the smallest detectable sizes (radius ~2 to 3 nm) of particle counters. Soot and ice contrail particles are significantly larger than the volatiles. An approximate stratospheric size distribution is shown for comparison. In contrast to soot and ice particles (see below), volatile particle spectra are mainly derived from numerical simulation models because of the lack of size-resolved, *in situ* particle measurements in the nanometer size range. However, the use (in field measurements) of multiple particle counters with different lower size-detection limits allows derivation of the mean sizes of observable particles as a function of fuel sulfur content and plume age (Kärcher *et al.*, 1998b; Yu *et al.*, 1998), thereby providing strong criteria to test the validity of model results.

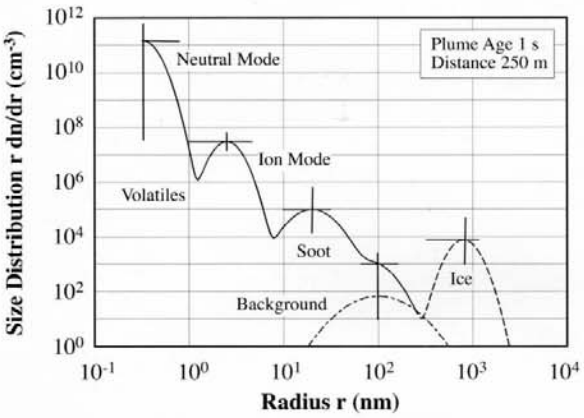

Figure 3-2: Size distribution of various aerosol types present in young jet aircraft exhaust plumes (adapted from Kärcher, 1998a). Shown are approximate size distributions (solid line) versus radius for volatile particles (neutral and chemi-ion modes) and soot (primary and secondary modes), when no contrail is produced by the aircraft. If a contrail is formed, these size distributions change (not shown), and ice particles are created (dashed line). Size distributions of soot and ice particles have been measured *in situ*. Mean sizes and numbers of ion mode particles have been deduced from particle counter measurements, and corresponding size distributions of volatile particles have been inferred from simulation models. Bars indicate the approximate range of variability resulting from variations of fuel sulfur content, engine emission parameters, and ambient conditions, as suggested by evaluation of current observations and modeling studies. An approximate background aerosol size distribution is included for comparison (dot-dashed line) (see Table 3-1).

Once formed, the new volatile particles interact with non-volatile and contrail ice particles through the processes of coagulation, freezing, condensation, and evaporation (Figure 3-1). Calculations show that the new liquid particles grow and shrink as a function of relative humidity, whereas H_2SO_4 molecules that enter the droplets stay in the liquid phase because of their very low saturation vapor pressure (Mirabel and Katz, 1974). They also suggest that volatile particles may take up HNO_3 and H_2O in the near field (Kärcher, 1996) to form particles with compositions similar to those found in cold regions of the stratosphere. These particles may persist in cold (< 200 K), HNO_3-rich stratospheric air but will be short-lived (< 1 min) otherwise. As the plume continues to dilute with ambient air, abundant newly formed volatile particles remain at nanometer sizes and therefore add substantially to the overall aerosol surface area and abundance (Danilin *et al.*, 1997). Their efficiency for heterogeneous chemistry and cloud formation, however, is size- and composition-dependent (Kärcher, 1997). They may be too small to act as efficient cloud- or ice-forming nuclei in the background atmosphere unless the air mass containing the aerosol is lifted or cooled or the relative humidity increases. Although studies exist on heterogeneous plume processing along selected trajectories (Danilin *et al.*, 1994), systematic investigations of heterogeneous chemistry coupled to plume aerosol dynamics remain to be performed (Chapter 2).

The evolution of volatile particles is significantly altered if a contrail forms. In contrails, volatile particles have to grow to sizes greater than about 100 nm via uptake of ambient H_2O before most of them freeze (Section 3.2.4.2). As ice particles grow in size by deposition of H_2O, they may also scavenge other volatile and soot particles (Anderson *et al.*, 1998a,b; Schröder *et al.*, 1998a). Thus, contrails are expected to contain fewer small particles than non-contrail plumes because of enhanced scavenging losses. After evaporation of contrail ice crystals, the residual volatile and soot cores remain as particles in the atmosphere (Figure 3-1). This contrail processing is expected to modify the particle size distribution and composition and may lead to efficient cloud condensation nuclei production (Yu and Turco, 1998b).

3.2.2.2. Observations and Modeling of Volatile Particles and Sulfur Conversion

Volatile particle abundances observed *in situ* in the plumes (mostly young, < 100 s) of subsonic and supersonic aircraft are summarized in Figure 3-3a. The data have been compiled from various field studies (Fahey *et al.*, 1995a,b; Schumann *et al.*, 1997; Anderson *et al.*, 1998a,b; Schröder *et al.*, 1998a). The results show EIs for ultrafine volatile aerosol particles (nominal radii > 2 to 3 nm) in the range of 10^{15} to 10^{16}/kg fuel for low to average fuel sulfur content values and exceeding 10^{17}/kg fuel for high-sulfur fuel. Besides the obvious dependence on fuel sulfur content, the spread in EI values may be explained by

differences in the emission characteristics of the engines, variations in the lower size detection limits of the particle counters, and differences in plume ages at the time of the observations. The increase in ultrafine particle abundance with increasing fuel sulfur content for the Advanced Technology Testing Aircraft System (ATTAS), T-38, and B757 aircraft strongly suggests an important role for fuel sulfur in the growth of volatiles from molecular clusters to detectable particles.

Only a few observations have been analyzed using detailed microphysical simulation models (Brown *et al.*, 1996a; Danilin *et al.*, 1997; Kärcher and Fahey, 1997; Yu and Turco, 1997, 1998a; Andronache and Chameides, 1998; Kärcher *et al.*, 1998a,b). Simulations show better agreement between calculated and observed particle concentrations when ion effects are taken into account. More important, the description of plume microphysics using binary homogeneous nucleation failed to explain a field measurement (Yu *et al.*, 1998). In two cases, condensation nucleus observations in the exhaust of the ATTAS and the Concorde (Figure 3-3a) have been explained in detail with a model that includes CI emissions on the order of 10^{17}/kg fuel. The observable (ion mode) particles have mean radii of about 2 to 4 nm in the young plume, for EI(S) ranging from average to high values. For decreasing levels of available H_2SO_4, the ion mode particles decrease in size. The number of detected particles falls below 10^{17}/kg fuel when the mean radius of their size distribution becomes smaller than the detection limit of the particle counters.

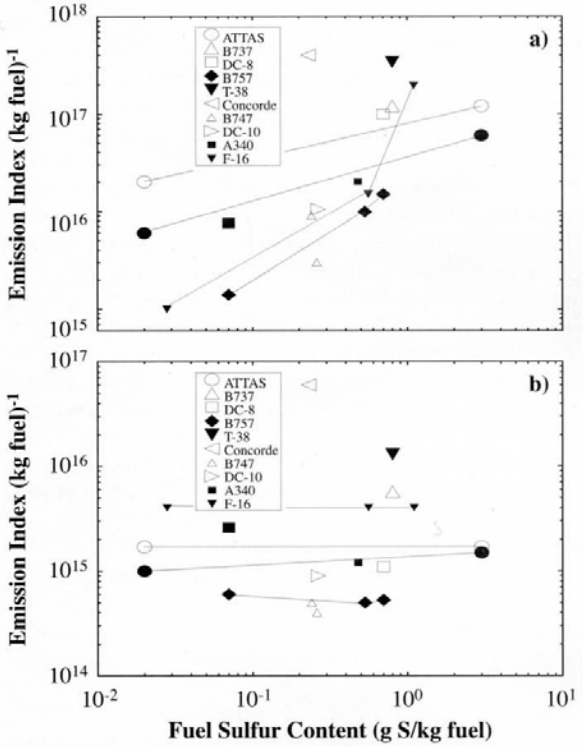

Figure 3-3: (a) Emission indices of detectable volatile particles in number per kg fuel measured *in situ* in plumes of various subsonic aircraft and the supersonic Concorde. The aircraft were examined as part of several missions in Europe and the United States of America; aircraft types are indicated in the legends. Ultrafine volatile particles with radii greater than 2 to 3 nm were measured at plume ages less than 20 s (ATTAS, B737, DC-8, B757, T-38, F-16), with radii greater than 4 to 5 nm at ages of 0.25 to 1 h (Concorde), and with radii greater than 6 nm at ages of 1 to 2 min (B747, DC-10, A340). Observations involving the same aircraft are connected by lines. Fuel sulfur content values were determined by chemical analysis of fuel or inferred from *in situ* SO_2 measurements (for B747 and DC-10). During the observations, a contrail either did (filled symbols) or did not (open symbols) form. (b) Same as (a), but for the emission indices of soot particles. Values from Howard *et al.* (1996) for a modern jet engine (about 10^{13}/kg) are below the range of values shown.

The extent of conversion of fuel sulfur to S(VI) necessary to explain the observed mass of volatile aerosol in young plumes seems to be variable. Direct measurements of H_2SO_4 have provided a lower bound of ~0.4% (for high-sulfur fuel, 2.7 g/kg fuel) and an upper bound of ~2.5% (for low-sulfur fuel, 0.02 g/kg fuel) for the conversion fraction in one case (Curtius *et al.*, 1998), consistent with calculated SO_3 emission levels (Brown *et al.*, 1996a,c). For the low fuel-sulfur case, it has been demonstrated that the observed volatile particles cannot be mainly composed of H_2SO_4 (Kärcher *et al.*, 1998b). In other cases, conversion fractions have been indirectly inferred from mass balance arguments involving observed or inferred particle size and number distributions, available sulfur as measured in fuel samples, and assumptions of aerosol composition. The dependence of the conversion fraction on EI(S) differs in the few studies performed to date (Fahey *et al.*, 1995a; Schumann *et al.*, 1996; Hagen *et al.*, 1998; Miake-Lye *et al.*, 1998; Pueschel *et al.*, 1998). The values deduced from these measurements range from the minimum value of 0.4% to more than 20%. Some of the indirect analyses may be affected by uncertainties (possibly about 20%) regarding the sulfur content in the fuels. Other experimental uncertainties are associated with these determinations, and the range of aircraft engines and operating parameters adds to the observed variability.

Generalization of these results cannot be done with confidence because of limited empirical knowledge of the S(VI) conversion fraction and emission levels of CIs representative of the exhaust as it enters the atmosphere. Part of the observed volatile aerosol may be composed of HNO_2 (Zhang *et al.*, 1996; Kärcher, 1997) or NMHCs (Kärcher *et al.*, 1998b), or it may result from unrecognized sulfur oxidation reactions (Danilin *et al.*, 1997; Miake-Lye *et al.*, 1998). Uptake of gaseous SO_2 and subsequent heterogeneous oxidation to sulfate in the new volatile particles is likely small (Kärcher, 1997), but the possibility of other condensational or aqueous-phase growth mechanisms has not yet been fully explored. On the other hand, CI emissions of about 10^{17}/kg fuel are consistent with observations (see Section 3.2.1.3), although they need to be confirmed by further measurements at the engine exit.

The best estimate for the S-to-H_2SO_4 conversion fraction in young plumes is 5%, with an estimated variability, or uncertainty range, of 1 to 20%. Combustion models predict a range of sulfur conversion up to about 10% and a potential for slightly higher values because of turbine blade cooling effects (Sections 3.2.1.2 and 7.6). Low conversion fractions of 2% are sufficient to explain observed volatile particle concentrations in the young plume behind the ATTAS when the effects of CIs are taken into account in simulation models of plume chemistry and microphysics (Kärcher *et al.*, 1998a,b; Yu and Turco, 1998a,b; Yu *et al.*, 1998). In contrast, the Concorde observations can be explained by assuming that about 20% of the fuel sulfur is converted to SO_3 before leaving the engine exit in such simulations (Yu and Turco, 1997).

In situ measurements detailing particle volatility and size distributions such as those included in Figure 3-3 have involved relatively young plumes. Further observations in aging plumes (> 1 h) as they dilute with the background atmosphere are currently lacking. Without detailed observations of the microphysical evolution and chemical composition of volatile exhaust particles from the engine exhaust plume to the global scale, important uncertainties remain in assessing the potential global impact of exhaust products on chemistry and cloudiness.

3.2.3. Soot and Metal Particles

3.2.3.1. Soot

Aircraft jet engines directly emit solid soot particles. Soot encompasses all primary, carbon-containing products from incomplete combustion processes in the engine. Besides the pure (optically black) carbon fraction, these products may also contain nonvolatile (gray) organic compounds (e.g., Burtscher, 1992; Bockhorn, 1994). Soot parameters of importance for understanding plume processes are concentration and size distribution at the engine exit, nucleating and chemical properties, and freezing ability.

Soot emissions for current aircraft engines are specified under the International Civil Aviation Organization (ICAO) using smoke number measurements (Chapter 7). The smoke number is dominated by the largest soot particles collected onto a filter. Sampling soot particles smaller than about 300 nm on such filters becomes inefficient. Correlations between smoke number and soot mass concentrations (e.g., Champagne, 1988) are used to estimate the soot mass EI from ICAO certification data. A mean value has been estimated to be approximately 0.04 g/kg fuel for the present fleet (Döpelheuer, 1997). Because soot emissions depend strongly on engine types, power settings, and flight levels, additional information is generally needed to relate smoke number to emissions under flight conditions. However, details of the size distribution and physicochemical properties of soot under flight conditions are generally not known and cannot be inferred from smoke number data.

Soot particle measurements for a variety of contemporary engines show values that scatter around 10^{15}/kg fuel (Figure 3-3b). Thus, soot is about 100 times less abundant in the plume than volatile aerosol particles; no significant, if any, dependence exists between soot and fuel sulfur content (Petzold *et al.*, 1997, 1999; Anderson *et al.*, 1998a; Paladino *et al.*, 1998). Values of 10^{14} to 10^{15}/kg fuel are consistent with a mass range of 0.01 to 0.2 g/kg fuel for individual engines using estimated size distributions. The older Concorde and T-38 engines show exceptionally high number EIs, whereas one modern subsonic engine emits much fewer soot particles (about 10^{13}/kg fuel) (Howard *et al.*, 1996). Soot particles are composed of individual, nearly spherical particles (spherules), which have a number mean radius between 10 and 30 nm and exceed the size of volatile aerosol particles in a young plume (Hagen *et al.*, 1992; Rickey, 1995) (Figure 3-2). Several spherical soot particles may aggregate and form a complex chain structure that may change with time (Goldberg, 1985). The smallest soot particles will be most rapidly immersed in background aerosol droplets by coagulation, consistent with the fact that only larger individual soot particles or agglomerates with radii larger than about 50 to 100 nm are observable at cruising levels (Sheridan *et al.*, 1994). Reported estimates of soot surface area at the engine exit are in the range of 5,000 to 10^5 μm^2 cm^{-3} (Rickey, 1995; Petzold *et al.*, 1999). These values continually decrease as the plume dilutes.

Much less information is available concerning the hydration properties of exhaust soot. In the initial stages of formation, graphite-like soot particles are hydrophobic. However, laboratory observations have shown that n-hexane soot particles and other black carbons are partially hydrated (e.g., Chughtai *et al.*, 1996). Soot particles fresh from jet engines very likely become hydrophilic by oxidation processes or deposition of water-soluble species present in the exhaust. Irregular surface features and chemically active sites can also increase chemical reactivity and amplify heterogeneous nucleation processes.

A clear correlation between fuel sulfur content and soluble mass fractions found on fresh exhaust soot suggests that soot hydrates more effectively with increasing EI(S) and that H_2SO_4 is the primary soluble constituent (Whitefield *et al.*, 1993). Hydration of carbon particles was observed under water-subsaturated conditions after treatment with gaseous H_2SO_4 (Wyslouzil *et al.*, 1994). This increase in H_2O adsorption is in qualitative agreement with an analysis of the wetting behavior of graphitic carbon under plume conditions (Kärcher *et al.*, 1996b). Heterogeneous nucleation of H_2SO_4 hydrates on soot was found to be unlikely under plume conditions. Soot hydration properties may also change after treatment with OH and ozone (Kärcher *et al.*, 1996b; Kotzick *et al.*, 1997).

Production of water-soluble material by the interaction of soot with SO_2 is unlikely because the sticking probabilities of gaseous SO_2 on amorphous carbon are too small (Andronache and Chameides, 1997; Rogaski *et al.*, 1997). However, SO_3 and H_2SO_4 might easily adsorb on soot prior to volatile particle formation and may explain measured soluble mass fractions on

soot (Kärcher, 1998b). Sulfur may also become incorporated into soot already within the engines, possibly via S-containing hydrocarbons involved in soot formation (Petzold and Schröder, 1998). Scavenging of small volatile droplets constitutes another soot activation pathway (Zhao and Turco, 1995; Brown *et al.*, 1996b; Schumann *et al.*, 1996). The resulting liquid H_2SO_4/H_2O coating increases with plume age and may enhance the ice-forming ability of soot, which is only poorly known (Section 3.2.4), or it may suppress reactions identified in the laboratory using dry soot surfaces (Gao *et al.*, 1998).

3.2.3.2 Metal Particles

Aircraft jet engines also directly emit metal particles. Their sources include engine erosion and the combustion of fuel containing trace metal impurities or metal particles that enter the exhaust with the fuel (Chapter 7). Metal particles—comprising elements such as Al, Ti, Cr, Fe, Ni, and Ba—are estimated to be present at the parts per billion by volume (ppbv) level at nozzle exit planes (CIAP, 1975; Fordyce and Sheibley, 1975). The corresponding concentrations of 10^7 to 10^8 particles/kg fuel (assuming 1-μm radius; see below) are much smaller than for soot. Although metals have been found as residuals in cirrus and contrail ice particles (Chen *et al.*, 1998; Petzold *et al.*, 1998; Twohy and Gandrud, 1998), their number and associated mass are considered too small to affect the formation or properties of more abundant volatile and soot plume aerosol particles.

3.2.4. Contrail and Ice Particle Formation

3.2.4.1. Formation Conditions and Observations

Contrails consist of ice particles that mainly nucleate on exhaust soot and volatile plume aerosol particles. Contrail formation is caused by the increase in relative humidity (RH) that occurs in the engine plume as a result of mixing of warm and moist exhaust gases with colder and less humid ambient air (Schmidt, 1941; Appleman, 1953). The RH with respect to liquid water must reach 100% in the young plume behind the aircraft for contrail formation to occur (Höhndorf, 1941; Appleman, 1953; Busen and Schumann, 1995; Jensen *et al.*, 1998a). The thermodynamic relation for formation depends on pressure, temperature, and RH at a given flight level; fuel combustion properties in terms of the emission index of H_2O and combustion heat; and overall efficiency η (Cumpsty, 1997). η, defined as the fraction of fuel combustion heat that is used to propel the aircraft, can be computed from engine and aircraft properties (Schumann, 1996a; see also Section 3.7). Only the fraction $(1-\eta)$ of the combustion heat leaves the engine with the exhaust gases. As the value of η increases, exhaust plume temperatures decrease for a given concentration of emitted water vapor, hence contrails form at higher ambient temperatures and over a larger range of altitudes in the atmosphere (Schmidt, 1941).

Several recent studies reported formation and visibility of contrails at temperatures and humidities as predicted by thermodynamic theory for a variety of aircraft and ambient conditions (Busen and Schumann, 1995; Schumann, 1996b; Schumann *et al.*, 1996; Jensen *et al.*, 1998a; Petzold *et al.*, 1998). These data are compiled in Figure 3-4. The mixing process in the expanding exhaust plume is close to isobaric, so the specific excess enthalpy and water content of the plume decrease with a fixed ratio as plume species dilute from engine exit to ambient values. Hence, plume conditions follow straight "mixing lines" in a plot of H_2O partial pressures versus temperature (Schmidt, 1941) (Figure 3-4). The thermodynamic properties of H_2O are such that the saturation pressures over liquid water and water-ice (solid and dashed lines) increase exponentially with temperature. Therefore, within the first second in the plume, the exhaust RH increases to a maximum, then decreases to ambient values. The ambient temperature reaches threshold values for contrail formation when the mixing lines touch the liquid saturation curve in Figure 3-4b. Contrails persist when mixing-line endpoints fall between the liquid and ice saturation pressures—that is, when the ambient atmosphere is ice-supersaturated. Without ambient ice supersaturation, contrail ice crystals evaporate on time scales of seconds to minutes. Short-lived contrails may also form without ambient water vapor if ambient temperatures are sufficiently low.

Contrails become visible within roughly a wingspan distance behind the aircraft, implying that the ice particles form and grow large enough to become visible within the first tenths of a second of plume age. Ice size distributions peak typically at 0.5 to 1 μm number mean radius (Figure 3-2). A lower limit concentration of about 10^4 cm^{-3} of ice-forming particles in the plume (at plume ages between 0.1 and 0.3 s) is necessary for a contrail to have an optical depth above the visibility threshold (Kärcher *et al.*, 1996b). These values and the corresponding mean radii of 1 μm of contrail ice particles are in agreement with *in situ* measurements in young plumes (Petzold *et al.*, 1997). Initial ice particle number densities increase from 10^4 to 10^5 cm^{-3} and mean radii decrease from 1 to 0.3 μm when the ambient temperature is lowered by 10 K from a typical threshold value of 222 K (Kärcher *et al.*, 1998a). Although aerosol and ice particle formation in a contrail are influenced by the fuel sulfur content (Andronache and Chameides, 1997, 1998), it has only a small (< 0.4 K) impact on the threshold temperature for contrail formation (Busen and Schumann, 1995; Schumann *et al.*, 1996).

Simulations of contrail formation further suggest that contrails would also form without soot and sulfur emissions by activation and freezing of background particles (Jensen *et al.*, 1998b; Kärcher *et al.*, 1998a). However, the resulting contrails would have fewer and larger particles.

Ice particle size spectra within and at the edge of young contrails systematically differ from each other (Petzold *et al.*, 1997). Ambient aerosol may play a larger role in contrail regions that nucleate at the plume edges, where the ratio of ambient to soot particles is largest and when ambient temperatures are low

(212 K) (Jensen *et al.*, 1998b). Ice particles may also nucleate on ambient droplets in the upwelling limbs of vortices and could contribute to contrail ice mass (Gierens and Ström, 1998). Metal (and soot) particles have been found as inclusions in contrail ice particles larger than 2 to 3 μm in radius (Twohy and Gandrud, 1998), but these particles are numerically unimportant compared with other plume particles.

Contrail ice crystals evaporate quickly when the ambient air is subsaturated with respect to ice, unless the particles are coated with other species such as HNO_3 (Diehl and Mitra, 1998). Simulations suggest that a few monolayers of HNO_3 may condense onto ice particle surfaces and form NAT particles in stratospheric contrails (Kärcher, 1996). These particles would be thermodynamically stable and longer lived and would cause a different chemical perturbation than would short-lived stratospheric contrails composed of water ice. However, the relevance of this effect on larger scales has not yet been studied because no parameterization of NAT particle nucleation in aircraft plumes exists for use in atmospheric models (Chapter 4).

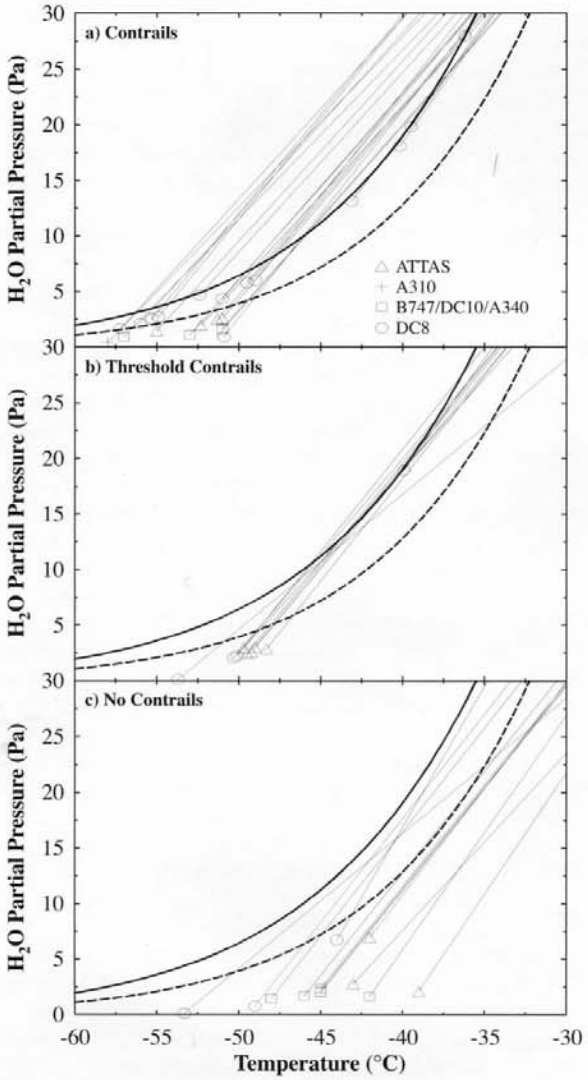

Figure 3-4: Water vapor partial pressure and temperature measurements and calculations from various contrail studies. Symbols indicate measured ambient conditions of temperature and H_2O abundance behind various identified aircraft. Measurements are grouped using visual observations of contrails into three categories: (a) The existence of contrails is confirmed, (b) contrails were just at the limit of formation or disappearance, and (c) contrails were not observed. Liquid and ice saturation pressure are given by full and dashed curves, respectively. The thin line connected to each symbol represents the mixing line of plume states between ambient and engine exit conditions. The mixing lines have altitude- and engine-dependent slopes given by the expression $EI(H_2O)\ c_p\ p\ [0.622\ Q(1 - \eta)]^{-1}$, which includes the emission index of water vapor, the specific heat capacity of air c_p, the ambient pressure p, the ratio of molar masses of water and air (0.622), and the effective specific combustion heat $Q(1 - \eta)$, where η is the overall efficiency of propulsion for the aircraft and Q is the fuel-specific heat of combustion. Because contrails are observed only when the mixing line crosses [in (a)] or at least touches [in (b)] the liquid water saturation curve, these observations are consistent with the modified Schmidt-Appleman criterion used to predict contrail occurrence (from Kärcher *et al.*, 1998a).

3.2.4.2. Freezing of Contrail Particles

In a young contrail, activated particles first grow to sizes > 0.1 μm by water uptake before many of them freeze homogeneously to form water-ice particles (Kärcher *et al.*, 1995; Brown *et al.*, 1997). The fraction of H_2SO_4/H_2O droplets that freezes depends on the actual droplet composition, which affects the homogeneous freezing rate, the time evolution of H_2O supersaturation and temperature in the plume, and possible competition with heterogeneous freezing processes involving soot (see Figure 3-1).

Pure water droplets freeze homogeneously (without the presence of a foreign substrate) at a rate that grows in proportion to droplet volume and becomes very large when the droplet is cooled to the homogeneous freezing limit near about -45°C (Pruppacher, 1995). Acidic solutions freeze at lower temperatures than pure water. Freezing is often induced heterogeneously by solid material immersed inside a droplet (immersion freezing) or in contact with its surface (contact freezing). Prediction of heterogeneous freezing rates requires detailed knowledge about the ice-forming properties of droplet inclusions (Pruppacher and Klett, 1997). If homogeneous and heterogeneous freezing processes are possible, the most efficient freezing

mode takes up available H_2O and may prevent the growth of other particle modes.

When the ambient temperature is near the threshold value for contrail formation, models suggest that volatile aerosol particles take up only a little water and stay below the critical size (radii > 2 to 5 nm) required for growth and subsequent freezing (Kärcher *et al.*, 1995). This critical size—hence freezing probability—depends on maximum supercooling reached in the expanding plume. Particle growth rates—hence freezing rates—are larger in cooler and more humid ambient air, so volatile particles may contribute considerably to ice crystal nucleation at temperatures below the contrail threshold value. This result is supported by observations of contrails and their microphysical properties for different fuel sulfur levels (Petzold *et al.*, 1997) and environmental temperatures

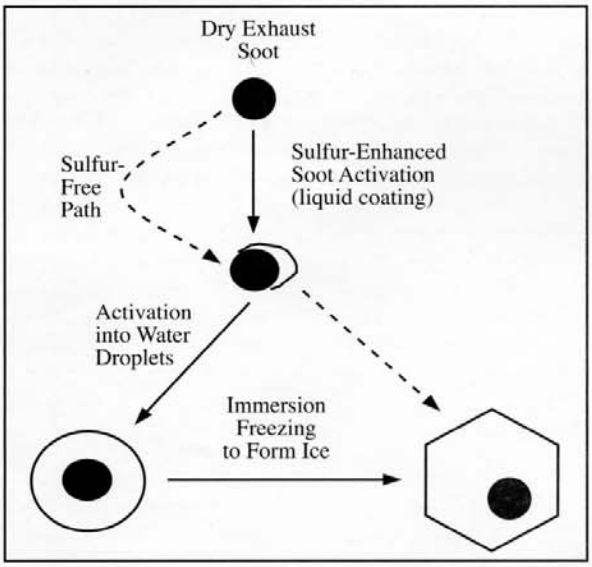

Figure 3-5: Soot activation and heterogeneous freezing in young aircraft exhaust plumes (Kärcher, 1998a). Observational evidence suggests the existence of a sulfur-free pathway (starting with the dashed arrow) for freezing of ice at threshold formation conditions. This pathway is probably dominant for low and very low fuel sulfur levels. The sulfur-enhanced path (solid arrows) is controlled by adsorption of oxidized sulfur molecules, water vapor, and scavenging of H_2SO_4/H_2O droplets. Activation into water droplets occurs when the relative humidity in the plume exceeds 100%. A few ice particles may nucleate below liquid water saturation (dashed arrow). Well below threshold formation temperatures, homogeneous freezing of volatile droplets from the nucleation mode (in which case ice crystals initially contain no soot inclusions) is thought to dominate over soot-induced immersion freezing in the formation of contrail ice particles. The hexagon is a schematic representation of ice particle shapes that are close to spherical in young contrails but may vary in aging contrails. Soot cores may reside inside the ice particles or be attached at their surfaces.

(Freudenthaler *et al.*, 1996). Volatile particles grown on charged droplets are more easily activated than neutral mode droplets (compare in Figure 3-2), therefore may play an enhanced role in contrail formation (Yu and Turco, 1998b). Ambient particles also contribute to ice crystal nucleation in the contrail (Twohy and Gandrud, 1998).

In contrail particle formation, heterogeneous freezing processes involving soot (see Figures 3-1 and 3-5) compete with homogeneous freezing of volatile plume particles. Volatile droplets will be prevented from freezing if rapid freezing of soot-containing particles occurs. Although this analysis is supported by model simulations and some observations (Gierens and Schumann, 1996; Kärcher *et al.*, 1996b, 1998a; Schumann *et al.*, 1996; Brown *et al.*, 1997; Konopka and Vogelsberger, 1997; Schröder *et al.*, 1998a; Twohy and Gandrud, 1998), the freezing probability of soot is poorly known because unique evidence that soot is directly involved in ice formation is difficult to obtain from *in situ* measurements. On the other hand, fresh soot particles do not act as efficient ice (deposition) nuclei in the exhaust (Rogers *et al.*, 1998), consistent with the absence of contrails at temperatures above the liquid water saturation threshold.

Contrails observed near threshold formation conditions are thought to result from freezing of water on soot particles (Kärcher *et al.*, 1996b; Schumann *et al.*, 1996; Brown *et al.*, 1997) (Figure 3-5). This result is supported by laboratory experiments (DeMott, 1990; Diehl and Mitra, 1998) that provide evidence that soot may induce ice formation by heterogeneous immersion freezing at temperatures colder than about 250 K. Water activation of soot may result from the formation of at least a partial surface coating of H_2SO_4/H_2O droplets, which likely develops for average to high fuel sulfur levels (Figure 3-5). Hence, more fuel sulfur leads to a greater number of ice particles. However, observations demonstrate that the number of ice particles (diameter > 300 nm) in young contrails increases by only about 30% when the fuel content increases from 6 to 2700 ppm (Petzold *et al.*, 1997), as model simulations of contrail formation also show (Kärcher *et al.*, 1998a).

Contrails at threshold conditions appear to be formed for very low (2 ppm) fuel sulfur content in the same manner as for average fuel sulfur content (260 ppm) (Busen and Schumann, 1995), but their properties differ measurably for larger fuel sulfur content (Schumann *et al.*, 1996). This result suggests that soot may take up water even at zero fuel sulfur content, though this uptake may be enhanced in the presence of sulfur emissions (Kärcher *et al.*, 1998a; see Figure 3-5).

The presence of liquid coatings may alter the chemical reactivity of dry exhaust soot, which is poorly known (Chapter 2). Soot particles acting as freezing nuclei have the potential to alter cirrus cloud properties (see Section 3.4). Present observations do not rule out the possibility that aircraft soot particles can act as freezing nuclei in cirrus formation, perhaps even without a H_2SO_4/H_2O coating. Information is lacking on how the chemical reactivity and freezing properties of soot might change in aging

plumes from interactions with background gases and particles or as a result of aerosol processing in contrails.

3.3. Regional and Global-Scale Impact of Aviation on Aerosols

3.3.1. Global Aircraft Emissions and Aerosol Sources

Aircraft emissions may cause changes in the background distribution of soot and sulfuric acid aerosols at regional and global scales. In this section, observations and model results are used to evaluate these potential aircraft-induced changes.

Soot and sulfur mass emissions from aircraft are small compared with other global emissions from anthropogenic and natural sources (Table 3-2). However, aircraft emissions occur in the upper troposphere and lower stratosphere, where background values are lower and removal processes are much less effective than near the Earth's surface. Moreover, aircraft aerosol particles tend to be smaller than background particles, so small emission masses may still cause large changes in aerosol number and surface area densities. In addition, aerosol particles from aircraft can participate in the formation of contrails and clouds in the upper troposphere, hence potentially alter the radiative balance of the atmosphere (Section 3.6).

About 93% of all aviation fuel is consumed in the Northern Hemisphere and 7% in the Southern Hemisphere (Baughcum *et al.*, 1996; see Chapter 9). Within the Northern Hemisphere, 76% of aviation fuel is consumed at mid- and polar latitudes (> 30°N). The geographical and altitude distribution of current aviation fuel consumption implies that the largest changes in aerosol and gas composition from aviation will be at northern mid-latitudes at altitudes of 10 to 12 km.

3.3.2. Sulfate Aerosol

3.3.2.1. Stratosphere

The background stratospheric sulfate layer is believed to be formed largely via the transport of carbonyl sulfide (OCS) into the stratosphere, its subsequent conversion to H_2SO_4 (Crutzen, 1976), and condensation of H_2SO_4 onto small particles nucleated primarily near the equatorial tropopause (Brock *et al.*, 1995; Hamill *et al.*, 1997). Current global photochemical models estimate that the natural source from OCS contributes 0.03 to

Table 3-2: *Emission indices and estimated global emission rates of exhaust products of the present (1992) aircraft fleet using representative emission indices. Emission sources other than aircraft and estimated magnitudes of these emissions are listed in the last two columns. Values in parentheses indicate estimated range (adapted from Fabian and Kärcher, 1997; Schumann, 1994).*

Fuel and Emissions	Emission Index (g pollutant/kg fuel)	Emission Rate (1992 fleet) (Tg yr^{-1})	Comparable Emissions (Tg yr^{-1})	Comparable Emission Source
Fuel	–	140 (139–170)[a]	3140	Total consumption of petrol
H_2O	1260	176	45	CH_4 oxidation in the stratosphere
			525000	Evaporation from Earth's surface
NO_x (as NO_2)	14 (12–16)[a]	2	2.9 ± 1.4	Flux from the stratosphere
			90 ± 35	All anthropogenic sources
Soot	0.04 (0.01–0.1)[b]	0.006	12[c]	Fossil fuel combustion and biomass burning
Sulfur	0.4 (0.3–0.5)	0.06	65[d]	Total from fossil fuel combustion
			10–50	Natural source, mostly as DMS[e]
			2.7[f]	Non-eruptive volcanoes
			4.0[g]	Eruptive volcanoes
C_xH_y	0.6 (0.2–3.0)	0.1	90	Anthropogenic emissions at Earth's surface

[a] From Chapter 9.
[b] Döpelheuer, 1997.
[c] Liousse *et al.*, 1996.
[d] Benkovitz *et al.*, 1996.
[e] Watson *et al.*, 1992.
[f] Spiro *et al.*, 1992.
[g] Chin *et al.*, 1996.

0.06 Tg S yr^{-1} into the stratosphere (Chin and Davis, 1995; Weisenstein *et al.*, 1997). Additional sources of stratospheric sulfur may be required to balance the background sulfur budget (Chin and Davis, 1995), such as a strong convective transport of SO_2 precursors (Weisenstein *et al.*, 1997). Large increases in H_2SO_4 mass in the stratosphere often occur in periods following volcanic eruptions (Trepte *et al.*, 1993). Increased H_2SO_4 increases the number and size of stratospheric aerosol particles (Wilson *et al.*, 1993). The relaxation to background values requires several years, as Figure 3-6 illustrates with aerosol extinction measurements derived from satellite observations. The relative effect of aircraft emissions will be reduced in periods of strong volcanic activity, particularly in the stratosphere, because the aircraft source of aerosol becomes small compared with the volcanic source (see Table 3-1).

The current subsonic fleet injects ~0.02 Tg S yr^{-1} into the stratosphere under the assumption that one-third of aviation fuel is consumed in the stratosphere (Hoinka *et al.*, 1993; Berger *et al.*, 1994) (see Table 3-2). This amount is 1.5 to 3 times less than natural sources of stratospheric sulfur in nonvolcanic periods. The enhanced sulfate aerosol surface area in the stratosphere affects ozone photochemistry through surface reactions that reduce nitrogen oxides and release active chlorine species (Weisenstein *et al.*, 1991, 1996; Bekki and Pyle, 1993; Fahey *et al.*, 1993; Borrmann *et al.*, 1996; Solomon *et al.*, 1997). The chemical impact of sulfate aerosol in the stratosphere is discussed in Chapters 2 and 4.

3.3.2.2. Troposphere

Anthropogenic and natural sources of sulfur are much larger in the troposphere than in the stratosphere (Table 3-2). Anthropogenic emissions of sulfur exceed natural sources by factors of 2 to 3 on a global scale, and emission in the Northern Hemisphere exceeds that in the Southern Hemisphere by a factor of 10 (Langner and Rodhe, 1991). Accordingly, aerosol abundance is larger in the upper troposphere than in the stratosphere and larger in the Northern Hemisphere troposphere than in the

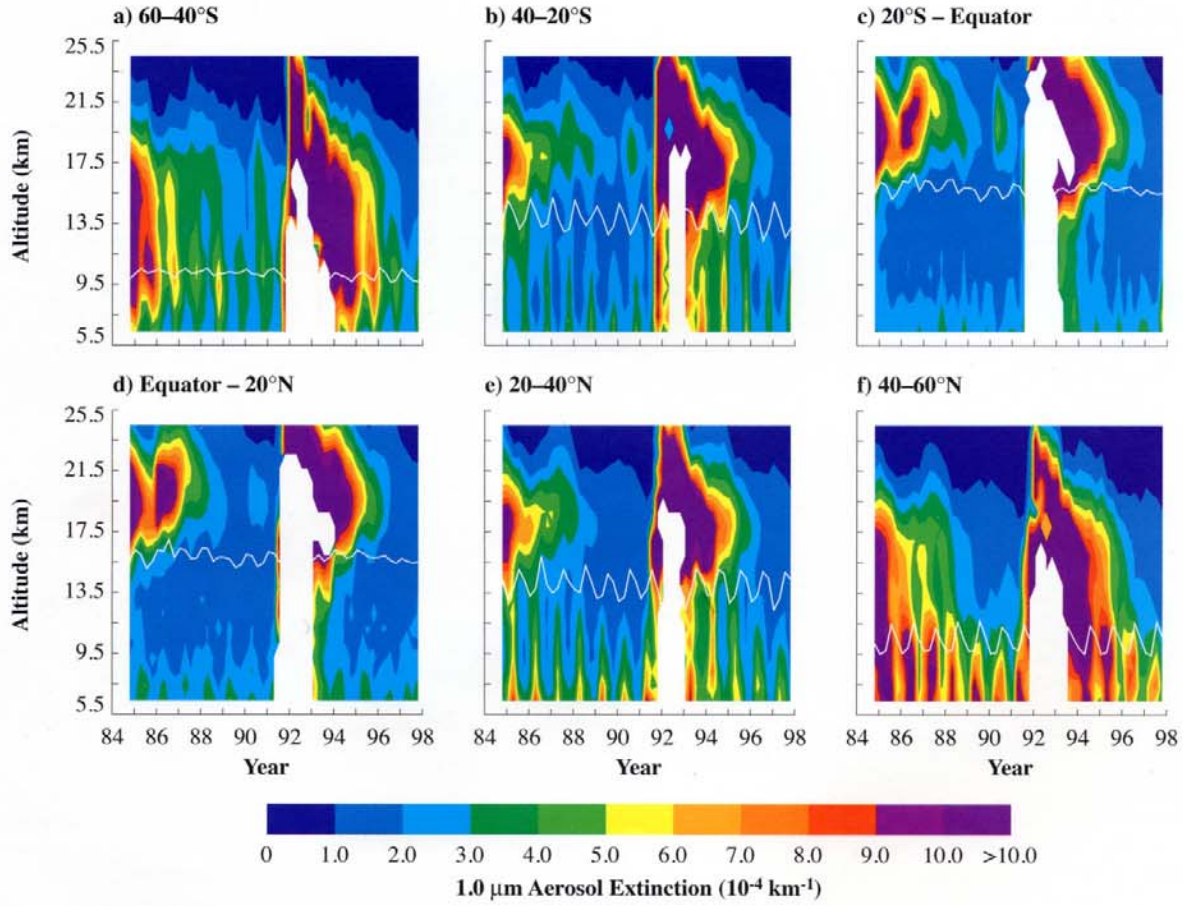

Figure 3-6: Aerosol extinction at 1.02 μm from SAGE II satellite observations at altitudes of 6.5 to 24.5 km. The time period covered is October 1984 to late 1997, with a resolution of 3 months. Each panel indicates mean values observed in a 20° latitude band. The white line indicates the location of the tropopause (extension of Plate 1 in Kent *et al.*, 1995).

Southern Hemisphere counterpart (Hofmann, 1993; Benkovitz *et al.*, 1996; Rosen *et al.*, 1997; Thomason *et al.*, 1997a,b) (Figure 3-6). Tropospheric aerosol concentrations are much larger than lower stratospheric concentrations under nonvolcanic conditions. Condensation nucleus number densities exceeding 1,000 cm^{-3} are not uncommon in the troposphere (Schröder and Ström, 1997; Hofmann *et al.*, 1998), whereas values in the lower stratosphere are less than 50 cm^{-3} in nonvolcanic periods (Wilson *et al.*, 1993).

The effect of aircraft sulfur emissions on aerosol in the upper troposphere and lower stratosphere is far larger than comparison of their amount with global sulfur sources suggests. The major surface sources of tropospheric sulfate aerosol include SO_2 and dimethyl sulfide (DMS), both of which have tropospheric lifetimes of less than 1 week (Langner and Rodhe, 1991; Weisenstein *et al.*, 1997). There is large variability in upper tropospheric aerosol particle number and size (Hofmann, 1993; Thomason *et al.*, 1997b) because of variability in tropospheric meteorology and the short lifetime of sulfur source gases. Surface emissions are known to reach the upper troposphere under certain conditions, such as during deep mid-latitude and tropical convection (Arnold *et al.*, 1997; Prather and Jacob, 1997; Dibb *et al.*, 1998; Talbot *et al.*, 1998). Only a small fraction of the surface sulfur emissions reaches the upper troposphere, however, because of the large removal rates of sulfur species near the surface.

3.3.2.3. *Differences between the Upper Troposphere and Lower Stratosphere*

The effects of aircraft emissions on aerosol particles and aerosol precursors depend on the amounts emitted into the troposphere and stratosphere. In addition to aerosol abundance and sources, stratospheric and tropospheric aerosols also differ in composition and residence time. Typical parameters for sulfate at 12 and 20 km at northern mid-latitudes are summarized in Table 3-1.

Sulfate is considered to be the dominant component of stratospheric aerosol; soot and metals are considered to be minor components (Pueschel, 1996). The composition of tropospheric aerosol, particularly near the surface, also includes ammonium, minerals, dust, sea salt, and organic particles (Warneck, 1988). The role of minor components of aerosol composition in affecting heterogeneous reaction rates is not fully understood. In general, the lower stratosphere contains highly concentrated H_2SO_4/H_2O particles (65–80% H_2SO_4 mass fraction) as a result of low relative humidity in the stratosphere and low temperatures (Steele and Hamill, 1981; Carslaw *et al.*, 1997). Higher H_2O abundances (by a factor of 10 or more) and similar temperatures cause particles in the upper troposphere to be more dilute (40–60% H_2SO_4). Surface reactions that activate chlorine are particularly effective on dilute H_2SO_4 particles and cirrus cloud particles at low temperatures in the tropopause region (Chapter 2).

Aircraft emissions injected into the stratosphere have greater potential to perturb the aerosol layer than those emitted into the troposphere, because in the stratosphere the background concentrations are lower and the residence times are longer. The initial residence time (1/e-folding time) of most of the stratospheric sulfate aerosol mass from volcanic eruptions is about 1 year as a result of aerosol sedimentation rates (Hofmann and Solomon, 1989; Thomason *et al.*, 1997b; Barnes and Hofmann, 1997) (see also Figure 3-6). The residence time of the remaining aerosol mass contained in smaller particles is several years. The residence time of upper tropospheric aerosol particles is much smaller, ranging from several days (Charlson *et al.*, 1992) to between 10 and 15 days (Balkanski *et al.*, 1993; Schwartz, 1996). Tropospheric particles are larger than those in the stratosphere (Hofmann, 1990), therefore sediment faster. They are also removed by cloud scavenging and rainout.

3.3.3. *Observations of Aircraft-Produced Aerosol and Sulfate Aerosol Changes*

Observations of aircraft-induced aerosols have increased substantially in recent years (see Section 3.2). Concentrations of aerosol particles and aerosol precursor gases well above background values have been observed in the exhaust plumes of aircraft operating in the upper troposphere and lower stratosphere. Although aircraft emissions are quickly diluted by mixing with ambient air to near background values, the accumulation of emissions in flight corridors used in the routing of commercial air traffic has the potential to cause notable atmospheric changes.

Estimated changes from aircraft emissions (Schumann, 1994; WMO, 1995) are small compared with natural variability, hence are not always apparent in observational data sets. However, regional enhancements in concentrations of aircraft-produced aerosol have been observed near air traffic corridors. During measurement flights across the North Atlantic flight corridor over the eastern Atlantic, signatures of NO_x, SO_2, and condensation nuclei (CN) were clearly evident in the exhaust plumes of 22 aircraft that passed the corridor at this altitude in the preceding 3 h, with values exceeding background ambient levels by 30, 5, and 3 times, respectively (Schlager *et al.*, 1997). A mean CN/NO_x abundance ratio of 300 cm^{-3} $ppbv^{-1}$ was measured. This ratio corresponds to a mean particle emission index of about 10^{16} kg^{-1} and implies CN increases of 30 cm^{-3} in corridor regions where aircraft increase NO_x by 0.1 ppbv (cf. Chapter 2). The regional perturbation was found to be detectable at scales of more than 1,000 km under special meteorological conditions within a long-lasting stagnant anticyclone (Schlager *et al.*, 1996). In an analysis of 25 years of balloon measurements in Wyoming in the western United States of America, subsonic aircraft are estimated to contribute about 5–13% of the CN concentration at 8–13 km, depending on the season (Hofmann *et al.*, 1998). This estimate provides only a lower bound of the aircraft contribution because smaller aircraft-produced particles (radius < 10 nm) are not detected. Additionally, regular lidar measurements have been made of aerosol optical depth at aircraft altitudes (10–13 km) in an area of heavy air traffic in southern Germany (Jäger *et al.*, 1998).

Table 3-3: *Non-volcanic upper tropospheric annual mean optical depth and % change per year, along with standard deviation, from SAGE satellite observations during 1979–97. Values in parentheses are for the Southern Hemisphere (adapted from Kent et al., 1998).*

Latitude Band	Annual Mean Optical Depth (10^{-4})	Change per Year (%)
80–60° N(S)	25.1 ± 4.7 (2.9 ± 0.9)	-0.4 ± 0.2 (-0.7 ± 0.6)
60–40° N(S)	18.1 ± 4.7 (7.0 ± 1.0)	0.4 ± 0.2 (1.4 ± 0.3)
40–20° N(S)	19.3 ± 2.9 (15.2 ± 2.5)	0.2 ± 0.1 (1.2 ± 0.2)
20–0° N(S)	19.6 ± 0.9 (18.2 ± 1.6)	0.2 ± 0.1 (0.8 ± 0.1)
Hemisphere N(S)		0.1 ± 0.1 (0.9 ± 0.3)
Globe		0.5 ± 0.2

Large optical depths on the order of 0.1 that could be attributed to the accumulation of aircraft aerosol were observed very rarely at this location.

Global changes in sulfate aerosol properties at subsonic air traffic altitudes were small over the last few decades. The examination of long-term changes in aerosol parameters suggests that aircraft operations up to the present time have not substantially changed the background aerosol mass. Multiyear observations for the upper troposphere and lower stratosphere are available from satellite and balloon platforms and ground-based lidar systems. Long-term variations of the optical depth in the upper troposphere from the SAGE satellite (Figure 3-6 and Table 3-3) have been analyzed with periods of volcanic influence excluded (Kent *et al.*, 1998). Data indicate that changes are less than about 1% yr^{-1} between 1979 and 1998, when observations are averaged over either hemisphere. A significant change in aerosol amounts is also not found in the 15- to 30-km region examined with lidar over Mauna Loa (20°N) for the period 1979 to 1996 (Barnes and Hofmann, 1997). Similarly, aerosol mass data above the tropopause derived from lidar soundings show no trend in a region of heavy air traffic in Germany (48°N) over the last 22 years (Figure 3-7) (Jäger and Hofmann, 1991; Jäger *et al.*, 1998).

Long-term changes in aerosol parameters measured *in situ* are also small. *In situ* measurements are important because the number of particles in the upper troposphere and lowermost stratosphere is dominated by sizes that are too small (< 0.15-μm radius) to be remotely detected. Long-term changes in CN are small in the 10- to 12-km region of the mid-latitude troposphere, where most of the current aircraft fleet operates (Hofmann, 1993). The 5% yr^{-1} increase in larger particle (radius > 0.15 μm) abundances found in lower stratospheric balloon measurements made between 1979 and 1990 was considered consistent with the accumulation of aircraft sulfur emissions (Hofmann, 1990, 1991). However, the absence of a change in observed stratospheric CN number suggests that the trend in the larger particles is the result of the growth of existing particles rather than nucleation of new particles. Model results show that the contribution of the current subsonic fleet to aerosol mass amounts between 15 and 20 km is about 100 times smaller than the observed aerosol amounts (Section 3.3.4; Bekki and Pyle, 1992). Previous balloon-borne CN counters did not measure particles below 10 nm in radius, which are now detected with more modern CN counters and dominate aerosol number in aircraft plumes. Moreover, the attribution of aerosol changes to aircraft is complicated by changes in surface sources of sulfur and episodic strong injections of sulfur from volcanic eruptions (Hitchman *et al.*, 1994; Barnes and Hofmann, 1997; Thomason *et al.*, 1997a,b). Hence, the contribution of aircraft emissions to changes or possible trends in these regions is difficult to determine at present.

3.3.4. Modeling Sulfate Aerosol Perturbations Caused by Aircraft

3.3.4.1. Subsonic Aircraft

Global models are required to evaluate the atmospheric impact of aerosol generated by subsonic aircraft (Friedl, 1997; Brasseur *et al.*, 1998). The global distribution of tropospheric

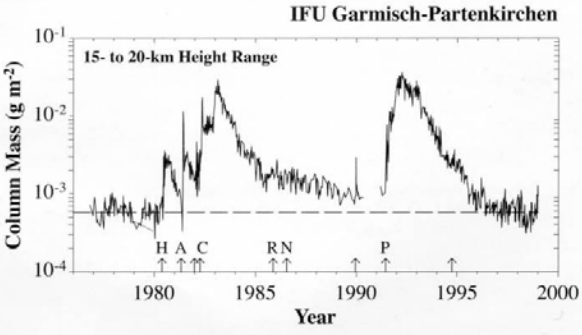

Figure 3-7: Aerosol-mass column between 15- and 20-km altitude, derived from backscatter measurements made by lidar at Garmisch-Partenkirchen, Germany, between 1976 and end of 1998. Dates of major volcanic eruptions are marked on the horizontal axis (H, St. Helens; A, Alaid; C, El Chichón; R, Ruiz; N, Nyamuragira; P, Pinatubo). The dashed line indicates the average value of 1979, which can be considered a background value free from volcanic influence (adapted from Jäger and Hofmann, 1991; Jäger *et al.*, 1998).

sulfur species has been investigated using various three-dimensional (3-D) models (Langner and Rodhe, 1991; Penner *et al.*, 1994; Chin *et al.*, 1996; Feichter *et al.*, 1996; Pham *et al.*, 1996; Schwartz, 1996). Because most models have been developed to investigate regional or global effects of surface emissions in the lower or middle troposphere, few have addressed the potential impact of aviation sources on aerosol parameters in the upper troposphere and lower stratosphere.

A systematic model study has been carried out with a suite of two-dimensional (2-D) and 3-D atmospheric models to determine upper bounds for the accumulation of aviation aerosol in the atmosphere (Danilin *et al.*, 1998). Each model computed the steady-state global distribution of a passive tracer emitted into the model atmosphere with the same rate and distribution as aviation fuel use, based on the NASA 1992 database (see Chapter 9). The only sink for the passive tracer is below 400 hPa (approximately 7 km), where it is removed with a 1/e-folding time of 5 days. The resultant global tracer distribution can be used to provide estimates of steady-state concentration change from a specific emission by multiplying the tracer value by the associated aircraft engine emission index (EI). Figure 3-8 shows steady-state tracer distributions in tracer-to-air mass mixing ratio units and annually and zonally averaged fuel source used in the simulation. Table 3-4 summarizes the main results of these simulations.

All models predict the largest perturbation at mid-latitudes in the Northern Hemisphere in the altitude range of 10–12 km. However, the magnitude of the perturbation varies by a factor of 10, ranging from 12.6 (ECHAM3) to 122 ng g^{-1} (GSFC-2D), reflecting differences in model resolution and current uncertainties in modeling of global atmospheric dynamics and turbulent diffusion. To mitigate the effects of model resolution, the tracer amount was summed in the 8- to 16-km altitude region between 30 and 90°N (shown by the thick dashed line in Figure 3-8). This region contains 34 (AER, ECHAM3) to 61% (GSFC-2D) of the total accumulated tracer. The absolute amount of tracer mass in this volume ranges from 2.9 (ECHAM3) to 14.5 Tg (GSFC-2D). The amount of the tracer above 12 km, which serves to diagnose the fraction of aircraft emissions transported toward the stratospheric ozone maximum, ranges from 14 (UCI/GISS, GSFC-2D) to 45% (UMICH, AER) of each model's global tracer amount. The global residence time of the fuel tracer, defined as the ratio of the steady-state tracer mass to the tracer source, varies from 21 days (TM3, ECHAM3) to 65 days (GSFC-2D, LLNL). The lower values are similar to the global residence times (approximately 18 days) found for air parcels uniformly released at 11 km between 20 and 60°N and followed with a trajectory model using assimilated wind fields (Schoeberl *et al.*, 1998). The 1/e-folding aircraft emissions lifetime of 50 days computed by Gettelman (1998) is consistent with the results of the fuel tracer experiment described here (Danilin *et al.*, 1998).

The model simulation results indicate that aircraft contribute little to the sulfate mass near the tropopause. For example, the sulfate aerosol mass density from the GSFC-2D model (see

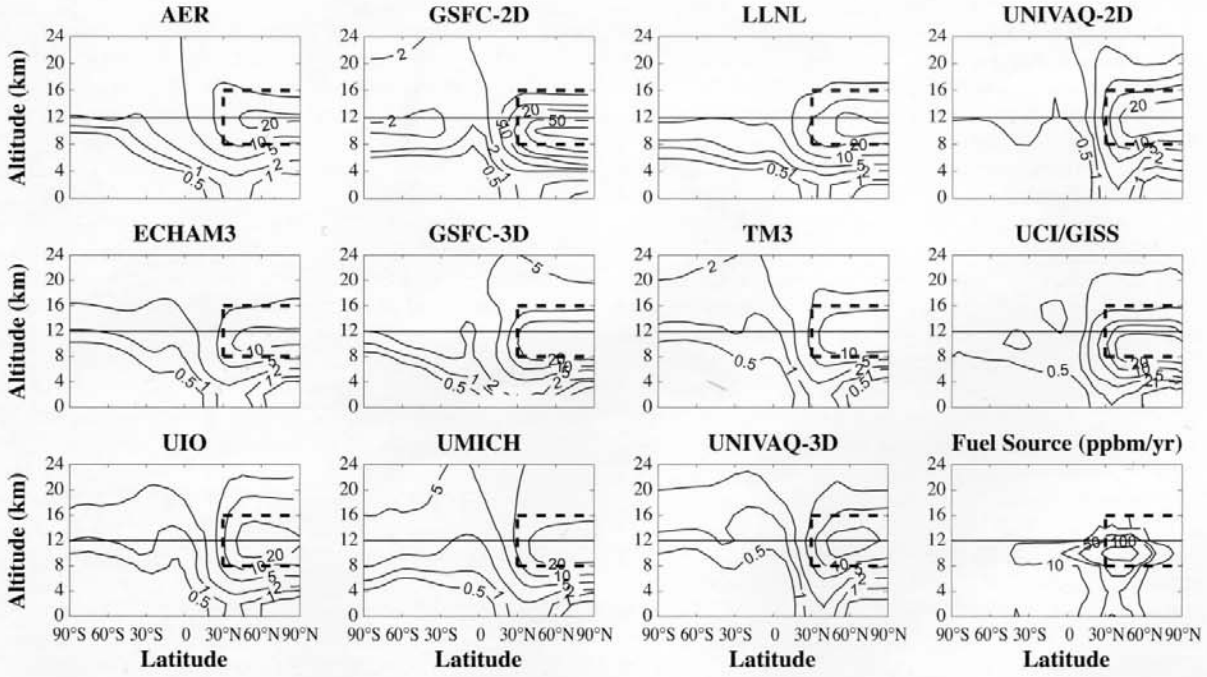

Figure 3-8: Zonally and annually averaged distribution of fuel tracer in ng(tracer)/g(air), according to indicated models. The fuel source is shown in the bottom right panel. The thick dashed line shows the region between 8–16 km and 30–90°N. The thin horizontal line indicates 12-km altitude (from Danilin *et al.*, 1998).

Table 3-4: *Results from the 1992 fuel tracer simulations (other results included in Table 3-1).*

Model[a]	Max. Tracer Value (ng g^{-1})	Latitude of Max. (°N)	Global Residence Time (days)	Tracer 8–16 km 30–90°N (%)	Tracer >12km (%)	Max. Tracer Column[b] (μg cm^{-2})	Global Soot Column (ng cm^{-2})	Global SO_4 Column[c] (ng cm^{-2})
2-D Models								
AER	26.7	55	38	34	45	6.6	0.11	3.5
GSFC-2D	122	55	62	61	16	22.9	0.20	5.9
LLNL	72.5	65	65	42	38	14.5	0.20	6.0
UNIVAQ-2D	36.4	60	23	58	33	7.7	0.08	2.2
3-D Models								
ECHAM3	12.6	50	22	34	31	4.1	0.07	2.0
GSFC-3D	46.7	50	52	44	29	11.7	0.16	4.9
TM3	20.1	80	21	45	40	4.9	0.07	2.0
UCI/GISS	34.4	55	27	49	14	8.2	0.09	2.6
UiO	28.2	55	29	50	40	7.8	0.09	2.7
UMICH	30.4	65	45	37	44	9.6	0.14	4.2
UNIVAQ-3D	38.4	50	25	50	41	7.7	0.08	2.3

[a] Models are denoted as follows: **2-D**—Atmospheric and Environmental Research (AER) (Weisenstein *et al.*, 1998), Goddard Space Flight Center (GSFC-2D) (Jackman *et al.*, 1996), Lawrence Livermore National Laboratory (LLNL) (Kinnison *et al.*, 1994), University of L'Aquila (UNIVAQ-2D) (Pitari *et al.*, 1993); **3-D**—German Aerospace Center (DLR) (ECHAM3) (Sausen and Köhler, 1994), Goddard Space Flight Center (GSFC-3D) (Weaver *et al.*, 1996), Royal Netherlands Meteorological Institute (KNMI) (TM3) (Wauben *et al.*, 1997), University of California at Irvine (UCI/GISS) (Hannegan *et al.*, 1998), University of Oslo (UiO) (Berntsen and Isaksen, 1997), University of Michigan (UMICH) (Penner *et al.*, 1991), UNIVAQ-3D (Pitari, 1993).

[b] Column amounts calculated between 0–60 km for all models except ECHAM3 and TM3 (0–32 km) and UiO (0–26 km).

[c] These values are calculated from model results with assumptions of EI(soot) of 0.04 g/kg fuel, EI(sulfur) of 0.4 g/kg fuel, and 100% conversion of sulfur to H_2SO_4.

Figure 3-8) is 0.055 μg m^{-3} at 10 km at 55°N, in contrast to background concentrations of 1 to 2 μg m^{-3} (Yue *et al.*, 1994). Other recent model studies (Danilin *et al.*, 1997; Kjellström *et al.*, 1998) show similar results for aerosol mass; these studies further conclude that aircraft emissions may noticeably enhance the background number and surface area densities (SAD) of sulfate aerosol (see Tables 3-1 and 3-4) because of the smaller radii of aircraft-produced particles.

Fuel tracer simulation also provides estimates of soot and sulfate column amounts that can be used to calculate the direct radiative forcing of current subsonic fleet emissions (see Chapter 6). Maximum tracer column values are located near 50 to 60°N and range from 4.1 (ECHAM3) to 22.9 μg cm^{-2} (GSFC-2D). To calculate instantaneous direct radiative forcing at the top of the atmosphere from aircraft soot emissions, globally averaged tracer column values (which are smaller than their maximum values by a factor of 3 to 4) are first multiplied by EI(soot) to obtain soot column values. For aircraft sulfur emissions, the tracer column is scaled by EI(S), the ratio of molar mass of SO_4 and S, and a 100% conversion fraction of sulfur to sulfate (see Table 3-4). For the suite of models in Table 3-4, the upper bound for the average soot column is 0.1 ng cm^{-2}, with a range from 0.07 to 0.20 ng cm^{-2}; for the average sulfate column the upper bound is 2.9 ng cm^{-2}, with a range from 2 to 6 ng cm^{-2}. If photochemical oxidation lifetime and tropospheric washout rate are taken into account, a 50% conversion fraction of sulfur to sulfate is a more suitable value than 100%. In this case, the average sulfate column is 1.4 ng cm^{-2}, with a range of 1 to 3 ng cm^{-2}.

In addition to the passive tracer simulation, the AER 2-D model also calculated the evolution of aerosol using a sulfur photochemistry and aerosol microphysics model designed for stratospheric conditions (Weisenstein *et al.*, 1997). This model calculates about 3.4 ng cm^{-2} for the perturbation in sulfate aerosol at 55°N, consistent with the AER model value in Table 3-4 but almost 30 times smaller than the background sulfate column amounts (~100 ng cm^{-2}). Figure 3-9 depicts the annually averaged increase of sulfate aerosol SAD calculated with the AER 2-D model, assuming 5% conversion of sulfur emissions into new particles (as recommended in Section 3.2) with a radius of 5 nm and fuel with 0.4 g S/kg. The maximum SAD perturbation, located at about 10–12 km in northern mid-latitudes, is about 0.3 μm^2 cm^{-3}, which is comparable to ambient values in nonvolcanic periods (Hofmann and Solomon, 1989; Thomason *et al.*, 1997b).

Table 3-1 presents upper-bound estimates of soot and sulfate aerosol number and surface area densities from 1992 fuel simulations. Present aircraft emissions noticeably increase the number and surface area densities of aerosol particles in the tropopause region despite the large CN background concentration in the upper troposphere. The estimates use the range of values

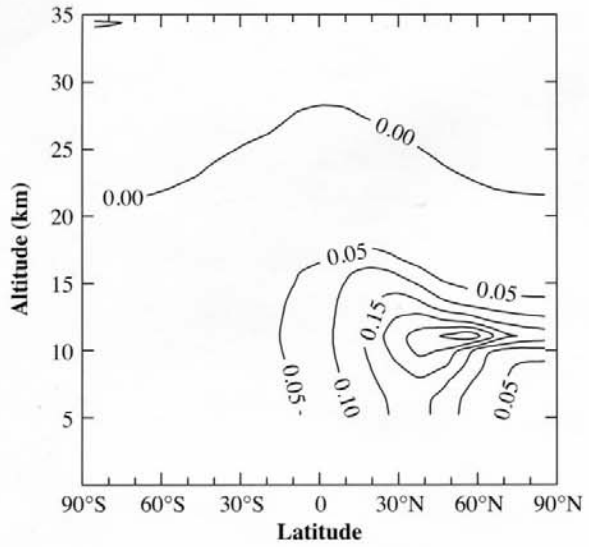

Figure 3-9: Latitude and altitude distribution of annually averaged increase of surface area density of sulfate aerosol (in μm^2 cm^{-3}), calculated with AER 2-D model assuming a 1992 aircraft fuel-use scenario, 0.4 g S/kg fuel, and 5% conversion of sulfur emissions into new particles with a radius of 5 nm (adapted from Weisenstein *et al.*, 1997).

of computed tracer concentrations from all models and the effective EIs of soot and sulfate mass and assume a mean particle size of 10(20) nm for sulfate (soot) particles and a 5% conversion of sulfur to sulfate aerosol. The results represent order-of-magnitude estimates of zonal mean maximum values at 12 km and can be compared with background aerosol properties in the lowermost stratosphere as given in Table 3-1. For these estimates, 5% of the emitted sulfur dioxide is assumed to be converted to sulfuric acid before dispersal out of the zonal region of maximum air traffic.

Tracer simulations strongly suggest that aircraft emissions are not the source of observed decadal H_2O changes at 40°N. The simulation results can be scaled by EI(H_2O) to provide an upper bound (neglecting precipitation from the upper troposphere) for the accumulation of water vapor above the tropopause as a result of aircraft emissions. The LLNL model shows the largest tracer accumulation at 40°N, with equivalent H_2O values smoothly decreasing from 55 ppbv at 10 km to 12 ppbv at 24 km. These values are small in comparison to current ambient values of 59 ppmv at 10–12 km and 4.2 ppmv at 22–24 km (Oltmans and Hofmann, 1995). Assuming 5% yr^{-1} growth in fuel consumption and EI(H_2O) of 1.23 kg/kg, the change in aircraft-produced H_2O ranges from 3.4 ppbv yr^{-1} at 10 km to 0.8 ppbv yr^{-1} at 24 km. These values represent a change of +0.006% yr^{-1} at 10 km and +0.018% yr^{-1} at 24 km and are more than of 20 times smaller than those found in long-term balloon observations (Oltmans and Hofmann, 1995).

3.3.4.2. Supersonic Aircraft

The impact of a future fleet of supersonic aircraft on sulfate aerosol abundance in the stratosphere has been discussed using measurements and model results (Bekki and Pyle, 1993; Fahey *et al.*, 1995a; Stolarski *et al.*, 1995; Weisenstein *et al.*, 1996, 1998). The results suggest that aerosol surface area density will be substantially greater than nonvolcanic background values in proposed fleet scenarios (Section 3.7 and Chapter 4). The consequences for stratospheric ozone changes depend on the simultaneous emissions of nitrogen oxides and chlorine and aerosol loadings of the atmosphere (Solomon *et al.*, 1997; Weisenstein *et al.*, 1998; see also Chapter 2).

3.3.5. Soot

The primary atmospheric source of soot or black carbon particles is combustion of fossil fuels and biomass burning at the Earth's surface, with total emission values near 12 Tg C yr^{-1} (Liousse *et al.*, 1996). This value exceeds reasonable estimates of the aircraft source of black carbon by several orders of magnitude (Bekki, 1997). For example, aircraft are estimated to have emitted 0.0015 to 0.015 Tg C as soot into the atmosphere in 1992 [with EI(soot) of 0.01 to 0.1 g C/kg fuel] (Friedl, 1997; Rahmes *et al.*, 1998). As in the case of sulfate aerosol, deposition and scavenging of black carbon near surface sources creates large vertical gradients in the lower atmosphere, with soot concentrations falling by 1 to 2 orders of magnitude between the surface and the lower stratosphere (Penner *et al.*, 1992; Cooke and Wilson, 1996; Liousse *et al.*, 1996). A possible meteoritic source of soot in the lower stratosphere has been considered but is not well quantified at present (Chuan and Woods, 1984).

Few direct measurements of soot abundance are available in the upper troposphere and lower stratosphere. The most extensive measurements in these regions are from aircraft impactor measurements (Pueschel *et al.*, 1992, 1997; Blake and Kato, 1995). The accuracy of such measurements depends on knowledge of the impactor for small soot particles. The results (Figure 3-10) are considered to represent a lower limit for soot number and mass because of size-selective sampling and because of scavenging of soot by background aerosol particles. Features of the measurements include a large gradient between the Northern and Southern Hemispheres and large variability with altitude at northern mid-latitudes. The large vertical variability of soot at northern mid-latitudes cannot be explained by the accumulation of aircraft soot emissions. With typical soot mass densities observed to be approximately 1 ng m^{-3}, soot is estimated to represent approximately 0.01% of the stratospheric aerosol mass (Pueschel *et al.*, 1992). In other sampling flights over southern Germany, measurements of absorbing mass (probably soot) at 8–12 km altitude and partly within cirrus clouds showed concentrations above 10 ng m^{-3}, with higher values correlated with local aviation fuel consumption (Ström and Ohlsson, 1998).

Modeling studies of soot distribution in the upper troposphere and lower stratosphere differ on the importance of aircraft

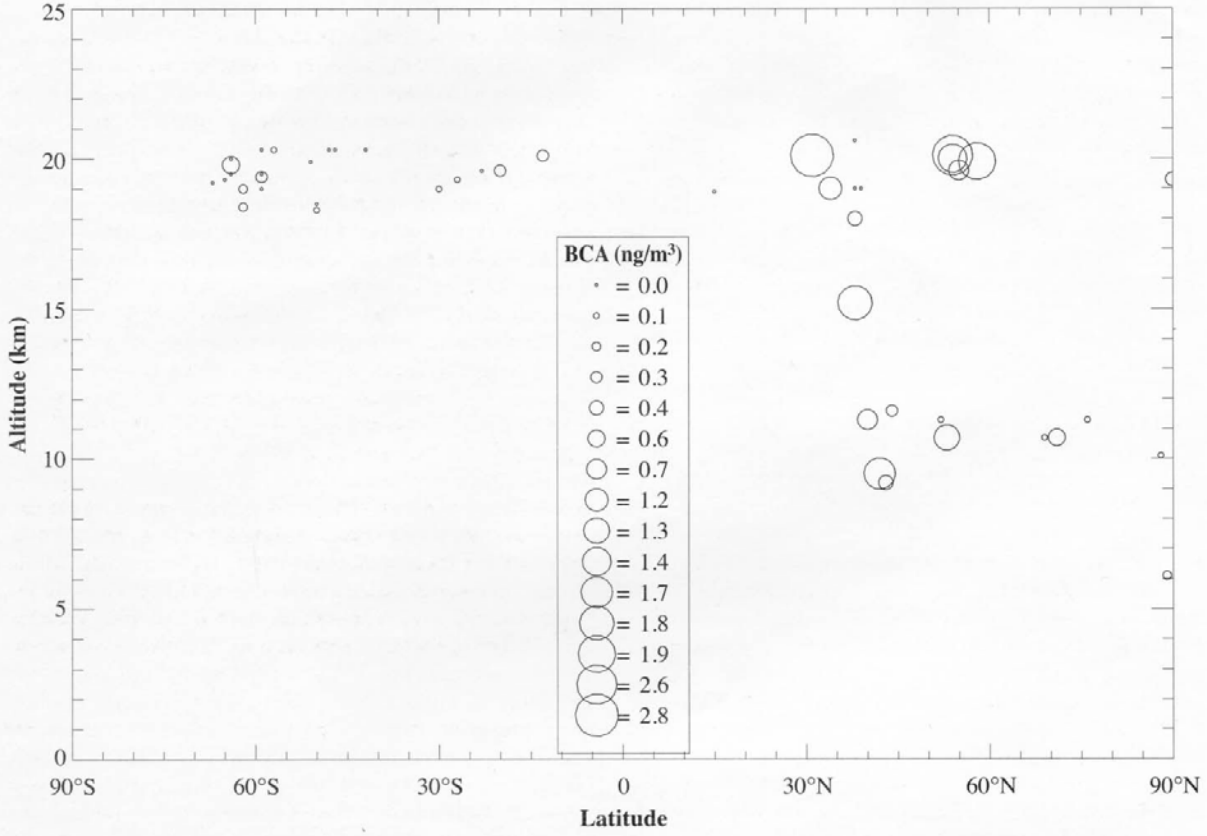

Figure 3-10: Latitude and altitude distribution of measured values of soot concentrations (BCA = black carbon aerosol) in upper troposphere and lower stratosphere (in ng m^{-3}). Measurements were obtained between November 1991 and April 1992 (Northern Hemisphere) and between April and October 1994 (Southern Hemisphere) (adapted from Pueschel *et al.*, 1997).

sources of soot. Some model simulations suggest that ground-level sources of soot (12 Tg C yr^{-1}) are as important as aircraft sources in the upper troposphere and predict maximum soot values there [2 to 5 ng m^{-3} in Liousse *et al.* (1996) and 10 to 50 ng m^{-3} in Cooke and Wilson (1996)] that exceed observed values near 200 hPa at northern mid-latitudes (Pueschel *et al.*, 1997). Other model results show that current aircraft could be a noticeable source of the soot near the tropopause at northern mid-latitudes (Bekki, 1997; Danilin *et al.*, 1998; Rahmes *et al.*, 1998). Tracer simulation results from the AER 2-D model (Section 3.5.1) were multiplied by EI(soot) of 0.04 g/kg fuel (Döpelheuer, 1997) to estimate the global distribution of soot. The results (Figure 3-11) show maximum values of 0.6 ng m^{-3} near 12 km at northern mid-latitudes. These values are in the middle of the range of other model results and are in the range of observed values (Figure 3-10). However, because the fleet-mean EI(soot) is uncertain and may range from 0.01 to 0.1 g/kg fuel, the effective range of the maximum in Figure 3-11 is 0.15 to 1.5 ng m^{-3}. At 20 km, fuel tracer simulations show aircraft-induced zonal mean soot perturbations to be approximately 100 times smaller than maximum observed values (Figure 3-10).

Observations of soot in the upper troposphere and lower stratosphere are too limited to provide an estimate of any long-term changes in soot concentrations in those regions. The possible consequences of heterogeneous reactions on soot (Bekki, 1997; Lary *et al.*, 1997) are discussed in Chapter 2.

3.3.6. Polar Stratospheric Clouds and Aircraft Emissions

During winter in the polar regions, low temperatures lead to the formation of polar stratospheric cloud (PSC) particles, which contain H_2SO_4, HNO_3, and H_2O (e.g., WMO, 1995; Carslaw *et al.*, 1997; Peter, 1997). PSCs activate chlorine, leading to significant seasonal ozone losses in the lower stratosphere, particularly in the Southern Hemisphere (WMO, 1995). PSC formation may be enhanced by the atmospheric accumulation of aircraft emissions of NO_x, H_2O, and sulfate, as well as through direct formation in aircraft plumes in polar regions (Section 3.2 and Chapter 4). If aircraft emissions change the frequency, abundance, or composition of PSCs, the associated ozone loss may also be modified (Peter *et al.*, 1991; Arnold *et al.*, 1992; Considine *et al.*, 1994; Tie *et al.*, 1996; Del Negro *et al.*, 1997). The effects of subsonic aircraft emissions on PSCs and stratospheric ozone are expected to be smaller than those of similar emissions from supersonic aircraft because subsonic

emissions occur in the 10- to 12-km region, whereas supersonic emissions will most likely occur in the 15- to 20-km region. Ambient temperatures in the 10- to 12-km region are usually too high (> 200 K) for PSCs to form with available H_2O and HNO_3, and ozone and total inorganic chlorine concentrations are much lower than near 20 km.

The impact of the subsonic fleet on PSC formation has not been well studied. The results of the fuel tracer simulation discussed in Section 3.3.4 can be used to estimate the increase of PSC SAD as a result of aircraft emissions of H_2O and NO_x. Assuming an EI(H_2O) of 1,230 g/kg, EI(NO_x) of 15 g/kg, complete conversion of NO_x to HNO_3, and formation of NAT particles at threshold temperatures, AER model results for a 1992 subsonic fleet show an additional condensation of HNO_3 on NAT particles ranging from 0.02 ppbv at 60°N to 0.12 ppbv at 85°N at 20 km in January. These values provide an increase of 0.08 μm^2 cm^{-3} in PSC SAD at 20 km and 85°N, assuming a unimodal distribution of PSC particles with diameter of 1 μm. The increase in spatial extent of PSCs both vertically and latitudinally is small in the model. PSC increases are very sensitive to background temperature, H_2O, and HNO_3 values and will differ considerably among models. The increases are not likely to significantly alter ozone changes in polar winter because the SAD increases are much less than typical values of 1–10 μm^2 cm^{-3} calculated for PSC events, and satellite data observations show that the probability of PSC formation below 14 km in the Arctic is generally very low (< 1%) (Poole and Pitts, 1994).

An important caveat related to the assessment of additional PSC formation as a result of aircraft emissions is that plume processes are not included. Global models generally assume that aircraft emissions are homogeneously distributed in a model grid box that is much larger than an aircraft plume. The consequences of this assumption have not yet been fully evaluated. In one model study, reactions on PSCs did not affect ozone chemistry in a subsonic plume at northern mid-latitudes in April (Danilin *et al.*, 1994). A further caveat is that estimated PSC changes from aircraft emissions have not accounted for projected cooling of the stratosphere, which may enhance PSC formation.

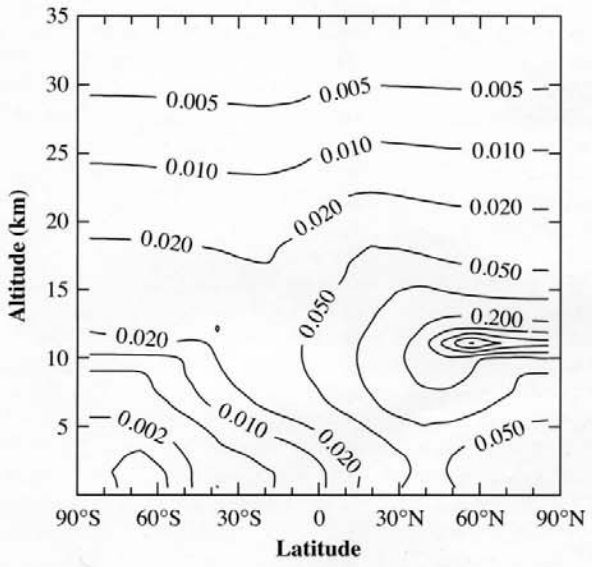

Figure 3-11: Latitude and altitude distribution of annually averaged increase in soot mass density calculated with the AER 2-D model, assuming a 1992 aircraft fuel-use scenario and a soot emission index of 0.04 g C/kg fuel. Contour values are in ng m^{-3} (adapted from Weisenstein *et al.*, 1997).

The chemical implications of increased PSC formation for ozone chemistry and atmospheric composition are further discussed in Chapter 2. The effects of future aircraft fleets on additional PSC formation and subsequent ozone response are presented in Chapter 4.

3.4. Contrail Occurrence and Persistence and Impact of Aircraft Exhaust on Cirrus

Aircraft cause visible changes in the atmosphere by forming contrails that represent artificially induced cirrus clouds. The conditions under which contrails form are discussed in Section 3.2.4. This section describes the formation, occurrence, and properties of persistent contrails and how they compare with natural cirrus.

3.4.1. Cirrus and Contrails

Cirrus clouds (Liou, 1986; Pruppacher and Klett, 1997) contain mainly ice crystals (Weickmann, 1945). The distinctive properties of cirrus and contrails derive from the physics of ice formation. Ice particle nucleation occurs either through homogeneous nucleation (when pure water droplets or liquid aerosol particles freeze) or through heterogeneous nucleation, when freezing of the liquid is triggered by a solid particle or surface that is in contact with the liquid or suspended within the liquid. Both processes depend strongly on temperature and relative humidity (Heymsfield and Miloshevich, 1995; see Section 3.2.4.2).

Comparisons of model simulations with observations suggest that we may understand homogeneous nucleation (Ström *et al.*, 1997; Jensen *et al.*, 1998b) and are making headway in understanding the potential contribution of heterogeneous nucleation (DeMott *et al.*, 1998; Rogers *et al.*, 1998). Each of these freezing mechanisms requires that the atmosphere be highly supersaturated with respect to the vapor pressure of ice before crystals can form. For instance, supersaturations in excess of 40–50% with respect to ice are needed for sulfuric acid particles to freeze homogeneously (Tabazadeh *et al.*, 1997) at temperatures above 200 K. Observations of relative humidity with respect to ice at the leading edges of wave clouds are consistent with the requirement of large ice supersaturations for nucleation of ice on the bulk of the atmospheric aerosol (Heymsfield *et al.*, 1998a; Jensen *et al.*, 1998c). Hence, there is a large supersaturation range in which

heterogeneous nuclei could lead to cirrus formation before the bulk of the atmospheric particles freeze (DeMott *et al.*, 1997). This potential for heterogeneous nuclei to cause ice formation at ice supersaturations that are relatively low compared to those needed to freeze sulfate particles leads to concern about the role of aircraft exhaust in modifying ambient clouds (Jensen and Toon, 1997).

Ice crystal number densities are limited by competition between increasing saturation as a result of cooling in vertical updrafts and decreasing saturation as a result of growth of ice crystals. The depletion of vapor as a result of growth of the first few ice crystals nucleated prevents further ice nucleation on the remaining particles (Jensen and Toon, 1994). Once ice crystals form and take up available water vapor, supersaturation declines and further nucleation of ice ceases. This selectivity causes ice crystals in cirrus to be larger relative to droplets in liquid water-containing clouds—apart from differences in saturation vapor pressures over ice compared to water, which causes more water vapor to be available for deposition on ice particles than on water droplets. Large ice particles may precipitate rapidly. Many cirrus clouds have a "fuzzy" appearance because rapid precipitation causes optically thin edges of clouds to be diffuse, and precipitation allows particles to spread in the wind, forming long tails of cloud. Ice crystal nucleation also depends on available aerosol in the upper troposphere, the properties of which are only poorly known (Ström and Heintzenberg, 1994; Podzimek *et al.*, 1995; Sassen *et al.*, 1995; Schröder and Ström, 1997). In some locations, upper tropospheric particles are dominated by sulfates (Yamato and Ono, 1989; Sheridan *et al.*, 1994). However, more recent data show that minerals, organic compounds, metals, and other substances may often be present in significant quantities (Chen *et al.*, 1998; Talbot *et al.*, 1998).

Cirrus clouds occur mainly in the upper troposphere. The mean tropopause altitude is about 16 km in the tropics and 10 km (250 hPa) north of 45°N latitude (Hoinka, 1998). The tropopause temperature at northern mid-latitudes varies typically between -40 and -65°C; it may reach below -80°C in the tropics. At mid-latitudes, the upper troposphere often is humid enough for cirrus and persistent contrails to form. The stratosphere is commonly so dry that cirrus (PSCs) and persistent contrails form only in polar winter (for $T > -60$°C and $p < 250$ hPa, a 10-ppmv H_2O mixing ratio corresponds to less than 15% relative humidity). Ground-based observers report a mean cirrus cover of 13% over oceans and 23% over land (Warren *et al.*, 1986, 1988). Satellite data (Wang *et al.*, 1996; Wylie and Menzel, 1999) identify larger cloud cover (~40%) by subvisible (optical depth τ at 0.55 μm below ~0.03) and semi-transparent ($0.1 < \tau < 0.6$) cirrus clouds. Cirrus clouds are typically 1.5 (0.1 to 4) km thick; are centered at 9 (4 to 18) km altitude; have a crystal concentration of 30 (10^{-4} to 10^{4}) L^{-1}, with crystal lengths of 250 (1 to 8000) μm (see Dowling and Radke, 1990); and have an optical depth at 0.55 μm of about 0.3 (0.01 to 30) (Wylie and Menzel, 1999). These typical values of cirrus crystal concentration and mean particle size may be biased by early studies that failed to make adequate measurements of ice crystals smaller than about 50 μm. More recent studies suggest that crystal concentrations in cirrus are often on the order of 1 cm^{-3} (Ström *et al.*, 1997; Schröder *et al.*, 1998b), although crystal concentrations in wave clouds can exceed 10 cm^{-3}. PSCs (between the tropopause and ~25-km altitude) and noctilucent clouds (~80-km altitude) contain ice and might therefore be included as very high altitude forms of cirrus clouds. Systems of cirrus clouds have a lifetime that may reach several hours or even days (Ludlam, 1980), but the lifetimes of particles within clouds is much shorter.

Persistent contrail formation requires air that is ice-supersaturated (Brewer, 1946). Ice-supersaturated air is often free of visible clouds (Sassen, 1997) because the supersaturation is too small for ice particle nucleation to occur (Heymsfield *et al.*, 1998b). Supersaturated regions are expected to be quite common in the upper troposphere (Ludlam, 1980). The presence of persistent contrails demonstrates that the upper troposphere contains air that is ice-supersaturated but will not form clouds unless initiated by aircraft exhaust (Jensen *et al.*, 1998a). Aircraft initiate contrail formation by increasing the humidity within their exhaust trails, whereas local atmospheric conditions govern the subsequent evolution of contrail cirrus clouds. Indeed, the ice mass in long-lasting contrails originates almost completely from ambient water vapor (Knollenberg, 1972).

Ice-supersaturated air masses are often formed when ice-saturated air masses are lifted by ambient air motions. While the air lifted, it may remain cloud-free until it is cooled adiabatically to near-liquid saturation (Ludlam, 1980). Other evidence for large supersaturation occurring in the upper troposphere is provided by cirrus fallstreaks that grow while falling through supersaturated air layers (Ludlam, 1980) and by a few localized humidity measurements (Brewer, 1946; Murphy *et al.*, 1990; Ovarlez *et al.*, 1997; Heymsfield *et al.*, 1998b). Recent humidity measurements by commercial aircraft show that—in flights between Europe, North and South America, Africa, and Asia—14% of flight time was in air masses that were ice-supersaturated with a mean value of 15% (Helten *et al.*, 1998; Gierens *et al.*, 1999).

3.4.2 Cirrus and Contrail Models

Small-scale, regional, and global models have been used to study cirrus clouds and contrails. Small-scale models simulate the details of cloud formation in a single parcel of air along some defined trajectory (e.g., Jensen *et al.*, 1994b). High-resolution 2-D models have simulated the dynamics and microphysics of cirrus (Starr and Cox, 1985) and contrails (Gierens, 1996; Chlond, 1998). Regional and global models describe the large-scale dynamics of clouds with simpler representations of microphysical cloud processes (Sundqvist, 1993; Lohmann and Roeckner, 1995; Fowler *et al.*, 1996; Westphal *et al.*, 1996). Regional-scale (typically 10-km horizontal grid-scale) and global-scale models are not able to resolve the vertical motions and small-scale temperature and humidity fluctuations (Gierens *et al.*, 1997) that drive supersaturations involved in

cirrus nucleation. However, global models with prescribed or parameterized contrail cover have been useful for understanding the radiative impact of a change in cloud cover as a result of aircraft emissions (Ponater *et al.*, 1996).

3.4.3. Contrail Occurrence

At plume ages between 1 min and 1 h, contrails grow much faster horizontally (to several km width) than vertically (200 to

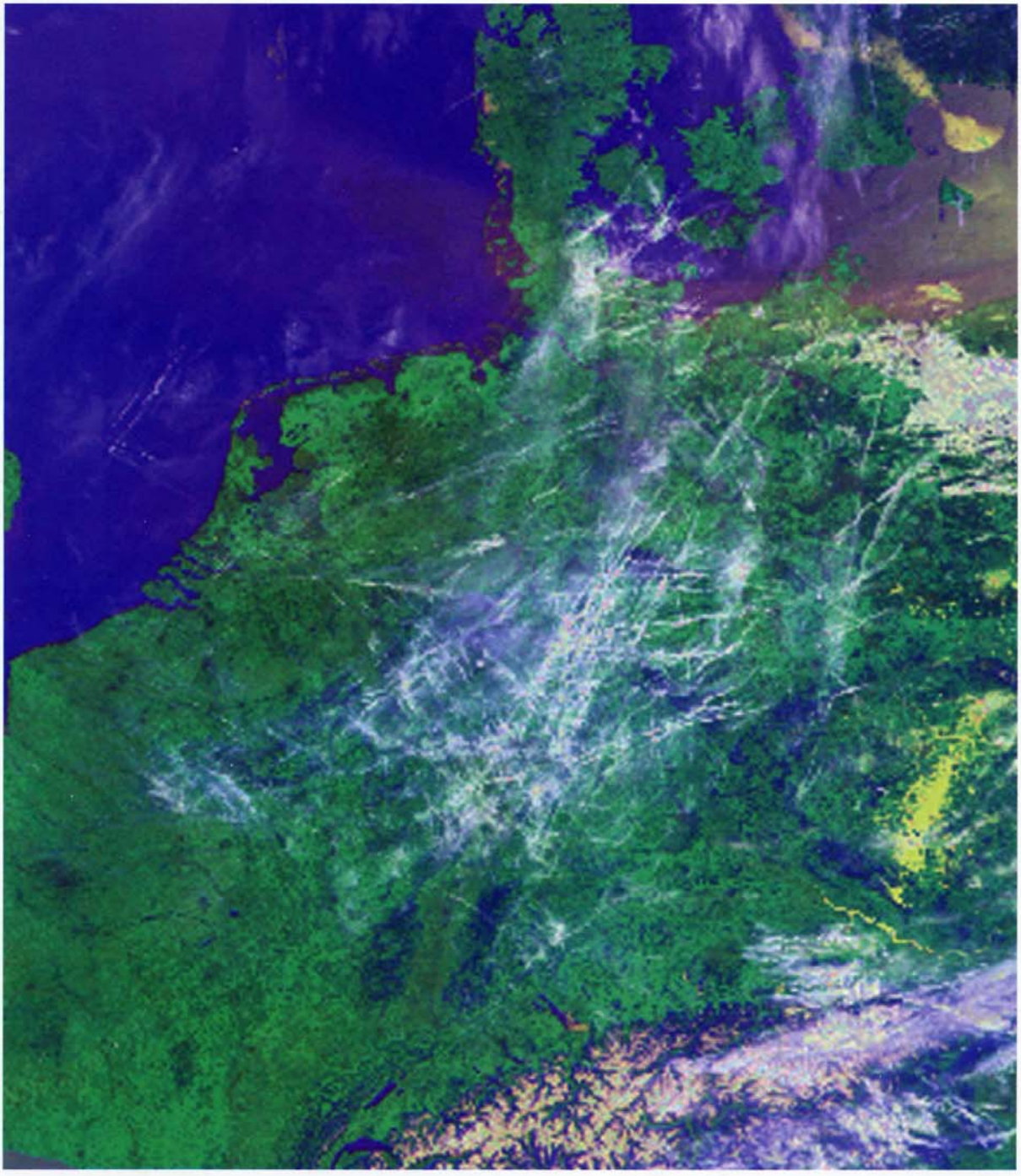

Figure 3-12: Contrails over central Europe on 0943 UTC 4 May 1995, based on NOAA-12 AVHRR satellite data (from Mannstein, 1997).

400 m), especially in highly sheared environments (Freudenthaler *et al.*, 1995, 1996; Sassen, 1997). Young contrails spread as a result of turbulence created by aircraft vortices (Lewellen and Lewellen, 1996; Gerz *et al.*, 1998; Jensen *et al.*, 1998a,b,c), shear in the ambient wind field (Freudenthaler *et al.*, 1995; Schumann *et al.*, 1995; Dürbeck and Gerz, 1996; Gierens, 1996), and possibly radiatively driven mixing (Jensen *et al.*, 1998d).

Contrails often become wide and thick enough to induce radiative disturbances that are sufficient to be detectable in multispectral satellite observations. They have been observed at 1-km spatial resolution with instruments such as the Advanced Very High Resolution Radiometer (AVHRR) on board National Oceanic and Atmospheric Administration (NOAA) polar-orbiting satellites (e.g., Lee, 1989) and at 4-km resolution in the infrared with the Geostationary Operational Environmental Satellite (GOES) (Minnis *et al.*, 1998a). The AVHRR channels in the 11- to 12-μm range (4 and 5) are particularly suited to detect thin ice clouds because of the different emissivity of ice particles in this spectral range (King *et al.*, 1992; Minnis *et al.*, 1998c). Figure 3-12 shows, for example, a mid-European scene derived from AVHRR data in these channels, combined with the visible channel to represent the surface, for a day when many line-shaped contrails were formed by heavy air traffic (Mannstein, 1997). The figure shows that aircraft trigger contrail cirrus that evolves into cirrus clouds that are much more extensive in scale than the initial contrails. Such spread and deformed contrail cirrus can no longer be distinguished from naturally occurring cirrus. In Figure 3-12, contrails that still have a line-shaped appearance cover about 5% of the scene.

Aged contrails often cannot be distinguished from cirrus, which poses an observational problem in determining the frequency and area of coverage by contrails. An important example of the persistence of contrails and their evolution into more extensive cirrus is shown in Figure 3-13. An initial oval contrail observed in GOES-8 satellite images diffused as it was advected over California until it no longer resembled its initial shape 3 h later (Minnis *et al.*, 1998a). The exhaust from this single aircraft flying for less than 1 h in a moist atmosphere caused a cirrus cloud that eventually covered up to 4,000 km^2 and lasted for more than 6 h. Other contrails and contrail clusters were observed to develop over periods of 7 to 17 h, spreading to cover areas of 12,000 to 35,000 km^2. Such dispersed contrails are usually indistinguishable from natural cirrus; hence, satellite detection algorithms based on the linear structures of young contrails will not detect these dispersed contrails.

At present, observations of actual frequency or areal coverage of Earth by contrails are limited to a few selected regions.

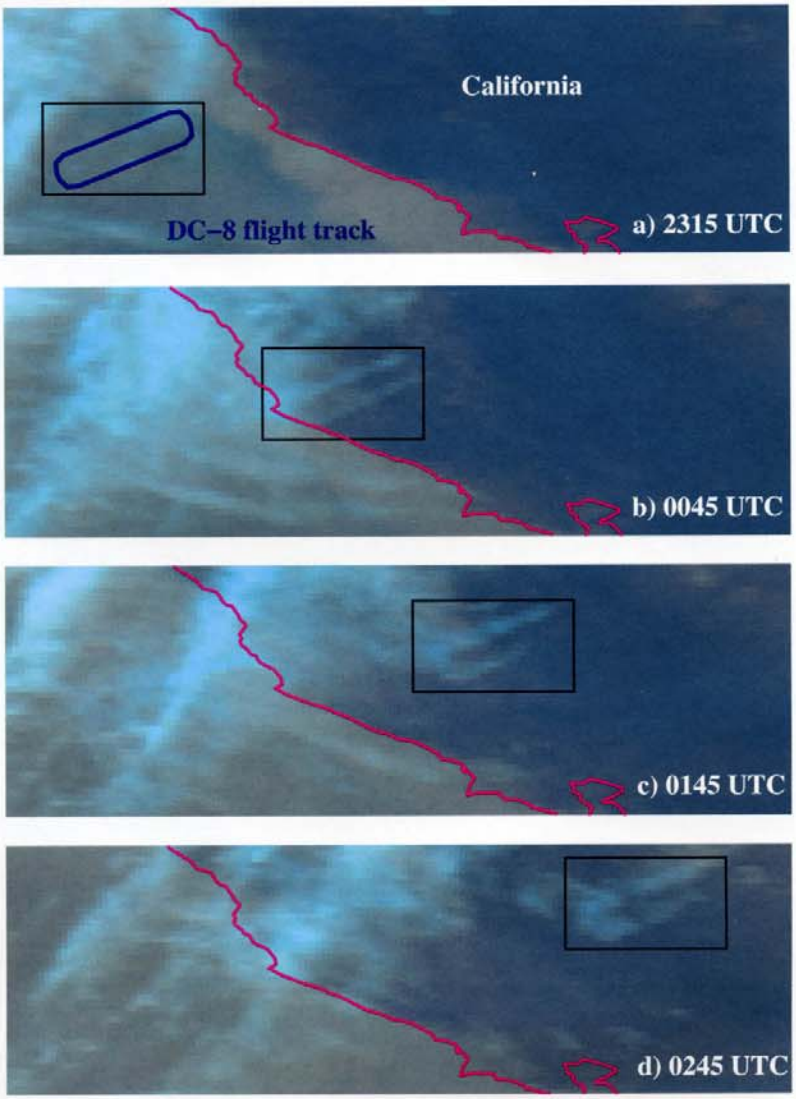

Figure 3-13: Time series of GOES-8 satellite images showing the evolution of a contrail from an initial oval shape to extensive cirrus clouds (from Minnis *et al.*, 1998a). The NASA DC-8 flew an oval flight pattern several times off the coast of California on 12 May 1996 (a), resulting in a visible contrail 15 minutes later (b). This contrail spread as it was advected over California (c), until it no longer resembled its initial shape 3 hours later (d). Satellite photographs courtesy of L. Nguyen of AS&M, Inc., Hampton, VA, USA.

Contrail frequency refers to the probability that a contrail will be observed somewhere within the scene being viewed; area of coverage refers to the fraction of the area of the scene in which contrails are observed. Estimates of contrail coverage or occurrence have been made directly or indirectly from surface (Detwiler and Pratt, 1984; Minnis *et al.*, 1997) and satellite observations (Joseph *et al.*, 1975; Carleton and Lamb, 1986; Lee, 1989; DeGrand *et al.*, 1990; Schumann and Wendling, 1990; Betancor-Gothe and Grassl, 1993; Bakan *et al.*, 1994; Mannstein *et al.*, 1999).

Data for the frequency of contrails are available from surface-based observations at 19 locations across the continental United States of America for every hour during 1993–94 (Minnis *et al.*, 1997). The data indicate that contrail frequency peaks around February/March and is at a minimum during July. Annual mean persistent contrail frequency (not the cover) for the 19 sites was 12%. When related to fuel use and extended to the remainder of the country, mean annual contrail frequency for the United States of America is estimated at 9% (Minnis *et al.*, 1997). The relationship between fuel consumption and contrail frequency from this data set is shown in Figure 3-14. The correlation implies that contrail coverage is limited mainly by the number of aircraft flights, not by atmospheric conditions at cruise altitudes. Pilots flying over the former Soviet Union have reported that contrails occur most frequently in winter and spring and less often during summer (Mazin, 1996). Sky photographs taken from 1986 to 1996 over Salt Lake City, Utah, reveal a seasonal cycle in contrail frequency, with a maximum in fall and winter and a minimum in July (Sassen, 1997). These data are similar to observations from a site 64 km north (Minnis *et al.*, 1997) of Salt Lake City. Sassen (1997) and Minnis *et al.* (1997) found that contrails occur with cirrus in approximately 80% of observations. The coincidence of cirrus and contrails suggests that cloud-free supersaturated regions are usually interspersed with areas in which natural clouds have actually formed.

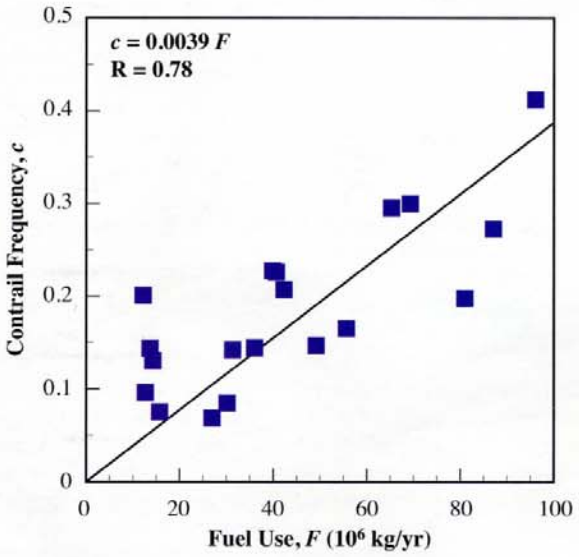

Figure 3-14: Correlation of mean annual contrail frequency and estimated May 1990 aircraft fuel usage above 7-km altitude. Contrail frequencies are based on 1993 to 1994 hourly surface observations from 19 stations in the United States of America (Minnis *et al.*, 1997). The fit to the data (solid line) is shown. R is the correlation coefficient.

From an analysis of AVHRR infrared images taken over the northeast Atlantic and Europe, a mean contrail cover of 0.5% was derived for 1979–81 and 1989–92 (Bakan *et al.*, 1994). A distinct seasonal cycle was found, with a southward displacement of the maximum cover during winter. Maximum coverage (~2%) occurred during summer, centered along the North Atlantic air routes. Using AVHRR channel 4 and 5 differences and a pattern-recognition algorithm to differentiate line-shaped clouds from fuzzy cirrus clouds, the contrail cover—defined as line-shaped clouds over mid-Europe—was systematically evaluated for all of 1996 using nearly all noon passages of the NOAA-14 satellite (see Figure 3-15) (Mannstein *et al.*, 1999). Contrails are not uniformly distributed; instead, they lie along air traffic corridors and accumulate near upper air route crossings. As with observations over the United States and the former Soviet Union, maximum coverage occurred during winter and spring. At noon on average over the year, line-shaped contrails cover about 0.5% of the area of the mid-European region shown in this figure. This coverage represents the lower bound for the actual contrail cover because the algorithm cannot identify non-line-shaped contrails. Contrail coverage at night over Europe is one-third of the noon-time contrail cover (Mannstein *et al.*, 1999).

Contrails often occur in clusters within regions that are cold and humid enough to allow persistent contrails to form. Contrail clusters observed in satellite data indicate that these air masses cover 10 to 20% of the area over mid-Europe (Mannstein *et al.*, 1999) and parts of the United States of America (Carleton and Lamb, 1986; Travis and Changnon, 1997), consistent with the fraction of air masses expected to be ice-supersaturated at cruise altitudes. Hence, as air traffic increases in these regions, persistent contrail coverage is also expected to increase, possibly up to a limit of 10–20%.

Estimates of global coverage by air masses that are sufficiently cold and humid for persistent contrails can be obtained using meteorological analysis data of temperature and humidity, a model to estimate the frequency of ice-saturation in each grid cell as a function of the analyzed relative humidity, and the Schmidt-Appleman criterion (depending on η; see Section 3.2.4.1) for contrail formation conditions. Using 11 years of meteorological data from the European Center for Medium Range Weather Forecast (ECMWF), the cover of suitable air masses is found to be largest in the upper troposphere, especially in the tropics (global mean value of 16%) (Sausen *et al.*, 1998). This coverage is similar in size to the area covered by clusters of contrails in satellite data and the frequency of ice-supersaturated air masses observed along commercial aircraft routes (Gierens *et al.*, 1999). The expected contrail cover is then computed from the product of the air mass coverage and the fuel consumption

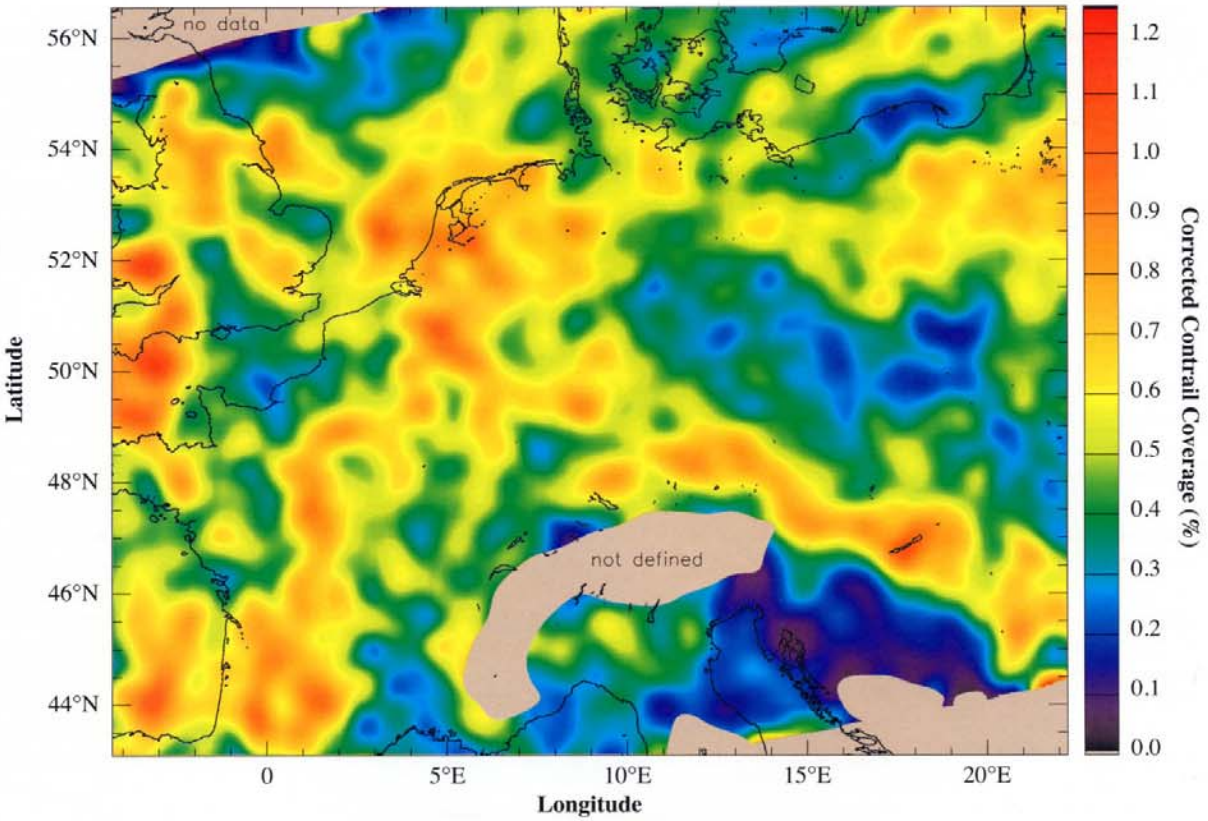

Figure 3-15: Annual mean corrected contrail coverage at noon over mid-Europe in 1996, as derived from AVHRR data from the NOAA-14 satellite (from Mannstein *et al.*, 1999).

rate in the same region, with the latter chosen as one of several possible measures of air traffic. The product is scaled to give a 0.5% mean contrail cover in the European/Atlantic region (30°W to 30°E, 35 to 75°N) as considered by Bakan *et al.* (1994). The resulting contrail cover (see Figure 3-16) for 1992 fuel emissions and $\eta = 0.3$ is 0.087% (about 0.1%) in the global mean, with a local maximum of 5% over the eastern United States of America. The computed contrail coverage over southeastern Asia is only slightly smaller than that over Europe and North America. Although air traffic is much less extensive over southeastern Asia, this high contrail coverage may result because this region more often has ice-supersaturated air. However, the predicted contrail coverage over North America and southeastern Asia has not yet been verified by observations. Predicted regional differences are sensitive to the representation of the number of aircraft in operation. For example, in some regions, a large fuel consumption density is caused by a few large aircraft (Gierens *et al.*, 1998). Studies have not been performed to evaluate the accuracy of humidity values provided by meteorological data. The results depend linearly on scaling by the cover observed in the reference region, as provided here by Bakan *et al.* (1994). Other data imply global cover values between 0.02 and 0.1% (Gierens *et al.*, 1998). A value larger than 0.1% (possibly 0.2%) cannot be excluded because the analysis uses only thermodynamic contrail formation conditions and the scaling is based solely on observed line-shaped contrail cover.

3.4.4. Contrail Properties

The relatively small particles present in newly formed contrails serve to distinguish contrail radiative properties from those of most natural cirrus (Grassl, 1970; Ackerman *et al.*, 1998; see also Section 3.6). Measurements of contrail particles with impactors and optical probes (see also Section 3.2.4 and Table 3-1) reveal a wide variety of size, shape, and spectral size distributions. The results depend on plume age, ambient humidity, ambient aerosol, and other parameters. At a plume age of 30 to 70 s, ice particles have been found to form a single-mode log-normal size distribution with a volume-equivalent radius in the range of 0.02 to 10 μm, a mean radius of about 2 μm, and maximum dimension of 22 μm. Particle shapes are mainly hexagonal plates, along with columns and triangles. The axial ratios of the columns were found to be less than 2, and the shapes of the crystals were already established for particles of about 1-μm radius (Goodman *et al.*, 1998). Contrail particle sizes increase with time in humid air. Ice particles observed in 2-min-old contrails typically have radii of 2 to 5 μm with shapes that are almost spherical, indicating frozen solution droplets (Schröder

et al., 1998b). On the other hand, some contrail particles strongly polarize light, indicating non-spherical shapes (Freudenthaler *et al.*, 1996; Sassen, 1997). After 10 min to 1 h, contrail particle size distributions may range from 32 to 100 μm or even 75 μm to 2 mm (Knollenberg, 1972; Strauss *et al.*, 1997).

Particle properties within a contrail core differ from those at the edges of the contrail. In the center of contrails, insufficient water vapor is available to allow the large number of ice particles to grow to large crystals. At the edges, ice supersaturation is greater, thereby sometimes allowing ice crystals to form up to 300 μm in diameter (Heymsfield *et al.*, 1998a). The larger particles have various shapes, with the largest being bullet rosettes (Lawson *et al.*, 1998). Such large particles are within the natural variability of cirrus particle sizes. As a consequence, old dispersed contrails appear to have particle sizes similar to those in surrounding cirrus (Duda *et al.*, 1998; Minnis *et al.*, 1998a).

Aircraft create a large number of new ice crystals that grow from ambient water vapor. As a contrail spreads, some evidence suggests that ice crystals are neither lost nor created in significant numbers. In one remote-sensing study, the total number of particles (about 2.6 x 10^9 ice crystals per cm of contrail length) in a contrail was found to remain constant as the contrail dispersed and the particle concentration (particles per unit volume) dropped (Spinhirne *et al.*, 1998). *In situ* measurements (Schröder *et al.*, 1998b) reveal 10^8 to 10^9 particles larger than 4.5-μm diameter formed per cm of contrail length. In contrast, changes in particle number will occur when some particles eventually sediment out of the contrail and new particles are nucleated as a result of air motions induced by the contrail. The ice water content of new contrails increases with time to exceed the amount of water emitted by the aircraft by more than two orders of magnitude. However, the water content per unit volume remained approximately constant in the case observed by Spinhirne *et al.* (1998). The optical depth of contrails remains nearly constant during the first hour despite horizontal spreading (Jäger *et al.*, 1998).

3.4.5. Impact of Aircraft Exhaust on Cirrus Clouds and Related Properties

Aircraft may perturb natural cirrus through the addition of water vapor, soot, and sulfate particles and by inducing vertical motions and turbulent mixing (Gierens and Ström, 1998). Observations of cirrus coverage in certain regions have found perturbations from anthropogenic aerosol (Ström *et al.*, 1997). Persistent contrails are often associated with or embedded in natural cirrus (Minnis *et al.*, 1997; Sassen, 1997). Such in-cloud contrails may be formed slightly above the Schmidt-Appleman temperature threshold because ambient ice particles that enter the engine inlet increase the humidity in the exhaust plume (Jensen *et al.*, 1998a; Kärcher *et al.*, 1998a). Some evidence associates in-cloud contrails with regions of enhanced absorbing

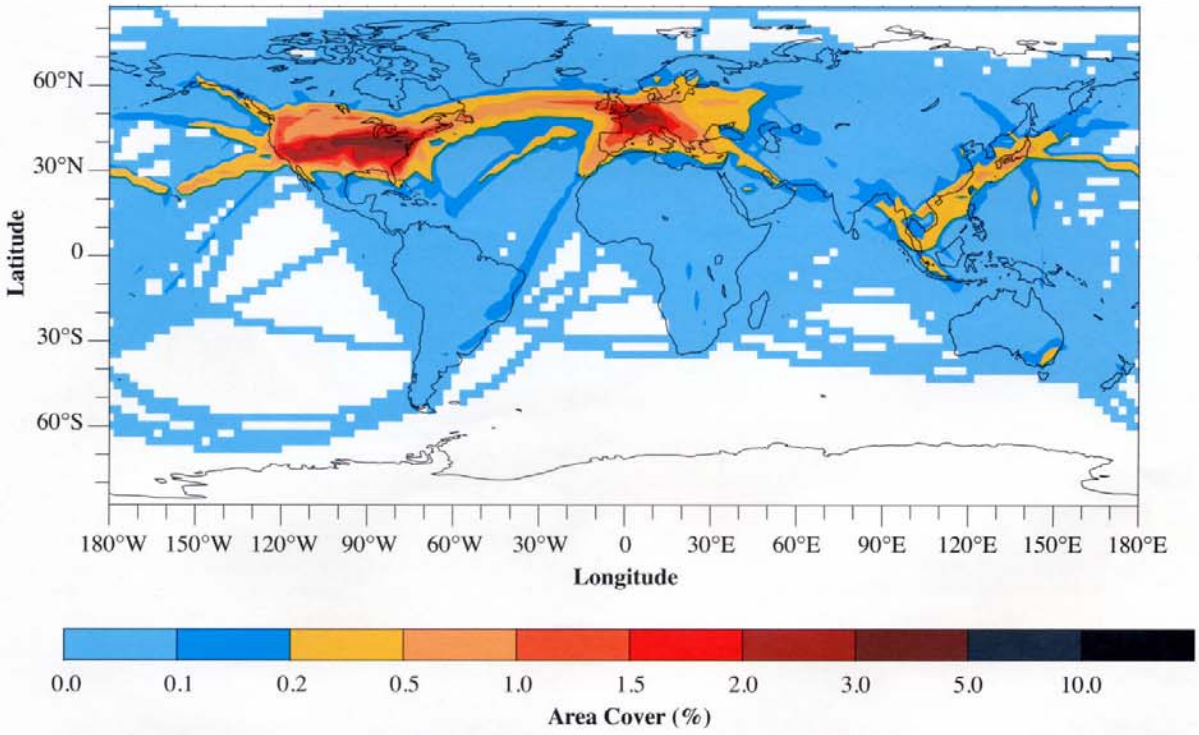

Figure 3-16: Persistent contrail coverage (in % area cover) for the 1992 aviation fleet, assuming linear dependence on fuel consumption and overall efficiency of propulsion η of 0.3. The global mean cover is 0.1% (from Sausen *et al.*, 1998).

material and enhanced ice crystal number densities (Ström and Ohlsson, 1998). The presence of HNO_3 may increase the hygroscopic growth of supercooled cloud droplets (Laaksonen *et al.*, 1997), and HNO_3 dissolved in sulfate solution droplets may change their freezing behavior. The importance of such perturbations has not been quantified.

Soot particles originating from aircraft exhaust may act as freezing nuclei. In an atmosphere with few freezing nuclei, this perturbation could lead to an expansion of cirrus cover, a change in average particle size, and related changes in cloud surface area and optical depth (Jensen and Toon, 1997)—hence have consequences for radiative forcing (see Section 3.6.5). For aircraft to alter cirrus properties, exhaust particles would need to be more efficient or more abundant than ice nuclei currently existing in the atmosphere. If the predominant particle that freezes to form ice contains sulfate, aircraft soot could serve as important ice nuclei because sulfate particles require a relatively high supersaturation before freezing occurs. Over the central United States of America, however, as many as 0.1 to 0.2 cm^{-3} freezing nuclei (effective at -35°C) have been found in the upper troposphere (DeMott *et al.*, 1998), indicating that the number of freezing nuclei is not always small. Some observations show that aircraft exhaust does not contain large numbers of ice nuclei active at temperatures above -35°C (Rogers *et al.*, 1998). Soot and metals were found to be significant, but not dominant, components of ice nuclei in contrails (Chen *et al.*, 1998; Petzold *et al.*, 1998; Twohy and Gandrud, 1998).

Aircraft measurements in and near clouds have indicated the presence of light-absorbing material contained inside ice crystals. The distribution pattern and the amount of measured absorbers suggest that the material is related to aircraft soot (Ström and Ohlsson, 1998) (Figure 3-17). For the same abundance of aerosol particles, clouds perturbed by absorbing material contained 1.6 to 2.8 times more ice crystals than unperturbed portions of clouds. These observations suggest that aircraft-produced particles enhance cloud ice particle concentrations, although they have not revealed the physical mechanism involved. Specifically, exhaust soot particles may have been involved in ice crystal formation within the cirrus or formed contrail ice particles within the exhaust plume before being incorporated into the cloud. These observations are roughly consistent with calculations of a cirrus cloud forming in a region of recent exhaust trails (Jensen and Toon, 1997).

Cirrus clouds may also be perturbed by enhanced sulfate aerosol. Small sulfate particles (e.g., 10-nm radius) are unlikely to be ice nuclei or cloud condensation nuclei. Larger particles would be more efficient. Such large particles may originate as ambient sulfate particles enlarged by growth from sulfur gases emitted by aircraft or by processing of liquid exhaust particles in short-lived contrails (see Section 3.2). Because ice nucleation processes tend to be self-limiting (Jensen and Toon, 1994), cirrus cloud properties would change only slightly if the number of sulfate particles increased while the size distribution and composition of ambient sulfate particles remained constant. On the other hand, large sulfate particles—such as those induced by the Mt. Pinatubo volcanic cloud—could lead to a significant increase in the number of ice crystals, optical depth, and radiative forcing of cirrus clouds (Jensen and Toon, 1992). Cloud modifications would require a large increase in the number of larger sulfate particles; such modifications would occur primarily in cirrus that were very cold (T < -50°C) and weakly forced by slow updrafts. Lidar observations of a cirrus cloud embedded in aerosol from the Mt. Pinatubo eruption show significantly higher than normal ice crystal concentrations (Sassen, 1992; Sassen *et al.*, 1995). Satellite data analyzed after the Mt. Pinatubo eruption suggest that the volcanic aerosol reduced the occurrence of cirrus clouds with high extinction coefficients, increased the occurrence of clouds with low extinction coefficients, and increased extinction in optically

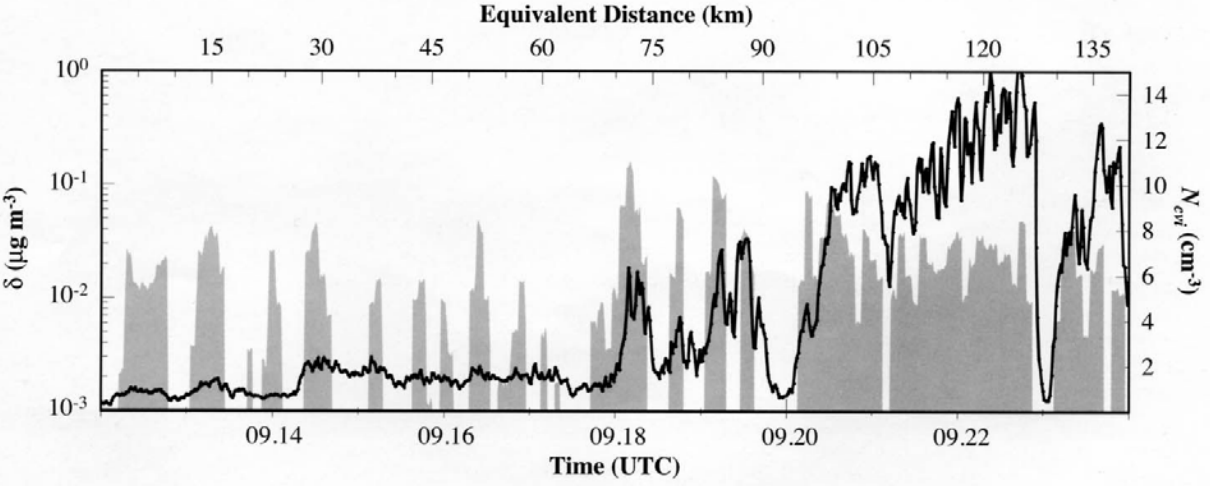

Figure 3-17: Time series of ice crystal concentration (N_{cvi}, thick line) and concentration of light-absorbing material contained in ice crystals (δ, shaded area) for a flight through a cirrus layer in a region with heavy air traffic (adapted from Ström and Ohlsson, 1998).

thick clouds (Minnis *et al.*, 1993; Wang *et al.*, 1995). Hence, some available models and data suggest that aircraft exhaust could play a significant role in modifying the properties of clouds. However, the magnitude and nature of these modifications are not well understood.

Sedimentation of large particles in persistent contrails may remove water vapor from the upper troposphere, possibly reducing radiative heating by water vapor, and cause seeding of lower level clouds (Murcray, 1970; Knollenberg, 1972). Sedimentation of ice crystals, which has been observed occasionally (Konrad and Howard, 1974; Schumann, 1994; Heymsfield *et al.*, 1998a), becomes important only in strongly supersaturated air (Hauf and Alheit, 1997) when large ice crystals form and have the potential to fall through lower-lying saturated air in which they will not evaporate readily. Because no attempts have been made to quantify the precipitation rate from contrails, the significance of this precipitation has not been assessed.

3.5. Long-Term Changes in Observed Cloudiness and Cloud-Related Parameters

Contrails have long been considered possible modifiers of regional climate (Murcray, 1970; Changnon, 1981). Contrails may increase total cloud and cirrus cloud amounts, and consequently change the Earth's radiation balance. As a result, surface and upper tropospheric temperatures may change (Detwiler, 1983; Frankel *et al.*, 1997). In the following sections, we examine changes in cloudiness and other climate parameters for their possible relationship to aircraft operations. Some data indicate changes in observed cirrus cloudiness. These observations are used to provide a first estimate of an upper bound on the increase in contrail-cirrus coverage since the beginning of the jet air traffic era. Limitations in attributing observed trends to aircraft are discussed in Section 3.5.3.

3.5.1. Changes in the Occurrence and Cover of Cirrus Clouds

3.5.1.1. Surface Observations

Although most studies reporting trends in cloud cover have considered total cloud cover (Henderson-Sellers, 1989, 1992; Angell, 1990; Plantico *et al.*, 1990; Karl *et al.*, 1993), we focus here on studies reporting trends in cirrus cloud cover, which is more relevant to the issue of aviation effects on cloudiness. Observations at Hohenpeissenberg, Germany, indicate that the frequency of high clouds during sunny hours increased from 45% in 1954 to 70% in 1995 (Vandersee, 1997; Winkler *et al.*, 1997). Such large changes are not atypical of regional cloud climatologies (e.g., Rebetez and Beniston, 1998). Over the same period, global radiation during sunshine hours decreased by about 10%, indicating that the observed cloud trend is not an artifact. Similarly, cirrus frequency increased between 1964 and 1990 under cloudy-with-sun conditions by 27% over Hamburg and 15% over Hohenpeissenberg (in northern and southern Germany, respectively) (Liepert *et al.*, 1994; Liepert, 1997). These changes are not directly attributable to aircraft, however; instead, they might be caused by an increase in tropopause altitude or higher relative humidity in the upper troposphere (Winkler *et al.*, 1997). Cirrus cover over Salt Lake City and Denver has increased from about 12% annual mean cover to 20% in the period from the early 1960s (i.e., since the beginning of the jet aircraft era) to the 1980s, possibly because of increased air traffic over those cities. These trends are significantly lower in the 1990s, and similar observations over Chicago and San Francisco show no obvious trends (Liou *et al.*, 1990; Frankel *et al.*, 1997).

Global trends of observed total and cirrus cover can be deduced from ground-based cloud observations over land and ocean (Warren *et al.*, 1986, 1988; Hahn *et al.*, 1994, 1996) for 1971–91. For the period 1982–91, mean global trends in cirrus occurrence frequency were 1.7 and 6.2% per decade over land and ocean, respectively (Boucher, 1999). The decadal trend was 5.6% over North America and 13.3% over the heavy air traffic region located in the northeastern United States of America. The computed average change in cirrus occurrence (1987–91 relative to 1982–86) as a function of aviation fuel use at the observation locations is shown in Figure 3-18. The results indicate a statistically significant (97% confidence level) increase in cirrus occurrence in the North Atlantic flight corridor compared with the rest of the North Atlantic Ocean (Boucher, 1998, 1999).

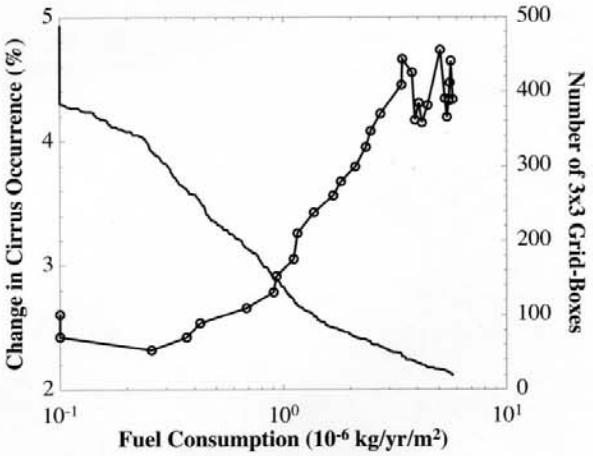

Figure 3-18: Change in cirrus occurrence frequency between 1987–1991 and 1982–1986 (in %) computed from surface observations over the North Atlantic Ocean averaged over grid boxes with fuel consumption above 8 km greater than indicated on the x-axis (open circles). Data are from surface observations of Hahn *et al.* (1996) and are averaged over 3°x3° grid boxes in the region 99°W to 21°E, 0°N to 72°N of the Atlantic Ocean. Only cloud reports satisfying the illuminance criterion defined by Hahn *et al.* (1995) are included in the statistics. The bold line indicates the number of grid boxes used for the average (adapted from Boucher, 1999).

From the same source of observations, cirrus cover was analyzed for the periods 1971–81 and 1982–91 and for a combined data set extending from 1971–92 (Minnis *et al.*, 1998b). Data were averaged for gross air traffic regions (ATRs) and the rest of the globe. ATRs are rectangular areas on the globe that contain most air traffic routes and constitute 26% of the available regions with data. The ATR trends are larger for cirrus clouds than for total cloudiness and are most significant in the first period (1971–81), with the largest annual values found in the United States of America (3%), western Asia (1.6%), and the North Pacific (1.7%). No significant ATR trends were found over Europe. Changes for the rest of the globe were significant only over land but with values less than those over the United States of America and western Asia. Averaged over all ATRs, the cirrus cover increase between 1971 and 1981 amounts to 1.5% per decade, compared with 0.1% for the rest of the globe. From 1982–91, cirrus cover increased over all areas except over non-ATR land and North Atlantic regions, where it changed by -0.4 and 0%, respectively.

The combined 1971–92 cirrus cover data set shows somewhat different results from the two separate data sets. The mean trend for land was 0% per decade for ATRs, compared to -1.1% per decade for other land regions. Over the United States of America, however, the ATR trend is significant at 1.2% per decade. Over oceans, the mean ATR trend is 1.2% per decade and 0.6% per decade over the rest of the oceans. The Pacific ATR trend is strongest, at 1.5% per decade. Averaging of apparent trends from the two separate data sets gives results that differ from the mean trends in the combined data set. However, the relative difference in the mean trends between the ATR regions and the rest of the globe is roughly 1.1% in both cases, indicating that cirrus coverage in areas with significant air traffic is increasing relative to that over the remainder of the globe.

Using ground-based data sets, Figure 3-19 shows the seasonal trends in cirrus coverage over the United States of America and Europe. The average trend of the two separate data sets is compared with the seasonal cycle of contrail occurrence frequency over the United States of America and cover over Europe. Contrail occurrence over the United States of America was derived from 1 year of surface station observations (Minnis *et al.*, 1997); contrail coverage over mid-Europe was computed from satellite data (Mannstein *et al.*, 1999). Over the United States of America, the seasonal trends in cirrus coverage (statistically significant at least at the 75% confidence level) are roughly in phase with the seasonal cycle of contrail occurrence (see Figure 3-19a), suggesting that cirrus changes are related to contrail occurrence. In contrast, the seasonal cycle of cirrus cover trends for Europe does not resemble the seasonal cycle of contrail cover (see Figure 3-19b). The European data, which are not statistically significant, show that the trends observed for the United States of America are not so obvious for other air traffic regions.

3.5.1.2. ISCCP Observations

Data from the International Satellite Cloud Climatology Project (ISCCP, C2) (Rossow and Schiffer, 1991) between 50°S and 70°N from 1984 to 1990 have also been inspected for trends in total and high cloud cover over land and ocean

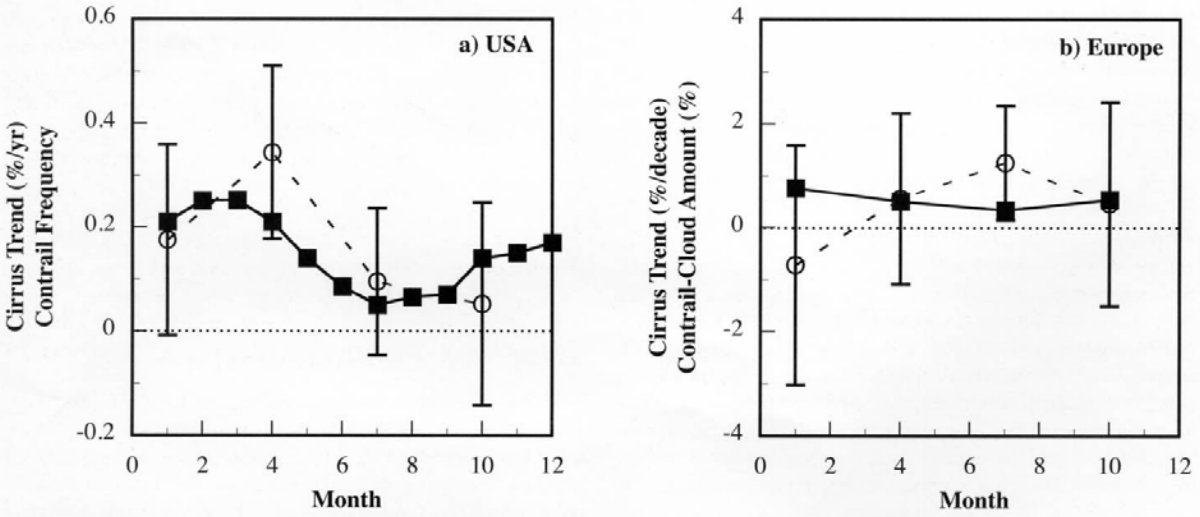

Figure 3-19: Observed monthly variation of contrail occurrence frequency (solid squares) and seasonal trends of cirrus cover (open circles) for (a) the United States of America (%/yr) and (b) Europe (%/decade). Contrail data from the United States of America are based on surface observations of contrail frequencies in 1993–1994 (Minnis *et al.*, 1997). The mid-Europe contrail data are derived from satellite analysis of line-shaped contrail cover for 1996 (Mannstein *et al.*, 1999). Seasonal mean trends of observed fractional cirrus cover in the time period 1971 to 1991 are mean values derived from separate data sets for 1971 to 1982 (Warren *et al.*, 1986) and 1982 to 1991 (Hahn *et al.*, 1996). Error bars indicate the standard error of the computed trends (from Minnis *et al.*, 1998b).

Table 3-5: *Computed trend values and differences of trend values in cirrus/high cloud amounts (% of Earth surface cover per decade) from surface and ISCCP satellite data sets taken between 1971 and 1991 for regions categorized as having a mean value of contrail coverage less than and greater than 0.5% as computed by Sausen et al. (1998) for 1992 aircraft operations (Minnis et al., 1998b). Differences in trends between contrail cover regions are shown as "trend difference" values. The last two rows (Global ISCCP, Global Surface) indicate global (ocean + land) trends in respective data sets. The time periods of the data sets are also indicated. Statistical significance refers to level of confidence in difference between trends for the two regions. An asterisk indicates insufficient resolution for analysis. Dashes indicate a confidence level less than 95%.*

	Period	Trend (% per decade) in Regions with Computed Contrail Cover		Trend Difference (% per decade)	Statistical Significance of Difference (%)
		< 0.5%	> 0.5%		
Ocean from ISCCP	1984–90	4.3	5.9	1.6	—
Land from ISCCP	1984–90	1.2	4.7	3.5	95
Ocean from surface	1971–81	*	*		*
Land from surface	1971–81	-0.21	2.1	2.3	99
Ocean from surface	1982–91	0.22	1.0	0.78	—
Land from surface	1982–91	-0.01	0.95	0.96	—
Ocean from surface	1971–92	0.75	0.24	-0.51	—
Land from surface	1971–92	-1.5	0.10	1.6	99
Global ISCCP	1984–90	3.2	5.2	1.9	99
Global surface	1984–90	0.0	1.0	1.0	—

regions (Minnis *et al.*, 1998b). The trends are similar to those found in the 1982–91 surface observations, though details differ. Over all land areas, total cloudiness decreased by 0.5% per decade; high cloud cover grew at a rate of 1.2% per decade. Over the United States of America, total cloudiness decreased by 2.3% per decade, but high cloud cover increased by 5.5% per decade. The trends over Europe were of the same sign but half the magnitude. Over Asia, total cloud cover increased by 4.8% per decade, and high cloudiness grew by 2.7% per decade. Thus, the satellite data suggest a relatively stronger increase in cirrus over the United States of America than surface observations suggest. Over ocean, total cloudiness decreased by 1.2% per decade, whereas high cloud cover was enhanced by 3.7% per decade overall. Some of the discrepancies between the satellite and surface data may originate from the different spatial sampling patterns, calibration, and orbit drift issues peculiar to the satellite data (Klein and Hartmann, 1993; Brest *et al.*, 1997). The satellite covers all regions almost equally, whereas surface observations are from fixed inhabited locations or from well-traveled ship routes.

Further analysis of the ISCCP satellite and the surface data sets was undertaken to isolate and quantify the effects of contrails (Minnis *et al.*, 1998b). The apparent trends were calculated separately for regions having a mean value of contrail coverage less than and greater than 0.5% as computed by Sausen *et al.* (1998) for 1992 aircraft operations (see Section 3.4.3). The mean values of the computed contrail coverage in the two regions are 0.04 and 1.4%, respectively (Figure 3-16). Satellite data and surface observations show larger increases in cirrus cloudiness where contrails are expected to occur most frequently than in all other areas (Table 3-5). Satellite data show that, over land, the increase in high cloudiness in contrail regions was almost four times that in other areas. Over ocean, the difference, though less significant statistically, amounts to a differential increase of 1.6% cover per decade in contrail areas with respect to non-contrail areas. Cirrus trends over contrail regions as derived from surface observations are 0.8 to 2.3% per decade greater than those in the remainder of the globe for the two periods from 1971–92. The single 1971–92 surface data set shows a significant increase (1.6%) in cirrus over land contrail regions compared to remaining land areas. Over oceans, the relative difference is negative but insignificant because of the small number of samples and large variance. Although the differences in these trends are significant at confidence levels of 95% only for the land and global ISCCP data and the 1971–81 land surface data, they show consistent tendencies.

3.5.1.3. HIRS Observations

High-Resolution Infrared Radiation Sounder (HIRS) data from NOAA satellites have been analyzed for the period June 1989 to February 1997 to determine total and high cloud cover (Wylie and Menzel, 1999). During this period, high clouds observed by the NOAA-10 and -12 satellites increased by 4–5% over land and ocean in the Northern Hemisphere (from 23 to 65°N) but only by about 2% in the tropics. High clouds increased by about 3% over southern mid-latitude oceans. The

trend values inferred from the NOAA-11 and -14 satellites are different and somewhat more uncertain because of orbit drift. Over oceans, they also indicate a larger high cloud increase in northern mid-latitudes (3.3%) than over the tropics (-0.4%). Further analysis of HIRS data is required to determine the extent of any contrail impact.

3.5.1.4. *SAGE Observations*

Data from the Stratospheric Aerosol and Gas Experiment (SAGE) II satellite instrument indicate that the frequency of subvisible cirrus clouds near 45°N is twice that at 45°S (Wang *et al.*, 1996). Aviation, as well as hemispheric differences in atmospheric conditions and background aerosol (Chiou *et al.*, 1997; Rosen *et al.*, 1997), may contribute to such differences (Sausen *et al.*, 1998).

3.5.1.5. *Upper Bound for Aviation-Induced Changes in Cirrus Clouds*

The line-shaped contrail cover and global extrapolation described in Section 3.4.3 (see Figure 3-16; Sausen *et al.*, 1998) provide only a lower bound for aviation-induced changes in cirrus cloud cover because they are based on satellite observations that identify only contrails and additional cirrus clouds that are line-shaped. Although estimates of an upper bound of aviation-induced cirrus cover have not yet been established, evidence for a correlation of long-term increases in cirrus cloudiness with air traffic has been published (Liou *et al.*, 1990; Frankel *et al.*, 1997; Boucher, 1998, 1999). Here, observations of cloudiness changes described above are used to provide a preliminary estimate of this upper bound.

Differences in trends derived from observations indicate a stronger mean increase of cirrus amounts in regions with large computed contrail cover than in regions with low computed contrail cover, at least over land (see Table 3-5). The trend difference values vary and are of different statistical significances. The values are considered more meaningful over land because there is less air traffic over the oceans. Of regions with large computed contrail cover, only 14% occurs over oceans, and most of these regions occur near the coasts. In addition, less correlation is expected between computed and observable contrail cover over oceans because actual flight tracks often deviate significantly from idealized great-circle routes. Over land, surface-based observations for 1971–81 suggest a differential increase in cirrus cover of 2.3% per decade. The 1982–91 trend difference is smaller but still positive, and the combined 22-year trend difference is 1.6% per decade. The 7 years of ISCCP satellite data suggest even larger trend differences, both globally and over land. If a trend difference of 1.6% per decade is adopted as most representative of available data, and if that trend is assumed to have persisted for the 3 decades since the beginning of the jet aircraft era (the end of the 1960s), then the current increase in cirrus coverage from aircraft is 4.8% in areas with contrail cover greater than 0.5%. This value is about three times the currently computed linear-contrail cover of 1.4% in those areas and is equivalent to about 0.3% coverage of the Earth's surface, 0.2% more than for line-shaped contrails. If no counteracting process took place that reduced cloudiness over this same period, this value gives an upper bound for total aviation-induced cloudiness.

3.5.2. *Changes in Other Climate Parameters*

3.5.2.1. *Sunshine Duration and Surface Radiation*

Observations from 100 stations over the United States of America showed that the mean value for total cloud cover over the years 1970–88 increased by 2.0 ± 1.3% relative to the years 1950–68 (Angell, 1990). Sunshine duration decreased by only 0.8 ± 1.2%, presumably because cirrus clouds are often too thin to reduce measured sunshine duration. Sunshine duration decreased by an average of 3.7% per decade over Germany between 1953 and 1989 (Liepert *et al.*, 1994). Contrails were estimated to be insufficient to account for the diminished sunshine. In an analysis of radiation trends in Germany from 1964 to 1990, solar radiation during cloudy periods with sun decreased strongly (by 20 to 80 W m^{-2}) (Liepert, 1997). The change might be attributable to aircraft, but the strong reduction in diffuse radiation revealed a more turbid atmosphere, which cannot be explained by increasing cirrus coverage alone.

3.5.2.2. *Temperature*

A substantial decrease in diurnal surface temperature range (DTR) has been observed on all continents (Karl *et al.*, 1984; Rebetez and Beniston, 1998). The reasons for this decrease are not clear; it could be caused by a change in aerosol burden, cloud amount, cloud ceiling height (Hansen *et al.*, 1995), soil moisture, or absorption of solar radiation by increased water vapor in the atmosphere (Roeckner *et al.*, 1998). A weak correlation was found between contrail occurrence data and DTR over the United States of America (DeGrand *et al.*, 1990; Travis and Changnon, 1997). The relationship was strongest during the summer and autumn and most significant over the southwestern United States of America. Rebetez and Beniston (1998) find large DTR trends in the Swiss Alps (a region with heavy air traffic) in correlation with low-level clouds but no reduction of DTR at higher elevation sites, contradicting a potential major impact on DTR from aviation-induced cirrus.

From data taken between 1901 and 1977 over the midwestern United States of America, increases of moderated temperatures (below average maximum and above average minimum), decreases in sunshine and clear days, and shifts in cloud cover, occurred after 1960; these changes were concentrated in the main east-west air corridor (Changnon, 1981). There are, however, many reasons for changes in global mean surface temperatures since 1880 (Halpert and Bell, 1997). The maximum increase in tropospheric temperatures occurred at northern mid-latitudes in the lower troposphere (Tett *et al.*, 1996; Parker *et al.*, 1997). However, radiative transfer models predict maximum heating

rates right below contrails and cirrus in the upper troposphere (Liou, 1986; Section 3.6). Studies using a full-feedback global circulation model (GCM) indicate a nearly constant increase in temperature with altitude for an increase in thin cirrus cloudiness (Hansen *et al.*, 1997). Thus, existing studies do not support the conclusion that aircraft-induced contrails and cloudiness caused changes in global tropospheric temperatures.

3.5.3. Limitations in Observed Climate Changes

The observations cited above suggest that some of the apparent trends in observed cirrus cloudiness and sunshine duration may be caused by air traffic. However, any observed change in cirrus cloudiness or climatic conditions may have other natural or anthropogenic causes (IPCC, 1996). Natural variability includes the El Niño Southern Oscillation (ENSO), the North Atlantic Oscillation (NAO), and the Pacific North America pattern (PNA). For example, the NAO index increased overall from the mid-1960s until 1995 (Hurrell, 1995; Halpert and Bell, 1997). However, there is no evident trend in the NAO index (Hurrell, 1995) and mean position of the Iceland low (Kapala *et al.*, 1998; Mächel *et al.*, 1998) over the period 1982–91 when significant increases in cirrus occurrence and cirrus amount were observed over the North Atlantic Ocean (Boucher, 1998, 1999). Changes in cirrus and subsequent changes in sunshine duration may reflect changes in cyclonic activity (Weber, 1990), ocean surface temperature and related atmospheric dynamics (Wallace *et al.*, 1995), upper troposphere temperature and relative humidity, tropopause altitude (Hoinka, 1998; Steinbrecht *et al.*, 1998), or volcanic effects (Minnis *et al.*, 1993)—or they may be a result of global climate change caused by increased greenhouse gases. Changes in anthropogenic or natural emissions of aerosol or aerosol precursors at the ground might also influence cirrus cloud formation (Plantico *et al.*, 1990; Hansen *et al.*, 1996; Hasselmann, 1997). Cirrus trend values deduced from surface observations may also be influenced by a variety of issues. For example, reported cirrus frequencies depend in an unknown manner on how observers classify contrails as cirrus. Reliable cloud observations are obtained mainly during daytime periods (Hahn *et al.*, 1995), which do not always correlate with the main air traffic periods. The significance of the statistical relationship between cloud changes and air traffic is limited because of the limited duration of satellite and surface cloud observations and the brief period of aircraft emissions in comparison to long-term climate variations. Thus, existing studies are not complete enough to conclude that aircraft-induced contrails and cloudiness have caused observable changes in surface and tropospheric temperatures or other climate parameters.

3.6. Radiative Properties of Aerosols, Contrails, and Cirrus Clouds

Aircraft emissions have an impact on the Earth's radiation budget and climate through direct and indirect changes in aerosols and cloudiness. Recent climate assessments have stressed the importance of natural and anthropogenic changes in aerosols on direct radiative forcing (Charlson *et al.*, 1990; Schwartz, 1996). Aerosols and contrails have direct effects (scattering and absorbing solar and longwave radiation) and indirect effects (modifying the formation of cloud particles and radiative properties of clouds). Several studies have addressed the direct impact of contrails (e.g., Detwiler and Pratt, 1984; Grassl, 1990; Liou *et al.*, 1990; Sassen, 1997). The indirect effect of contrails has not yet been investigated in detail. The direct radiative impacts of aircraft soot emissions (Pueschel *et al.*, 1992, 1997) and sulfate aerosol have been evaluated as being small (Friedl, 1997; Brasseur *et al.*, 1998). The indirect radiative effect of aircraft-induced aerosols on clouds is essentially unknown. In fact, the indirect radiative effect of non-aviation aerosol has been studied for liquid water clouds (IPCC, 1996), but the indirect effect of changing cirrus is not yet known either. Here, the discussion focuses on the impact of aircraft-generated aerosol and that of contrails and changed cirrus clouds.

Radiative forcing is defined as the net radiative flux change at some level in the atmosphere calculated in response to a perturbation, such as a change in cloud cover. The definition of radiative forcing used here is the "instantaneous" or "static" flux change at the top of the atmosphere (TOA) (IPCC, 1996) (see Chapter 6). A positive net flux change represents an energy gain, hence a net heating of the Earth system.

3.6.1. Direct Radiative Impact of Aerosols

The direct radiative impact of aircraft-induced aerosol is much smaller than that of volcanic stratospheric or regional tropospheric aerosol and smaller than other aircraft-induced radiative forcing values (see Chapter 6). Radiative forcing by aerosol depends on many parameters (Haywood and Ramaswamy, 1998). For aerosol in the size range 0.1 to 1 μm, the increase in solar reflectance (albedo effect) exceeds the trapping of terrestrial radiation (greenhouse effect), causing a surface cooling (Lacis *et al.*, 1992, Minnis *et al.*, 1993; Minnis *et al.*, 1998c). Aircraft-induced aerosols could have an importance similar to that of natural stratospheric aerosol variations if their optical depth in the solar range were of comparable magnitude to that of natural stratospheric aerosol. The optical depth of aerosol is proportional to its column load. The maximum zonally averaged column load from soot emissions and aircraft-induced sulfuric acid is estimated (see Section 3.3) to be less than 1 and 6 ng cm^{-2}, respectively. Small sulfuric acid particles are nonabsorbent but scatter strongly in the shortwave spectrum, with mass scattering efficiencies of 7 (4–10) $m^2\ g^{-1}$ in the solar range depending on relative humidity (Boucher and Anderson, 1995; Lacis and Mishchenko, 1995). Soot is a strong absorber of solar energy, with mass extinction coefficients of about 10 $m^2\ g^{-1}$ (Pueschel *et al.*, 1992; Penner, 1995; Petzold and Schröder, 1998). As a consequence of the product of given column load and extinction efficiency, the maximum change in zonal-mean optical depth from aircraft soot and sulfate aerosol is less than 4×10^{-4}. For comparison, the solar optical depth of

stratospheric aerosol varies typically between 0.005 and 0.15, depending on volcanic aerosol loading (Sato *et al.*, 1993). Regionally, within the main flight corridors, a particle concentration change of approximately 30 cm^{-3} at 0.1-μm mean diameter over a vertical layer of 2 km cannot be ruled out (Schumann *et al.*, 1996; Friedl, 1997; Schlager *et al.*, 1997), implying a mass load on the order of 10 ng cm^{-2} and a solar optical depth of about 0.001. This regional change is small compared with other regional variations. Tropospheric aerosol layers with optical depth of 0.1 to 0.5 occur frequently off the coasts of North America and Europe (Russell *et al.*, 1997).

3.6.2. Radiative Properties of Cirrus Clouds

Contrails are ice clouds with radiative effects similar to thin cirrus cloud layers (Liou, 1986; Raschke *et al.*, 1998). At the TOA, thin layers of cirrus clouds or contrails tend to enhance radiative forcing and hence the greenhouse effect because they cause only a small reduction of the downward solar flux but have relatively larger impact on the upward terrestrial radiative flux. An increase in cloud cover by thin cirrus clouds may therefore cause an increase in the net energy gain of the planet (Stephens and Webster, 1981; Fu and Liou, 1993). Contrails and cirrus clouds also have an impact on the radiative energy budget at the Earth's surface. Although radiative forcing at the TOA is most important for long-term and global climate changes, forcing at the surface may have short-term regional consequences.

Longwave (LW) radiative forcing by cirrus or contrails is greatest when clear-sky radiative flux to space is large (i.e., larger over warm than over cool surfaces, larger in a dry than in a humid atmosphere) and cloud emissivity is large (Ebert and Curry, 1992; Fu and Liou, 1993). For thin clouds, emissivity increases with ice water path, which is the product of the ice water content (IWC) of the cloud and its geometrical depth. The emissivity of ice particles in a cirrus layer is much larger, in particular at 8 to 12 μm (King *et al.*, 1992; Minnis *et al.*, 1998c), than that of the same amount of water in gaseous form. Hence, absorption and emission from an atmospheric layer increase when ice particles form at the expense of ambient water vapor (Detwiler, 1983; Meerkötter *et al.*,1999).

Shortwave (SW) radiative forcing of cirrus clouds is determined mainly by solar zenith angle, surface albedo, and cloud optical depth (which increases with ice water path) (Ebert and Curry, 1992; Platt, 1997). For fixed ice water path, clouds containing smaller particles have larger optical depth and exhibit larger solar albedo (Twomey, 1977; Betancor-Gothe and Grassl, 1993). Aspherical particles cause a larger albedo than spherical ones (Kinne and Liou, 1989; Gayet *et al.*, 1998). SW forcing is negative when the cloud causes an increase of system albedo. In general, SW forcing has a greater magnitude over dark surfaces than over bright surfaces.

The net radiative forcing of clouds is the sum of SW and LW flux changes and may be positive or negative. Thin cirrus clouds cause a small but positive radiative forcing at the TOA; thick cirrus clouds may cause cooling (Stephens and Webster, 1981; Fu and Liou, 1993). In the global mean, an increase in cirrus cloud cover warms the Earth's surface (Hansen *et al.*, 1997). Maximum heating is reached at intermediate ice water path, corresponding to an optical depth of about 2 to 3, and the effect shifts to small cooling for optical depths greater than about 10 to 20 (Platt, 1981; Jensen *et al.*, 1994a). Net forcing also varies with particle size but less than its two spectral components. For thin cirrus, smaller particles (but > 3-µm radius) tend to cause stronger heating by increasing cloud albedo less strongly than emissivity (Fu and Liou, 1993).

3.6.3. Radiative Properties of Contrail Clouds

Contrails are radiatively important only if formed in ice-supersaturated air, where they may persist and spread to several-kilometer lateral widths and a few hundred meters vertical depth (Detwiler and Pratt, 1984; Jäger *et al.*, 1998) (see also Section 3.4.4). In contrast, shorter lived contrails have much smaller spatial and temporal scales, hence contribute much less to the radiation budget (Ponater *et al.*, 1996). The impact of contrails on transmission of radiation depends on their optical depth. In the solar range (near a wavelength of 0.55 μm), the optical depth of observed persistent contrails varies typically between 0.1 and 0.5 (Kästner *et al.*, 1993; Sassen, 1997; Jäger *et al.*, 1998; Minnis *et al.*, 1998a). Occasionally, very thick contrails (on the order of 700 m) with optical depths greater than 1.0 are found at higher temperatures (up to -30°C) (Schumann and Wendling, 1990; Gayet *et al.*, 1996). The optical depth in the 10-μm range is about half that near 0.55 μm (Duda and Spinhirne, 1996). Particles in young persistent contrails are typically smaller (mean diameter 10 to 30 μm) than in other cirrus cloud types (greater than 30 μm) (Brogniez *et al.*, 1995; Gayet *et al.*, 1996) but grow as the contrail ages and may approach the size of natural cirrus particles within a time scale on the order of 1 h (see Section 3.4) (Minnis *et al.*, 1998a). The number density of ice crystals in contrails (on the order of 10 to 200 cm^{-3}) is much larger than in cirrus clouds (Sassen, 1997; Schröder *et al.*, 1998b). Reported IWC values in aged contrails vary between 0.7 and 18 mg m^{-3} (Gayet *et al.*, 1996; Schröder *et al.*, 1998b), consistent with results from numerical studies (Gierens, 1996). As for cirrus clouds (Heymsfield, 1993; Heymsfield *et al.*, 1998b), the IWC of contrails is expected to depend on ambient temperature (Meerkötter *et al.*, 1999) because the amount of water mass available between liquid and ice saturation (for temperatures < -12°C) increases with temperature (Ludlam, 1980). Hence, contrails may be optically thicker at lower altitudes and higher temperatures. Contrail particles have been found to contain soot (see Section 3.2.3). Soot in or on ice particles may increase absorption of solar radiation by the ice particles, hence reduce the albedo of the contrails. The importance of soot depends on the type of internal or external mixing and the volume fraction of soot enclosures. Because soot particles are typically less than 1 µm in diameter, their impact on the optical properties of ice particles in aged contrails is likely to be small. Contrail particles often deviate from a spherical shape (see Section 3.4.4).

The magnitude and possibly even the sign of the mean net radiative forcing of contrails depends on the diurnal cycle of contrail cover. For the same contrail cover, the net radiative forcing is larger at night. Satellite data reveal a day/night contrail cover ratio of about 2 to 3 (Bakan *et al.*, 1994; Mannstein, 1997). Aviation fuel consumption inventories suggest a longitude-dependent noon/midnight contrail cover ratio of 2.8 as a global mean value (Schmitt and Brunner, 1997).

3.6.4. Radiative Forcing of Line-Shaped Contrail Cirrus

Model studies indicate the importance of contrails in changing the Earth's radiation budget. One-dimensional (1-D) models represent contrails as plane-parallel clouds in a homogeneously layered atmosphere and use area-weighted sums for fractional contrail cover (Fortuin *et al.*, 1995; Strauss *et al.*, 1997; Meerkötter *et al.*, 1999). As a consequence, contrail forcing grows linearly with contrail cover in these models. Inhomogeneity effects may be large in natural cirrus (Kinne *et al.*, 1997) and small for vertically thin contrail clouds (Schulz, 1998) but may be important for thick and narrow contrails. Computations of radiative forcing by contrails have been done for fixed atmospheric temperatures in the North Atlantic flight corridor (Fortuin *et al.*, 1995). Normalized to 100% contrail cover (as provided by 1-D models), these computations found a net forcing in the range of -30 to +60 W m^{-2} in summer and 10 to 60 W m^{-2} in winter. The negative forcing values apply to clouds that are much thicker than typical contrails. A radiative convective model used to simulate the climatic conditions of a mid-European region (Strauss *et al.*, 1997) found a radiative flux change of almost 30 W m^{-2} at the tropopause for 100% contrail cover with 0.55-μm optical depth of 0.28, and a surface temperature increase on the order of 0.05 K for a 0.5% increase in current contrail cloud cover. With a 2-D radiative convective model, a 1 K increase was found in surface temperature over most of the Northern Hemisphere for an additional cirrus cover of 5% (Liou *et al.*, 1990). The potential effects of contrails on global climate were simulated with a GCM that introduced additional cirrus cover with the same optical properties as natural cirrus in air traffic regions with large fuel consumption (Ponater *et al.*, 1996). The induced temperature change was more than 1 K at the Earth's surface in Northern mid-latitudes for 5% additional cirrus cloud cover in the main traffic regions.

Table 3-6: *Instantaneous TOA radiative flux changes averaged over a day for shortwave (SW), longwave (LW), and net (= SW + LW) radiation for 100% contrail cover in various regions and seasons, with prescribed surface albedo, contrail ice water content (IWC), and computed optical depth τ of contrail at 0.55 μm. Results are for spherical particles (model M, upper values) and hexagons (four-stream version of model FL, lower values).*[a]

Region	Surface Albedo	IWC (mg m^{-3})	τ	SW (Wm^{-2})	LW (Wm^{-2})	Net (Wm^{-2})
Mid-latitude summer continent, 45°N	0.2	21	0.52	-13.4 -22.0	51.6 51.5	38.2 29.5
Mid-latitude winter continent, 45°N	0.2	7.2	0.18	-4.2 -4.6	18.4 18.3	14.2 13.7
Mid-latitude winter continent with snow, 45°N	0.7	7.2	0.18	-2.3 -2.0	18.4 18.3	16.1 16.3
North Atlantic summer ocean, 55°N	0.05	21	0.52	-21.5 -32.7	53.3 50.9	31.8 18.2
Tropical ocean (Equator, June)	0.05	23	0.57	-16.0 -25.9	63.0 57.4	47.0 31.5
Subarctic summer ocean, 62°N	0.05	28.2	0.70	-30.8 -45.3	55.7 49.1	24.9 3.7
Subarctic winter ocean ice, 62°N	0.7	7.2	0.18	-0.6 -0.7	14.6 13.2	14.0 12.5

[a]The contrail is embedded as a homogeneous cirrus cloud of 200-m vertical depth with a top at 11-km altitude (9 km in the subarctic); temperature-dependent IWC as listed; spherical ice particles with measured size spectrum (Strauss *et al.*, 1997) (volume-mean particle diameter of 16 μm); an otherwise clear atmosphere with continental or maritime aerosol (WMO, 1986) of 0.28 or 0.08 total 0.55-μm optical depth; a Lambertian surface with a spectrally constant SW albedo as listed; and a LW emissivity of 1. Reference atmospheres are prescribed according to McClatchey *et al.* (1972). Results are normalized for 100% contrail cover. See Meerkötter *et al.* (1999) for further details.

Table 3-7: *Sensitivity of daily mean of instantaneous net forcing at top of the atmosphere by contrails to a range of values for various parameters[a] for 100% contrail cover. The first two rows contain results from models FL, M, and N; the others are from model N.*

Case		Optical Depth τ at 0.55 μm	Net Forcing (Wm^{-2})
Reference (models FL, M, and N)		0.52	37.1–37.2
Different aspherical particles (models FL, M, and N)		0.4	22–36
Parameters	**Range**		
Solar zenith angle	60°–21°	0.52	37–49
Ice water content (IWC)	7.2–42 mg m^{-3}	0.2–1.0	19–51
Particle diameter	10–40 μm	0.85–0.21	41–20
Surface temperature	289–299 K	0.52	35–39
Cloud cover/optical depth of underlying clouds	0–1 / 0–23	0.52	37–40
Surface albedo	0.05–0.3	0.52	31–40
Relative humidity	reference – 80%	0.52	37–31
Contrail vertical depth (for fixed ice water path)	200 m – 1 km	0.52	37.1–36.7
Lower contrail top (for fixed IWC)	11–10 km	0.52	37–31
Lower contrail top (for temperature-dependent IWC)	11–10 km	0.52–1.32	37–45

[a] Details in Meerkötter *et al.* (1999). Reference case for mid-latitude summer (McClatchey *et al.*, 1972) as in Table 3-6; spherical particles; solar zenith angle of 60°; diurnal sunshine fraction of 50%; IWC of 21 mg m^{-3}; volume mean particle diameter of 32 μm; surface temperature of 294 K; no low-level clouds; relative humidity of reference profile (McClatchey *et al.*, 1972) varying from 77% at the surface to 11% at 12-km altitude; contrail depth 200 m; and contrail top at 11-km altitude.

Meerkötter *et al.* (1998) applied three established radiation transfer models to compute the static radiative forcing due to a prescribed additional cloud cover by contrails. These models, which assume plane parallel cloud cover, are the two- and four-stream models of Fu and Liou (1993) (FL); the matrix operator method of Plass *et al.* (1973), also used by Strauss *et al.* (1997) (M); and the four-stream model of Nakajima and Tanaka (1986, 1988) (N). The FL and M models have participated in model comparison exercises (Ellingson and Fouquart, 1990). Table 3-6 on the previous page shows the results of a parameter study that was carried out for various regions and seasons using models M and FL for spherical and hexagonal particles. The contrails cause a net forcing that is positive in all cases after summing over negative SW and positive LW flux changes. The magnitude of SW forcing is larger over dark ocean than over bright snow surfaces and larger for hexagonal ice particles than for spheres. LW forcing is larger in the tropics than in polar regions. Despite the small ocean albedo, net forcing is largest in the tropics because it has the warmest lower atmosphere. These results are consistent with the expectation that net forcing is smallest over cool and dark surfaces. Net forcing over the mid-latitude continent is larger in summer than in winter. Hexagonal particles cause a larger albedo than spherical ones, therefore less net forcing. These results show that contrail heating generally prevails over cooling in the atmosphere-surface system. However, this finding does not preclude situations in which contrails cause a net cooling—for example, very cold surface, high atmospheric humidity, low surface albedo, very small particles (< 10 μm; the limit depends on the ice water path in the cloud), or large optical contrail depth (> 10).

TOA radiative forcing depends mainly on the cover and on parameters that determine the solar optical depth of contrails and to a minor degree on other parameters. Forcing is very weakly sensitive to the methods used for radiative transfer calculations. This sensitivity can be seen from Table 3-7, which lists the results of a parameter sensitivity study with models FL, M, and N (Meerkötter *et al.*, 1999). Except for the first two rows of Table 3-7, results are from model N only because the results of the three models agree with each other to within 3%. The largest model differences are found for aspherical particles, which are represented by different shapes in various spectral regions in the models, but all models show smaller net forcing for aspherical particles than for spherical ones, as expected (Kinne and Liou, 1989). The results also depend rather strongly on solar zenith angle, ice water content, particle diameter, surface albedo, and relative humidity. Low-level clouds with large cover and optical depth reduce SW and LW forcing of the cloud-free case below a contrail, causing a small net increase of forcing. Variations in surface temperature (here ± 5 K) cause small LW flux changes. Lowering the altitude of a contrail for fixed IWC reduces the LW effect slightly. Lowering the altitude of the contrail and using the IWC that is expected for the higher temperature at lower levels makes the lower contrail optically thicker and radiatively more effective than the higher contrail. Hence, TOA radiative forcing by contrails grows with increasing surface temperature, surface albedo, and IWC. For the same IWC, contrails with small ice particles are more effective in radiative forcing than contrails with larger particles. Representative forcing values are approximately 25 to 40 W m^{-2} for 100% contrail cover and 0.55-μm optical depth of 0.5.

Radiative forcing by contrails depends strongly on the optical depth of the contrails and is different at the surface than at the TOA. Figure 3-20 shows computed SW, LW, and net change in radiative fluxes at the TOA (actually 50 km) and at the surface for 100% contrail cloud cover for the mid-latitude summer continental reference case with spherical ice particles. The ice water content was varied to yield different values of the 0.55-μm optical depth τ. The trends are consistent with those found in cirrus studies (Fu and Liou, 1993). At the TOA, LW forcing is larger than SW forcing, giving a net heating of the atmosphere that is maximum near $\tau = 3$. The flux increases slightly less than linearly with optical depth for small values of τ. The net forcing changes sign and becomes negative for $\tau > 10$ (not shown), but contrails are probably never that optically thick. This analysis indicates that contrails heat the atmosphere below them.

In all cases, TOA and top of the troposphere radiative flux changes from contrails differ by only about 10%; therefore, the instantaneous or static flux change gives a reasonable approximation for the adjusted radiative forcing as considered in IPCC (1996).

At the Earth's surface, LW flux changes are much smaller because water vapor closes much of the infrared radiation window in the lower atmosphere. In contrast, SW flux changes are only a little smaller than at TOA. Hence, the daytime SW contribution dominates and cools the surface in the daily mean. A reduction of solar radiation by 40 W m^{-2} has been measured locally in the shadow of contrails, although the simultaneous change in infrared flux in the shadow of contrails was very small (Sassen, 1997). Hence, the Earth's surface is locally cooled in the shadow of contrails. This analysis does not exclude warming of the entire atmosphere-surface system driven by the net flux change at TOA. As radiation-convection models show, for example, vertical heat exchange in the atmosphere may cause a warming of the surface even when it receives less energy by radiation (Strauss *et al.*, 1997). Cooling of the atmosphere below contrails is also suggested by measurements of solar and infrared upward and downward fluxes above and below a few persistent contrails (Kuhn, 1970). These measurements show a strong (10–20%) reduction of net downward radiation just below approximately 500-m-thick contrails with little change in LW fluxes. Further investigation is required to demonstrate how these results depend on the geometry and age of contrails.

Contrail cirrus induce a heat source by the change in divergence of solar and infrared radiation fluxes mainly within but also below the contrail in the upper troposphere (Liou *et al.*, 1990; Strauss *et al.*, 1997; Meerkötter *et al.*, 1999). In the atmosphere below a contrail, the change in heat source is on the order of 0.3 K/day for 100% cover. When the contrail is located above a thick lower level cloud, the atmosphere is heated only above the lower cloud; the heat source is essentially zero below the lower cloud.

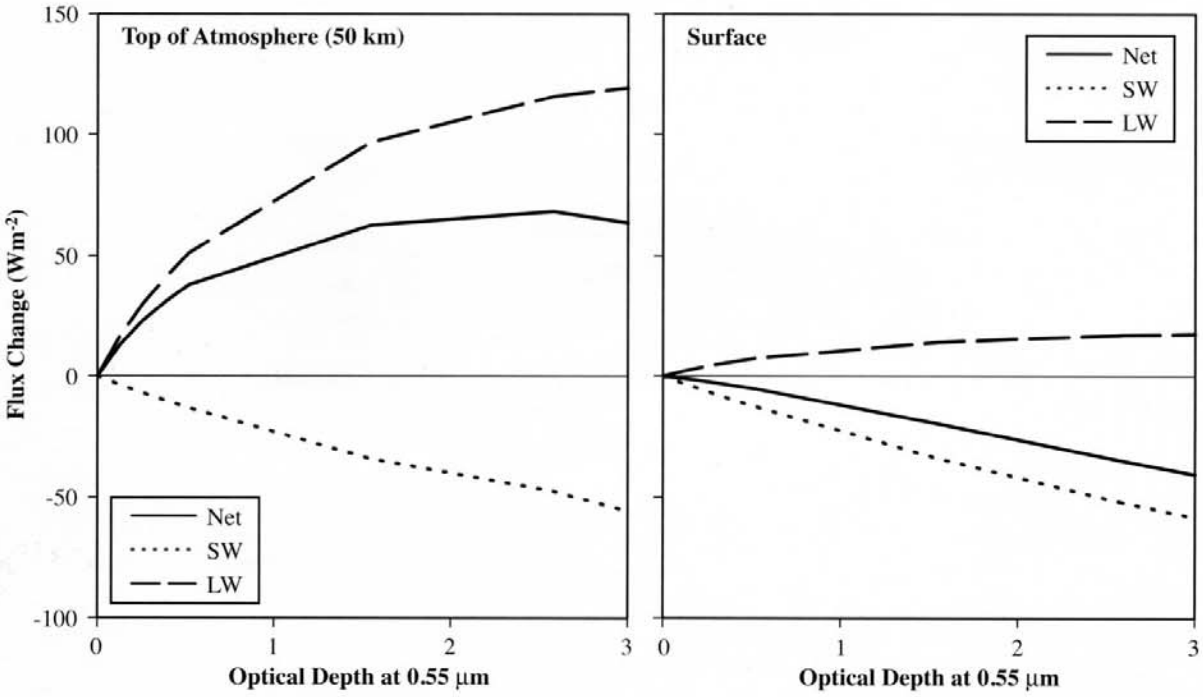

Figure 3-20: Shortwave (SW), longwave (LW), and net instantaneous radiative flux change from contrails with 100% cover under mid-latitude summer conditions averaged over a day as a function of optical depth (0.55 μm): Near the top of the atmosphere (50 km) and surface (0 km) (from Meerkötter *et al.*, 1999).

In the diurnal cycle, radiative forcing by contrails is positive and strongest during the night because of the absence of negative SW forcing (see Table 3-6). For small optical depth, net forcing at TOA is also positive during the day, hence always positive regardless of the diurnal cycle of contrail cover. Negative SW forcing is maximum not at noon but during morning or afternoon hours, when the solar zenith angle is near 70°. Other than at TOA, the net flux change is negative at the surface even for thin contrails during the day, in particular at intermediate zenith angles. The maximum day-night difference in net radiative forcing at the surface for cloudless summer mid-latitude conditions is about 20 W m^{-2} for constant 100% contrail cover with optical depth of 1 and constant surface temperature, and slightly less when accounting for the daily temperature cycle.

The global distribution of radiative forcing from contrails can be estimated using a radiation transfer model, the expected contrail cover, and a realistic representation of the cloudy atmosphere and surface (Minnis *et al.*, 1999). Global contrail cover for 1992, for example, is shown in Figure 3-16 (see Section 3.4.3). Global mean values for TOA radiative flux are summarized in Table 3-8, along with details of the calculations. As expected, SW forcing is negative and LW and net forcings are positive. All three values increase less than linearly with solar optical depth τ. The resulting 1992 global distribution of TOA net forcing for τ of 0.3 is shown in Figure 3-21. Forcing is largest in regions of heavy air traffic, with maximum values over northeast France (0.71 W m^{-2}) and near New York (0.58 W m^{-2}). Although the contrail amount is higher over the northeast United States of America, net contrail forcing over Europe is greater because of the greater LW forcing term. The global mean net forcing for τ between 0.3 and 0.5 is about 0.02 W m^{-2}; the zonal mean value is largest near 40°N, with a value five times larger than the global mean.

Computed results for global radiative forcing by contrails depend on assumed values for contrail cover and mean optical depth of contrails. Neither is well known. Here, the computed global contrail cover was normalized to yield 0.5% observed cover by line-shaped contrails over Europe, guided by satellite data. Because satellite data mainly reveal thicker contrails, a larger cover resulting from the presence of optically thin contrail cirrus might not be accurately detected. Therefore, the results for larger τ values (0.3 to 0.5) are considered in combination with the given contrail cover (0.1% globally) as being most representative for real forcing conditions. Hence, in the diurnal and annual mean, a global 0.1% increase in thin contrail cloud cover causes a net heating of the Earth-atmosphere system of approximately 0.02 W m^{-2}. The difference between the largest and smallest net forcing values in Table 3-8 suggests an error bound on the order of 0.01 W m^{-2}. Based on Section 3.5, the actual global cover may (with 2/3 probability) be 2 to 3 times smaller or larger than the derived line-shaped contrail cover. The optical depth value is likely known to a factor of 2 to 3. Thus, for assumed Gaussian behavior of individual uncertainties, the radiative forcing value may differ from the best estimate by a factor of about 3 to 4.

Based on computations using estimates of line-shaped contrail occurrence for the 1992 fuel scenario (0.1% cover), the best estimate of global-mean radiative forcing is positive, has a value of about 0.02 W m^{-2} with an uncertainty factor of 3 to 4, and may range from 0.005 to 0.06 W m^{-2} for present climate conditions. Certainly, the state of our understanding is only fair. Future investigations may result in considerable changes to the best estimates.

Global radiative forcing by contrails obviously is much smaller than that attributed to other anthropogenic changes in the past century—1.5 W m^{-2}, which represents about the median of the range of values given in IPCC (1996) but comparable to the forcing by past CO_2 emissions by aircraft (Brasseur *et al.*, 1998; see Chapter 6). A mean radiative forcing of 0.02 W m^{-2} induces a vertically averaged heat source in the troposphere equivalent to approximately 0.0002 K day^{-1}. The atmosphere reacts to this

Table 3-8: *Shortwave (SW), longwave (LW), and net radiative flux changes (Wm^{-2}) at top of atmosphere in global mean as caused by contrails in 1992 and 2050 scenario Fa1 (see Section 3.7.2 and Chapter 9), for contrail cover as shown in Figure 3-16 and for solar optical depths of 0.1, 0.3, and 0.5 for contrails (Minnis et al., 1999). The last line gives the results for temperature-dependent ice water content (IWC) with variable optical depth.*[a]

	1992			2050 (Scenario Fa1)		
Optical Depth at 0.55 μm	SW	LW	Net	SW	LW	Net
0.1	-0.0030	0.0111	0.0081	-0.018	0.067	0.049
0.3	-0.0081	0.0246	0.0165	-0.049	0.148	0.099
0.5	-0.0124	0.0327	0.0203	-0.075	0.197	0.122
Variable (from temperature-dependent IWC)	-0.0038	0.0135	0.0097	-0.024	0.084	0.060

[a]Cloud amount, cloud distribution, and cloud optical depth are 1986 ISCCP 3-h data interpolated to 1 h, for 4 months (January, April, June, October), with mean cloud cover of 68% of the Earth surface. Ice particles are modeled as hexagons with mean diameters of 20 μm. Water clouds consist of droplets with 60-μm mean diameter. Surface skin temperature and surface albedo are taken from ISCCP and Staylor and Wilber (1990). Winter and standard temperature and moisture profiles are assumed for pressures < 50 hPa, and numerical weather analysis monthly mean profiles of National Meteorological Center (NMC; now National Center for Environmental Protection, NCEP) are used for pressures > 50 hPa. Continental and marine aerosols were also included in the model. Contrails are assigned at a pressure of 200 hPa and assumed to be 220-m thick with aspherical ice particles of 24-μm volume mean diameter. IWC in contrails was adjusted to result in an optical depth of 0.1, 0.3, or 0.5. A case with IWC set to half the amount of water available for ice formation from vapor at 100% humidity relative to liquid saturation (temperature-dependent IWC) is also considered (variable optical depth). Net TOA forcing is computed with model FL as difference of results with and without contrails.

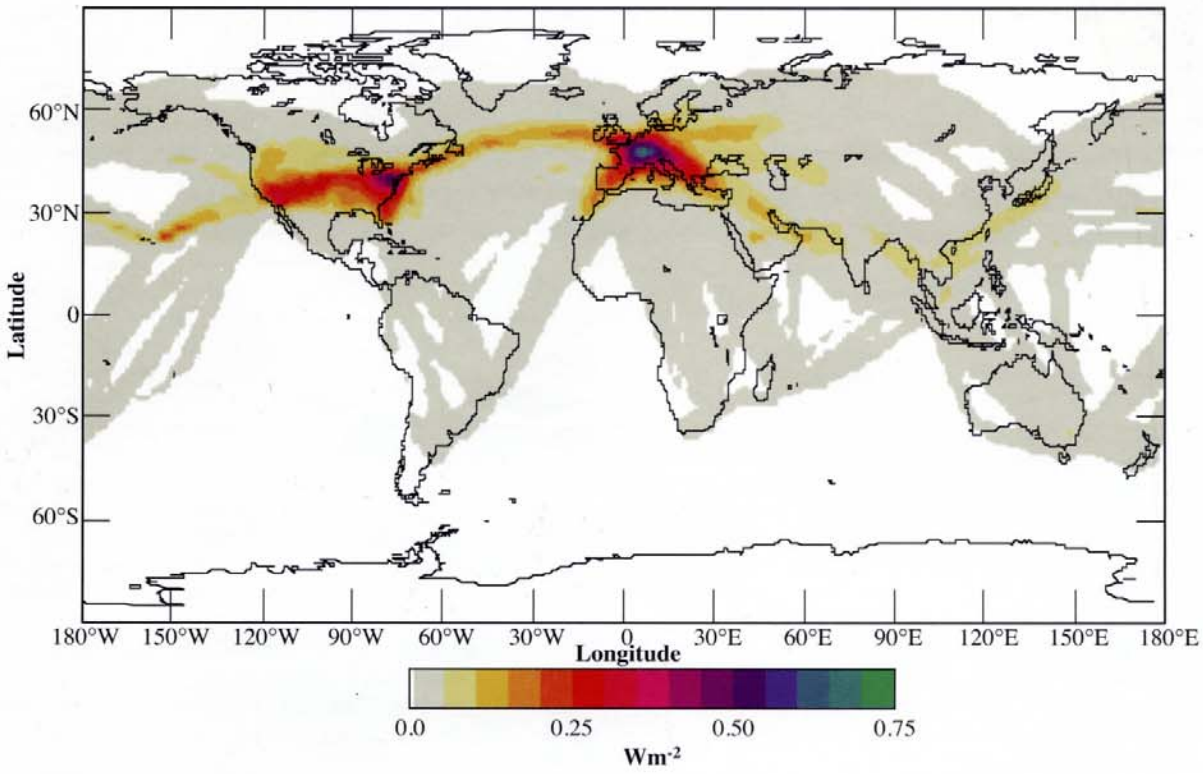

Figure 3-21: Global distribution of net instantaneous radiative forcing at the top of atmosphere in daily and annual average for present (1992) climatic conditions and analyzed contrail cover (see Figure 3-16) and 0.55-μm optical depth of 0.3 (Minnis *et al.*, 1999).

heat source in a complex manner (Ponater *et al.*, 1996) and may take decades to reach a steady-state temperature response. In steady state, the mean surface temperature may increase by about 0.01 to 0.02 K globally if climate sensitivity from contrail forcing is comparable to that of well-mixed greenhouse gases (IPCC, 1996; see Chapter 6.2.1). In comparison to the global mean value, annually averaged zonal mean values are larger by a factor of about 5, and regional values are larger by a factor of up to 40 (see Figure 3-21). The pattern of the climate response differs from the pattern of radiative forcing, in particular at small regional scales. Zonal mean steady-state temperature changes of between 0.01 and 0.1 K appear to be possible for present contrail cover when previous studies as scaled to the cover and radiative forcing found here (Liou *et al.*, 1990; Ponater *et al.*, 1996; Strauss *et al.*, 1997). Regional contrail forcing may have short-term consequences for the daily temperature range in such a region if contrail forcing persists for at least a day. These temperature changes appear to be too small to be detectable in comparison to atmospheric temperature variations.

3.6.5. Radiative Impact of Additional or Changed Cirrus and Other Indirect Effects

Besides forcing by line-shaped contrail cirrus, the global radiation balance may also be perturbed if there is a significant indirect effect of aircraft-induced aerosol, water vapor, and contrails on the coverage and properties (particle size distribution, number density, and composition) of "natural" cirrus clouds. In addition, there might be other indirect cloud-related effects, such as changes in humidity and precipitation. The principal effects might be similar to those caused by volcanic aerosol mixed down into the troposphere (see Section 3.4.5).

Radiative forcing will be enhanced by any increase in the cover of thin cirrus caused by aircraft beyond that of line-shaped contrail cirrus. If the additional global cirrus cover is as large as 0.2% (the estimated upper bound for 1992; see Section 3.5.1.5), and if the optical properties of this additional cirrus are the same as for line-shaped persistent contrails (optical depth of about 0.3, as also found often for natural cirrus; see Section 3.4.1), then the radiative forcing from the additional cirrus may be as large as 0.04 W m^{-2}—which is twice the value for line-shaped contrail cirrus.

Aircraft emissions may also change the properties of natural cirrus clouds (see Section 3.4.5). In a high-traffic region, cirrus was found to be affected by soot emissions from aircraft, causing an approximate doubling of the ice particle concentration (Ström and Ohlsson, 1998). Smaller particles cause larger optical depth for constant ice water content. Radiative forcing is strongly sensitive to particle size (see Table 3-7). As Figure 3-20

Table 3-9: *Global radiative forcing by contrails and indirect cloud effects in 1992 and 2050 (scenario Fa1). No entry indicates insufficient information for best-estimate value.*

Radiative Forcing	Best Estimate or Range	Uncertainty Range with 2/3 Probability	Status of Understanding
1992			
Line-shaped contrail cirrus	0.02 Wm^{-2}	0.005–0.06 Wm^{-2}	fair
Additional aviation-induced cirrus clouds	0–0.04 Wm^{-2}	—	very poor
Other indirect cloud effects	—	either sign, unknown magnitude	very poor
2050			
Line-shaped contrail cirrus	0.10 Wm^{-2}	0.03–0.4 Wm^{-2}	fair
Additional aviation-induced cirrus clouds	0–0.16 Wm^{-2}	—	very poor
Other indirect cloud effects	—	either sign, unknown range	very poor

indicates, an increase in optical depth causes additional heating if the cirrus cloud was optically thin but cooling if it was optically thick (Wyser and Ström, 1998). One recent study suggests that the indirect heating effect of aviation-induced changes in cirrus ice particle number density for fixed cloud cover may be positive and comparable to or even larger than that from increases in cloud cover (Meerkötter *et al.*, 1999).

While the impact of particle changes on radiative forcing by cirrus clouds may be studied parametrically, our understanding is very poor with respect to other indirect effects. Although comprehensive investigations are missing, there is no evidence that any of the indirect effects are important. Table 3-9 summarizes the assessment of global radiative forcing by aviation-induced cloudiness for 1992. The results for 2050 are explained in Section 3.7.

3.7. Parameters of Future Changes in Aircraft-Produced Aerosol and Cloudiness

The future effects of aircraft depend on trends in climate and air traffic amount and changes in the technical properties of aircraft. Our current understanding of the formation of aviation-induced aerosol and cloudiness can be used to estimate how future changes may affect the impacts of aviation and to identify mitigation options that would be effective in reducing these impacts.

3.7.1 Changes in Climate Parameters

If climate change occurs in the future, atmospheric parameters related to aerosols and contrails will also have changed. Of particular importance to aviation-induced aerosol and cloudiness are changes in temperature and humidity in the upper troposphere and lower stratosphere; changes in the height, temperature, and humidity of the tropopause region; changes in the abundance of particles; and changes in cloudiness. Table 3-10 summarizes how changes in these parameters may be reflected in aviation-related impacts.

General circulation models of the atmosphere predict that the climate of 2050 will reflect global warming from the accumulation of greenhouse gases. In this new climate, models predict increases in the amounts of cirrus clouds, the height of the tropopause, and upper tropospheric temperature (IPCC, 1996; Timbal *et al.*, 1997). A higher tropopause would cause more contrails, at least at high latitudes. Observed temperature changes (e.g., Parker *et al.*, 1997) do not reveal the expected temperature increase in the upper troposphere. Some models predict a higher tropopause if the surface temperature increases (about 200-m altitude increase for 1 K surface temperature increase) (Thuburn and Craig, 1997). Increases on the order of 100 m were analyzed in polar regions and at mid-latitudes (Hoinka, 1998; Steinbrecht *et al.*, 1998). Such changes may be forced by cooling of the lower stratosphere as a result of changes in ozone concentration (Hansen *et al.*, 1997) and increases in moisture as a result of increasing methane concentrations. Stratospheric temperatures between 50 and 100 hPa have decreased by about 1 to 2 K since 1980 (Ramaswamy *et al.*, 1996; Halpert and Bell, 1997). An increase in water vapor concentration has been observed in the lower stratosphere, with the largest trend (0.8%/yr) in the 18- to 20-km region (Oltmans and Hofmann, 1995). Because few contrails currently form in the lower stratosphere, small changes in stratospheric conditions will not create significant changes in contrail abundance. Aerosol loading in the troposphere and lower stratosphere may increase because of changed climate conditions and increased surface emissions. Surface emissions from fossil fuel burning were projected to grow by a factor of 1.5 to 2.1 from 1990 to 2040 (Wolf and Hidy, 1997).

3.7.2. Changes in Subsonic Aircraft

By the year 2050, the number of aircraft flying in the upper troposphere is expected to have increased significantly (see Chapter 9). In scenario Fa1, global annual aviation fuel consumption in 2050 will have increased by a factor of 3.2 compared with 1992, with a larger increase (factor of 4.3) above 500 hPa. Scenarios Fc1, Fe1, and Eah (see Chapter 9) assume increases by factors of 1.8, 5, and 14, respectively, in

Table 3-10: *Parameters affecting future changes in aircraft-produced aerosols and cloudiness and their impacts on contrails and aerosol abundance. Symbols indicate sign of change in the parameter and in the impact. Question marks indicate uncertainty in sign or importance of an impact. The symbol x indicates lack of a known or important impact.*

Parameter	Sign of Change	Global Contrail and Induced-Cirrus Coverage	Global Contrail Radiative Forcing	Aerosol Abundance
Upper troposphere temperature	+?	–	–	x
Lower stratosphere temperature	–	x	x	+
Humidity of lower stratosphere	+	x	x	+
Humidity of upper troposphere	+?	+	+	+
Tropopause altitude	+	+	+	x
Number of aircraft	+	+	+	+
Global aviation fuel consumption	+	+	+	+
Overall efficiency of propulsion	+	+	+	x
Cruise altitude at mid-latitudes	+	-	-	+
Cruise altitude in the tropics	+	+	+	x
Traffic in tropical regions	+	+	+	x
Soot emissions	–?	–?	–?	x
Fuel sulfur content	–?	–?	–?	–
Fuels with higher hydrogen content	+?	+	?	–

total fuel consumption compared to 1992. The frequency of contrail formation is expected to increase with traffic because large regions of the atmosphere are humid and cold enough to allow persistent contrails to form and because such regions are not at present fully covered with optically thick cirrus or contrail clouds (see Sections 3.4.1 and 3.4.3). The number of aircraft may grow slightly less rapidly than fuel consumption when smaller aircraft are replaced by larger ones. This factor is important because the amount of persistent contrail cover may depend mainly on the number of aircraft triggering contrails and less on fuel consumption.

As aircraft engines become more fuel efficient, contrails will form more frequently at lower flight levels because exhaust plumes of more efficient engines are cooler for the same water content (see Section 3.2.4.1). The overall efficiency η (Cumpsty, 1997) with which engines convert fuel combustion heat into propulsion of cruising subsonic aircraft was close to 0.22 in the 1950s, near 0.37 for modern engines in the early 1990s, and may reach 0.5 for new engines to be built by 2010 (see Figure 3-22). An increase of η from 0.3 to 0.5 in a standard atmosphere increases the threshold formation temperature of contrails by about 2.8 K (equivalent to 700-m lower altitude) (Schumann, 1996a).

The change in persistent contrail coverage because of changed traffic has been determined using thermodynamic analysis of meteorological data from 1983 to 1992 and fuel consumption data (Sausen *et al.*, 1998) (see Section 3.4). This method has been used to estimate future changes in contrail cover resulting from changes in air traffic, assuming a fixed climate, fuel consumption scenarios, and expected engine performance specifications (Gierens *et al.*, 1998). The computed contrail cover (Figure 3-23) for the 2050 Fa1 fuel scenario using present analysis data and η of 0.5 shows a global and annual mean contrail cover of 0.47%, with values of 0.26% and 0.75% for

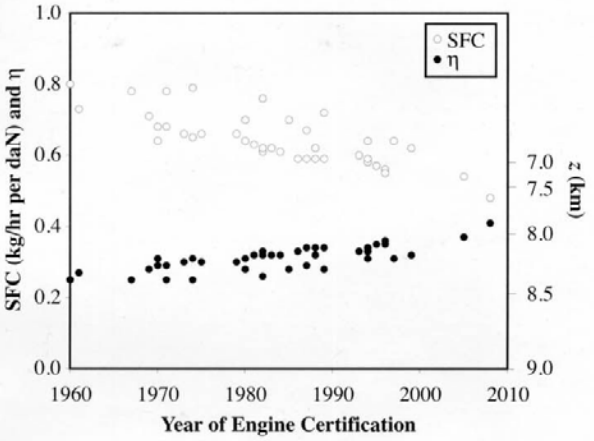

Figure 3-22: Trend in overall efficiency of propulsion η (solid circles), computed from aircraft specific fuel consumption (SFC) data (open circles; data as in Figure 7-9), according to $\eta = V(Q\ \mathrm{SFC})^{-1}$, with V as the aircraft speed (~240 m s^{-1}) and Q as the specific heat of combustion of aviation fuels (43 MJ kg^{-1}). Solid circles also denote the critical altitude z (right axis) above which contrails form (for 100% relative humidity in the mid-latitude standard atmosphere) for the years 1960 to 2010. SFC data were taken from a figure *Subsonic Engine-Specific Fuel Consumption at Cruise Versus Certification Date* originating from a NASA report and presented by H.G. Aylesworth at the Working Group Meeting CAEP-4, WG3 Emissions, International Civil Aviation Organization, 20-23 May 1997, Savannah, GA, USA.

scenarios Fc1 and Fe1. Values may be as high as 1 to 2% for scenario Eah, which does not specify the spatial distribution of future traffic and in which contrail cover may become limited by the amount of cloud-free ice-supersaturated air masses. In comparison, values are 0.087% for the 1992 DLR fuel inventory with η of 0.3 and 0.38% for the 2050 scenario with η of 0.3. Hence, contrail cover is expected to increase by a factor of about 5 over present cover for a 3.2-fold increase in annual aviation fuel consumption from 1992 to 2050, even under constant climate conditions. Increased efficiency of propulsion by future engines causes about 20% of the computed increase in contrail cover. In the year 2050, the maximum contrail coverage is expected to occur over Europe (4.6%, 4 times more than 1992), the United States of America (3.7%, 2.6 times more), and southeast Asia (1.2%, 10 times more). Contrail-induced increases in cirrus cloud cover may depend also on wind shear, vertical motions, and existing cirrus cover, which this thermodynamic analysis does not take into account. In addition, changes in climate conditions may influence future contrail formation conditions.

Radiative forcing from contrails was calculated for 2050 using the Fa1 fuel scenario and the same method as described in Section 3.6.3 (Minnis *et al.*, 1999). For the contrail cover shown in Figure 3-23, values of SW, LW, and net forcing were found to be about 6 times larger than in 1992 (see Table 3-8). The increase in radiative forcing from 1992 to 2050 is larger than the increase in contrail cover (factor of 5) during the same period because additional contrails in the subtropics and over Asia over relatively warm and cloud-free surfaces are more effective in increasing radiative forcing. The global distribution of radiative forcing calculated with this procedure is shown in Figure 3-24 for an assumed optical depth of 0.3. Radiative forcing grows more strongly globally than in regions of present peak traffic. Global mean forcing is 0.1 W m^{-2} in this computation, with maximum values of 3.0 and 1.4 W m^{-2} (3.3 and 2.4 times more than 1992) over northeast France and the eastern United States of America, respectively.

For an optical depth of 0.3, the best-estimate value of the global radiative forcing in 2050 (scenario Fa1) is 0.10 W m^{-2}. The uncertainty range is a little larger than in 1992, and estimated to amount to a factor of 4. Hence, the likely range of forcing extends from 0.03 to 0.4 W m^{-2} (see Table 3-9). The forcing for other scenarios has not been computed in detail, but rough estimates scale with the fuel consumption. The climatic consequences of this forcing are discussed in Chapter 6.

An estimate of the range of aviation-induced cirrus cloudiness in 2050, as required for this assessment, is not available in the scientific literature. For 1992, a range for the best estimate of the additional aviation-induced cirrus clouds was derived from decadal trends in high fuel-use regions (0–0.2% global cover; Section 3.5.1.5). For the 2050 time period, a different approach

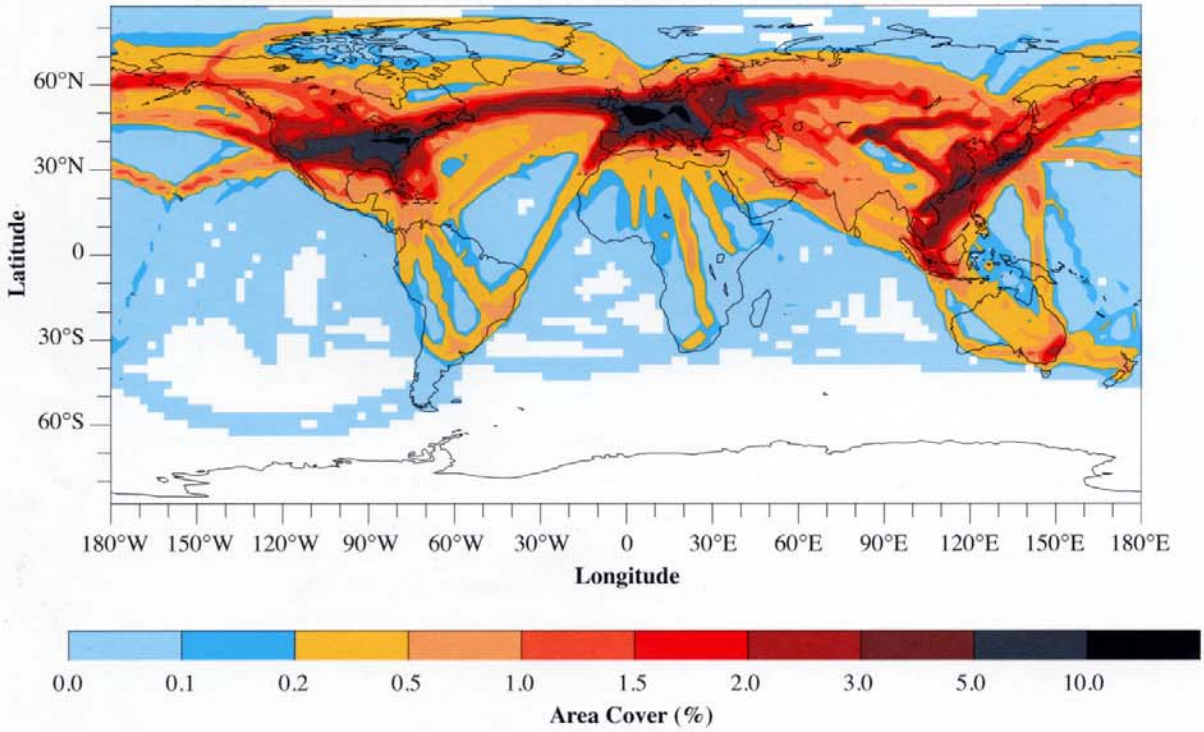

Figure 3-23: Persistent contrail coverage (in % area cover) based on meteorological analysis data and on fuel emission database for 2050 (Fa1 fuel consumption scenario for 2050), assuming linear dependence on fuel consumption and overall efficiency of propulsion η of 0.5; global mean cover is 0.5%. Compare with Figure 3-16 (from Gierens *et al.*, 1998).

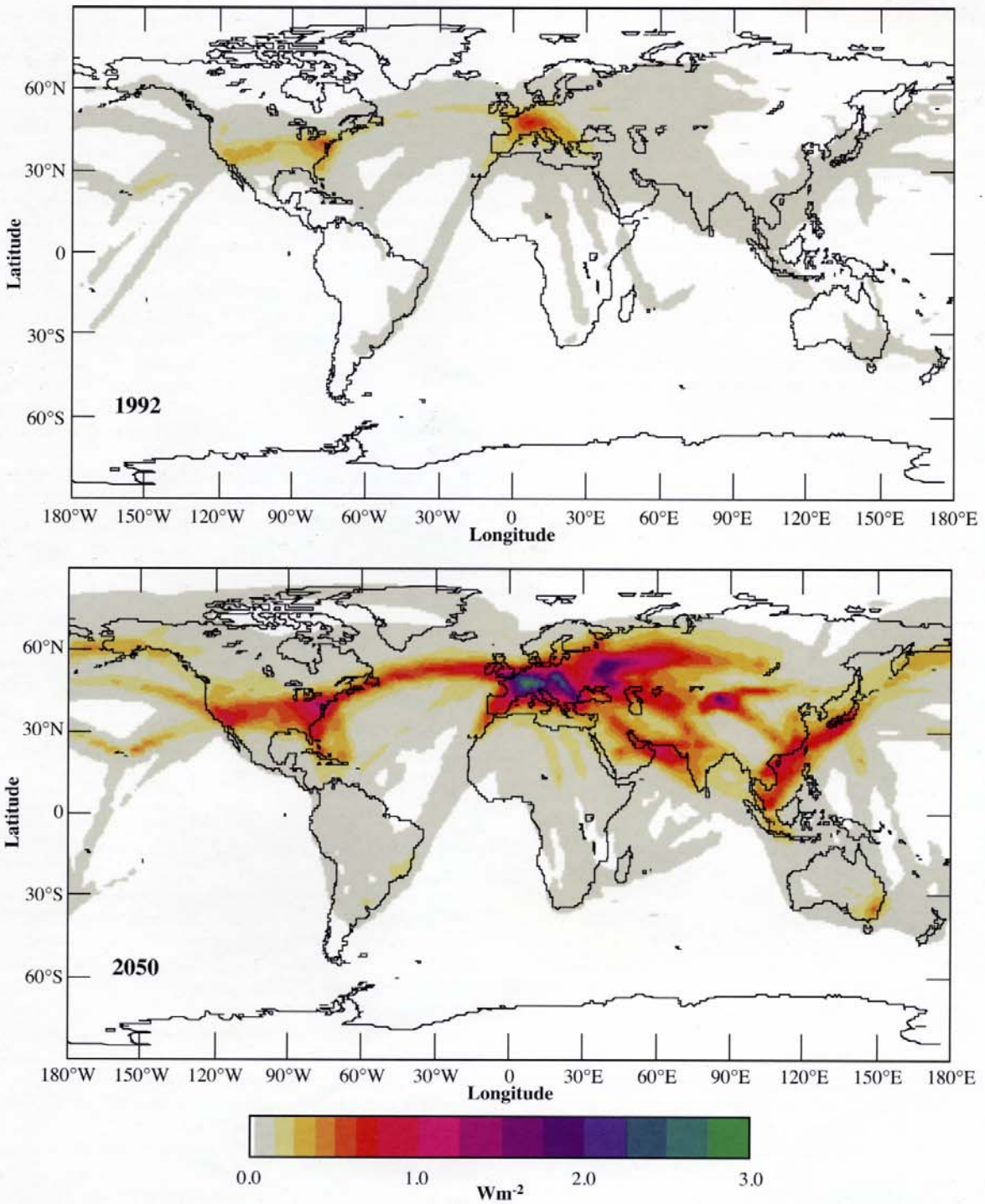

Figure 3-24: Global distribution of net radiative forcing at top of atmosphere in daily and annual average for contrails with 0.55-μm optical depth of 0.3: For 1992, as in Figure 3-21; and for the 2050 scenario with contrail cover as shown in Figure 3-23 (Minnis *et al.*, 1999).

is required. Observed contrail frequencies and trends in cirrus occurrence have been found to correlate with aviation fuel consumption (see Figures 3-14 and 3-18). Therefore, the aviation-induced cirrus cloudiness between 1992 and 2050 is projected to grow in proportion to the total aviation fuel consumption in the upper troposphere. This fuel consumption grows by a factor of 4 between 1992 and 2050 in scenario Fa1. Hence, the best-estimate of additional global cirrus cover in 2050 would range from 0 to 0.8%. For the same radiative sensitivity as in 1992, the associated radiative forcing could be between 0 and 0.16 W m^{-2} or up to 1.6 times the value given for line-shaped contrail cirrus in 2050 (see Table 3-9). The forcing could be outside this range if future aviation causes strong changes in the optical properties of the cirrus clouds. Saturation effects (Sausen *et al.*, 1999) will likely limit any increase in cirrus cover in heavy air traffic regions. Because of these uncertainties the status of understanding of radiative forcing from additional aviation-induced cirrus clouds in 2050 is very poor. The assessment of the other indirect effects (Section 3.6.5) is beyond the scope of present understanding.

Modern subsonic aircraft cruise most efficiently at flight altitudes of 9 to 13 km. Trends in aircraft cruise altitudes are discussed in Chapter 7. If mean flight levels of global air traffic were to increase, the frequency of persistent contrails in the troposphere at mid-latitudes would be reduced and the frequency in the upper troposphere in the tropics would be increased. In addition, the formation of polar stratospheric clouds in the lower polar stratosphere (Peter *et al.*, 1991) may be enhanced as a result of increased emissions in the stratosphere. At mid-latitudes, a 1-km flight-level increase causes a moderate reduction of contrail cover because of increased flights in the dry stratosphere (e.g., 12% less contrail cover over the North Atlantic compared with the nominal-altitude cover). Despite these changes, the global change in contrail cover from an altitude increase is small because of compensating changes in the tropics. The stronger increase of contrail cover in the tropics may cause a stronger positive radiative forcing because of the warmer surface in the tropics compared with mid-latitudes (see Table 3-7). A reduction in flight levels generally has the opposite effect (more contrails at high latitudes and fewer contrails in the tropics). Results for Europe and parts of the United States of America are different in that computed contrail coverage decreases slightly for both an increase and a decrease in mean flight levels because air traffic currently occurs in the cold and humid upper troposphere in those regions, and a shift toward the drier stratosphere or the warmer mid-troposphere reduces contrail coverage (Sausen *et al.*, 1998). A change in mean altitude of contrails may change their radiative impact even for constant areal coverage. A contrail at higher altitude in the troposphere will likely contain less ice mass and produce less radiative forcing, therefore, despite lower ambient temperatures (see Table 3-7).

Trends in soot emissions would be important if soot influences ice particle formation (see Section 3.4) or the chemistry of ozone (see Chapter 2). A soot mass emission index of 0.5 to 1 g kg^{-1} (and larger) is not uncommon for older aircraft engines. The soot mass emission index of the present aircraft fleet is estimated as 0.04 g kg^{-1} (see Chapter 7). The soot emission index decreased with new engine technology until about 1980 but has showed no significant trend thereafter (Döpelheuer, 1997). The mass of soot emitted may decrease despite increases in fuel consumption. No data exist on trends for the number and surface area of soot aerosol emissions.

Atmospheric models and fuel consumption scenarios suggest that aircraft emissions contribute little to the tropospheric mass of sulfate and soot aerosol in today's atmosphere and in 2050 (see Section 3.3). However, aircraft-induced particles will increase with growing emission rates of condensable sulfur compounds and soot particle mass. A reduction in fuel sulfur content is not to be expected for the near future (see Chapter 7). The fraction of condensable sulfur compounds formed from fuel-sulfur depends on the details of the chemistry between the combustor and the engine exit (Brown *et al.*, 1996a; Lukachko *et al.*, 1998). The dependence of this fraction on expected changes in engine technology is not known (see Chapter 7).

Engines burning liquid hydrogen (liquid methane) instead of kerosene (Wulff and Hourmouziadis, 1997) emit 2.6 (1.5) times more water vapor for the same amount of combustion heat. Therefore, such engines trigger contrails at about 1 to 2 km lower altitude (4 to 10 K higher ambient temperature) than comparable kerosene engines. Therefore, an increase in contrail coverage is expected with such fuels. Because of larger water emissions, such contrails will grow to larger diameters before evaporating in ice-subsaturated ambient air. On the other hand, aircraft using hydrogen (methane) fuels will emit no (little) soot and sulfur compounds, hence may cause contrails that have fewer and larger ice particles, smaller optical thickness, and a lesser impact on radiative fluxes (Schumann, 1996a) (compare Table 3-7).

3.7.3. *Expected Changes for Supersonic Aircraft*

The expected emissions of future high speed civil transports (HSCTs) flying above 16-km altitude would substantially add to aerosol amounts in the stratosphere. A fleet of 500 HSCTs is expected to consume about 72 Tg fuel yr^{-1} in 2015 (Baughcum and Henderson, 1998). This level of consumption will cause emissions of sulfur and soot of 14.4 and 2.9 Gg yr^{-1}, for emission indices of 0.2 g S kg^{-1} and 0.04 g soot kg^{-1}, respectively. Microphysical calculations by the AER 2-D model (Weisenstein *et al.*, 1997) show that 28 Gg of sulfate will accumulate in the global atmosphere, assuming that 10% of sulfur emissions are converted in the plume to new particles with a radius of 10 nm. The globally averaged aircraft-produced sulfate column is equal to 5.4 ng SO_4 cm^{-2}, with a maximum of 13.6 ng SO_4 cm^{-2} near 50°N. This value is about twice that computed for present subsonic aviation (Table 3-4). The annually and zonally averaged perturbation of sulfate aerosol SAD as shown in Figure 3-25 is used for scenario SA5 in Chapter 4 and in calculations in Chapters 5 and 6. The chemical consequences of these SAD changes are discussed in detail in Section 4.3.3.

Though supersonic aircraft may have better engine efficiency than subsonic aircraft (0.38 for the Concorde), supersonic aircraft are expected to form few persistent contrails because the probability of ice-supersaturated air at cruise altitudes is small, except in the polar regions and near the tropical tropopause (Miake-Lye *et al.*, 1993). However, the accumulation of supersonic aircraft emissions in the polar atmospheres and local H_2O, HNO_3, and aerosol concentration increases in aircraft plumes may enhance the occurrence of polar stratospheric clouds. The impact on tropospheric cloud formation of supersonic aircraft cruising in the stratosphere is very likely much smaller than the impact of major volcanic events.

3.7.4. Mitigation Options

In the following discussion, options related to aircraft and aircraft operations are briefly considered for the reduction of volatile and nonvolatile particle emission and formation and for the reduction of contrail formation and contrail impact.

Volatile particle growth is controlled mainly by oxidized sulfur, chemi-ions, and water vapor present in aircraft exhaust. With current engines and fuels, no practical options exist to reduce water vapor emission indices. The oxidation of sulfur depends on the emission of SO_3 or the formation of H_2SO_4 in the engine and plume. The emission of SO_3 depends on the details of the reactive flow in and beyond the engine combustion chambers (Chapter 7). The processes controlling condensable sulfur oxides and chemi-ion production are not yet sufficiently understood for a meaningful assessment of mitigation options. A reduction of sulfur content in fuel reduces plume levels of SO_3 and H_2SO_4, but not necessarily by the same factor (Brown *et al.*, 1996a). In addition, for low fuel sulfur content, volatile particles may remain that result from the emissions of other condensable material (Yu *et al.*, 1998; see Section 3.2) and thus require separate mitigation strategies.

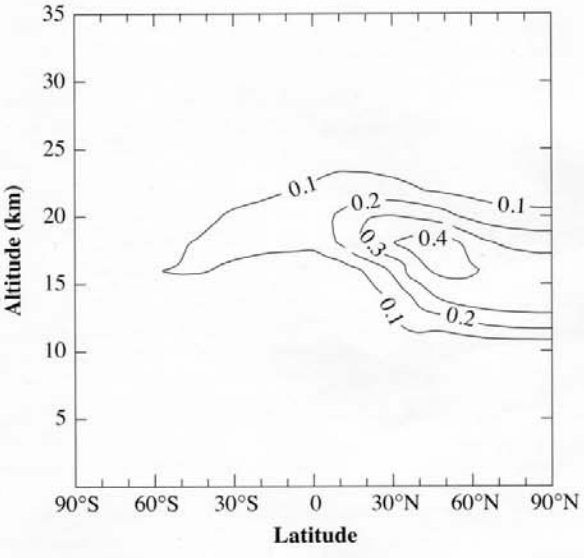

Figure 3-25: Annually and zonally averaged perturbation of sulfate aerosol surface area density (in $\mu m^2\ cm^{-3}$) caused by an HSCT fleet of 500 aircraft flying at Mach 2.4 according to AER 2-D model (Weisenstein *et al.*, 1997). A sulfur emission index of 0.2 g kg^{-1} and a 10% conversion to sulfate particles with 10-nm radius in the plume are assumed in these calculations.

Options to reduce soot emissions require changes in the combustion process (Chapter 7). Soot may be activated by H_2SO_4 and possibly other exhaust species. If soot activation by H_2SO_4 is to be avoided, fuel sulfur contents of less than 10 ppm would be required.

Simulations suggest that contrails would form even without any soot and sulfur emissions by activation and freezing of background particles (Jensen *et al.*, 1998b; Kärcher *et al.*, 1998a). Hence, the formation of contrails cannot be avoided completely by reducing exhaust aerosol emissions. Contrails formed in plumes with fewer exhaust particles are likely to be composed of fewer and larger particles, have smaller optical depths (Schumann, 1996a), hence cause less radiative forcing. Reduced soot and sulfate particle emissions may also lead to the formation of cirrus clouds with fewer but larger particles and less radiative forcing.

An increase in engine efficiency may change the global effects of contrails. Improvements in engine efficiency measured as specific fuel consumption (SFC) per unit thrust or overall efficiency, η, would reduce fuel consumption at cruise altitudes for a given amount of air traffic. Because more efficient engines increase the altitude range over which persistent contrails form (see Section 3.2.4.1 and 3.7.2), contrail frequency and cover would likely increase for a given air traffic amount. On the other hand, the number of ice crystals forming per aircraft-km would likely be reduced for lower SFC because aerosol and aerosol precursor emissions would be reduced. Fewer ice crystals could result in less radiative impact for a given amount of air traffic in altitude regions where contrails form at present. Hence, the balance of changes in contrail occurrence and the radiative impact that would result from changes in engine efficiency depend on a variety of factors, not all of which are well known enough at present.

Reducing the frequency of contrails for a given amount of air traffic could otherwise be effected by reducing the number of flights in the humid and cold regions of the upper and middle troposphere. Numerical weather prediction schemes may be used to predict and circumvent such regions on long-distance flights. Contrail-forming regions could also be avoided by flying at generally higher altitudes, but the climatic impact of contrails may not be reduced because of counteracting effects. For example, higher flight altitudes at low latitudes could increase contrails, possibly causing a net increase instead of a decrease in global radiative forcing by contrails. In addition, more flights in the lower stratosphere could result in enhanced aerosol and chemical impacts not related to contrails.

References

Ackerman, S.A., C. Moeller, K.I. Strabala, H.E. Gerber, L.E. Gumley, W.P. Menzel, and S-C. Tsay, 1998: Retrieval of effective microphysical properties of clouds: a wave cloud case study. *Geophysical Research Letters,* **25,** 1121–1124.

Anderson, B.E., W.R. Cofer, J.W. Barrick, D.R. Bagwell, C.H. Hudgins, and G.D. Nowicki, 1998a: Airborne observations of aircraft aerosol emissions. 1. Total and nonvolatile particle emission indices. *Geophysical Research Letters,* **25,** 1689–1692.

Anderson, B.E., W.R. Cofer, D.R. Bagwell, J.W. Barrick, C.H. Hudgins, and K.E. Brunke, 1998b: Airborne observations of aircraft aerosol emissions. 2. Factors controlling volatile particle production. *Geophysical Research Letters,* **25,** 1693–1696.

Andronache, C. and W.L. Chameides, 1997: Interactions between sulfur and soot emissions from aircraft and their role in contrail formation. 1. Nucleation. *Journal of Geophysical Research,* **102,** 21443–21451.

Andronache, C. and W.L. Chameides, 1998: Interactions between sulfur and soot emissions from aircraft and their role in contrail formation. 2. Development. *Journal of Geophysical Research,* **103,** 10787–10802.

Angell, J.K., 1990: Variation in United States cloudiness and sunshine duration between 1950 and the drought year of 1988. *Journal of Climate,* **3,** 296–308.

Appleman, H., 1953: The formation of exhaust contrails by jet aircraft. *Bulletin of the American Meteorological Society,* **34,** 14–20.

Arnold, F., J. Scheid, T. Stilp, H. Schlager, and M.E. Reinhardt, 1992: Measurements of jet aircraft emissions at cruise altitude. I. The odd-nitrogen gases. *Geophysical Research Letters,* **19,** 2421–2424.

Arnold, F., J. Schneider, M. Klemm, J. Scheid, T. Stilp, H. Schlager, P. Schulte, and M.E. Reinhardt, 1994: Mass spectrometric measurements of SO_2 and reactive nitrogen gases in exhaust plumes of commercial jet airliners at cruise altitude. In: *Impact of Emissions from Aircraft and Spacecraft upon the Atmosphere* [Schumann, U. and D. Wurzel (eds.)]. Proceedings of an international scientific colloquium, 18–20 April 1994, Cologne, Germany. DLR-Mitteilung 94-06, Deutsches Zentrum für Luft- und Raumfahrt (German Aerospace Center), Oberpfaffenhofen and Cologne, Germany, pp. 323–328.

Arnold, F., J. Schneider, K. Gollinger, H. Schlager, P. Schulte, P.D. Whitefield, D.E. Hagen, and P. van Velthoven, 1997: Observation of upper tropospheric sulfur dioxide- and acetone-pollution: potential implications for hydroxyl radical and aerosol formation. *Geophysical Research Letters,* **24,** 57–60.

Arnold, F., T. Stilp, R. Busen, and U. Schumann, 1998a: Jet engine exhaust chemi-ion measurements: implications for gaseous SO_3 and H_2SO_4. *Atmospheric Environment,* **32,** 3073–3077.

Arnold, F., K.-H. Wohlfrom, M.W. Klemm, J. Schneider, K. Gollinger. U. Schumann, and R. Busen, 1998b: First gaseous ion composition measurements in the exhaust plume of a jet aircraft in flight: implications for gaseous sulfuric acid, aerosols, and chemi-ions. *Geophysical Research Letters,* **25,** 2137–2140.

Bakan, S., M. Betancor, V. Gayler, and H. Grassl, 1994: Contrail frequency over Europe from NOAA-satellite images. *Annales Geophysicae,* **12,** 962–968.

Balkanski, Y.J., D.J. Jacob, G.M. Gardner, W.C. Graustein, and K.K. Turekian, 1993: Transport and residence times of tropospheric aerosols inferred from a global three-dimensional simulation of ^{210}Pb. *Journal of Geophysical Research,* **98,** 20573–20586.

Barnes, J.E. and D.J. Hofmann, 1997: Lidar measurements of stratospheric aerosol over Mauna Loa Observatory. *Geophysical Research Letters,* **24,** 1923–1926.

Baughcum, S.L. and S.C. Henderson, 1998: *Aircraft Emission Scenarios Projected in Year 2015 for the NASA Technology Concept Aircraft (TCA) High Speed Civil Transport.* NASA/CR-1998-207635, National Aeronautics and Space Administration, Hampton, VA, USA, 21 pp.

Baughcum, S.L. T.G. Tritz, S.C. Henderson, and D.C. Pickett, 1996: *Scheduled Civil Aircraft Emission Inventories for 1992: Database Development and Analysis.* NASA-CR-4700, National Aeronautics and Space Administration, Hampton, VA, USA, 205 pp.

Bekki, S., 1997: On the possible role of aircraft generated soot in the middle latitude ozone depletion. *Journal of Geophysical Research,* **102,** 10751–10758.

Bekki, S. and J.A. Pyle, 1992: Two-dimensional assessment of the impact of aircraft sulphur emission on the stratospheric sulphate aerosol layer. *Journal of Geophysical Research,* **97,** 15839–15847.

Bekki, S. and J.A. Pyle, 1993: Potential impact of combined NO_x and SO_x emissions from future high speed civil transport aircraft on stratospheric aerosols and ozone. *Geophysical Research Letters,* **20,** 723–726.

Benkovitz, C.M., M.T. Scholtz, J. Pacyna, L. Tarrason, J. Dignon, E.V. Voldner, P.A. Spiro, J.A. Logan, and T.E. Graedel, 1996: Global gridded inventories of anthropogenic emissions of sulfur and nitrogen. *Journal of Geophysical Research,* **101,** 29239–29253.

Berger, B., U. Schumann, and D. Wurzel, 1994: Fuel consumption by airliners above and below the tropopause analyzed from operational flight plan data. In: *Impact of Emissions from Aircraft and Spacecraft upon the Atmosphere* [Schumann, U. and D. Wurzel (eds.)]. Proceedings of an international scientific colloquium, 18–20 April 1994, Cologne, Germany. DLR Mitteilung 94-06, Deutsches Zentrum für Luft- und Raumfahrt, Oberpfaffenhofen and Cologne, Germany, pp. 71–75.

Berntsen, T. and I.S.A. Isaksen, 1997: A global three-dimensional CTM for the troposphere. 1. Model description and CO and ozone results. *Journal of Geophysical Research,* **102,** 21239–21280.

Betancor-Gothe, M. and H. Grassl, 1993: Satellite remote sensing of the optical depth and mean crystal size of thin cirrus and contrails. *Theoretical and Applied Climatology,* **48,** 101–113.

Blake, D.F. and K. Kato, 1995: Latitudinal distribution of black carbon soot in the upper troposphere and lower stratosphere. *Journal of Geophysical Research,* **100,** 7195–7202.

Bockhorn, H. (ed.), 1994: *Soot Formation in Combustion. Mechanisms and Models.* Springer-Verlag, Berlin, Germany, 596 pp.

Borrmann, S., S. Solomon, J.E. Dye, and B.P. Luo, 1996: The potential of cirrus clouds for heterogeneous chlorine activation. *Geophysical Research Letters,* **23,** 2133–2136.

Borrmann, S., S. Solomon, J.E. Dye, D. Baumgardner, K.K. Kelly, and K.R. Chan, 1997: Heterogeneous reactions on stratospheric background aerosol, volcanic sulfuric acid droplets, and type I polar stratospheric clouds: effects of temperature fluctuations and differences in particle phase. *Journal of Geophysical Research,* **102,** 3639–3648.

Boucher, O. and T.L. Anderson, 1995: GCM assessment of the sensitivity of direct climate forcing by anthropogenic sulfate aerosols to aerosol size and chemistry. *Journal of Geophysical Research,* **100,** 26117–26134.

Boucher, O., 1998: *Is the Observed Trend in Cirrus Occurrence Due to Aviation?* Note Interne du LOA No. 1, Laboratoire d'Optique Atmosphérique, UFR de Physique, Université de Lille-I, Villeneuve d'Ascq, France, 17 pp.

Boucher, O., 1999: Influence of air traffic on cirrus occurrence. *Nature,* **397,** 30–31.

Brasseur, G.P., R.A. Cox, D. Hauglustaine, I. Isaksen, J. Lelieveld, D.H. Lister, R. Sausen, U. Schumann, A. Wahner, and P. Wiesen, 1998: European scientific assessment of the atmospheric effects of aircraft emissions. *Atmospheric Environment,* **32,** 2329–2418.

Brest, C.L., W.B. Rossow, and M.D. Roiter, 1997: Update of radiance calibrations for ISCCP. *Journal of Atmospheric and Oceanic Technology,* **14,** 1091–1109.

Brewer, A.W., 1946: Condensation trails. *Weather,* **1,** 34–40.

Brock, C.A., P. Hamill, J.C. Wilson, H.H. Jonsson, and K.R Chan, 1995: Particle formation in the upper tropical troposphere: a source of nuclei for the stratospheric aerosol. *Science,* **270,** 1650–1653.

Brogniez, G., J.-C. Buriez, V. Giraud, F. Parol, and C. Vanbauce, 1995: Determination of effective emittance and a radiatively equivalent microphysical model of cirrus from ground-based and satellite observations during the International Cirrus Experiment: the 18 October 1989 case study. *Monthly Weather Review,* **123,** 1025–1036.

Brown, R.C., M.R. Anderson, R.C. Miake-Lye, C.E. Kolb, A.A. Sorokin, and Y.I. Buriko, 1996a: Aircraft exhaust sulfur emissions. *Geophysical Research Letters,* **23,** 3603–3606.

Brown, R.C., R.C. Miake-Lye, M.R. Anderson, C.E. Kolb, and T.J. Resch, 1996b: Aerosol dynamics in near-field aircraft plumes. *Journal of Geophysical Research,* **101,** 22939–22953.

Brown, R.C., R.C. Miake-Lye, M.R. Anderson, and C.E. Kolb, 1996c: Effect of aircraft exhaust sulfur emissions on near field plume aerosols. *Geophysical Research Letters,* **23,** 3607–3610.

Brown, R.C., R.C. Miake-Lye, M.R. Anderson, and C.E. Kolb, 1997: Aircraft sulfur emissions and the formation of visible contrails. *Geophysical Research Letters,* **24,** 385–388.

Burtscher, H. 1992: Measurements and characteristics of combustion aerosols with special consideration of photoelectric charging and charging by flame ions. *Journal of Aerosol Science,* **23,** 549–595.

Busen, R. and U. Schumann, 1995: Visible contrail formation from fuels with different sulfur contents. *Geophysical Research Letters,* **22,** 1357–1360.

Calcote, H.F., 1983: Ionic mechanisms of soot formation. In: *Soot in Combustion Systems and its Toxic Properties* [Lahaye, J. and G. Prado (eds.)]. Plenum Press, London, United Kingdom, pp. 197–215.

Carleton, A.M. and P.J. Lamb, 1986: Jet contrails and cirrus clouds: a feasibility study employing high-resolution satellite imagery. *Bulletin of the American Meteorological Society,* **67,** 301–309.

Carslaw, K.S., T. Peter, and S.L. Clegg, 1997: Modeling the composition of liquid stratospheric aerosols. *Review of Geophysics,* **35,** 125–154.

Champagne, D.L., 1988: *Standard Measurement of Aircraft Gas Turbine Engine Exhaust Smoke*. ASME 71-GT-88, American Society of Mechanical Engineers, New York, NY, USA, 11 pp.

Changnon, S.A., 1981: Midwestern sunshine and temperature trends since 1901: possible evidence of jet contrail effects. *Journal of Applied Meteorology,* **20,** 496–508.

Charlson, R.J., J. Langner, and H. Rodhe, 1990: Sulphate aerosol and climate. *Nature,* **348,** 22.

Charlson, R.J., S.E. Schwartz, J.M. Hales, R.D. Cess, J.A. Coakley, Jr., J.E. Hansen, and D.J. Hofmann, 1992: Climate forcing by anthropogenic aerosols. *Science,* **255,** 423–430.

Chen, Y., S.M. Kreidenweis, L.M. McInnes, D.C. Rogers, and P.J. DeMott, 1998: Single particle analyses of ice nucleating aerosols in the upper troposphere and lower stratosphere. *Geophysical Research Letters,* **25,** 1391–1394.

Chin, M. and D.D. Davis, 1995: A reanalysis of carbonyl sulfide as a source of stratospheric background sulfur aerosol. *Journal of Geophysical Research,* **100,** 8993–9005.

Chin, M., D.J. Jacob, G.M. Gardner, M.S. Foreman-Fowler, P.A. Spiro, and D.L. Savoie, 1996: A global three-dimensional model of tropospheric sulfate. *Journal of Geophysical Research,* **101,** 18667–18690.

Chiou, E.W., M.P. McCormick, and W.P. Chu, 1997: Global water vapor distributions in the stratosphere and upper troposphere derived from 5.5 years of SAGE II observations (1986–1991). *Journal of Geophysical Research,* **102,** 19105–19118.

Chlond, A., 1998: Large-eddy simulation of contrails. *Journal of Atmospheric Sciences,* **55,** 796–819.

Chuan, R.L. and D.C. Woods, 1984: The appearance of carbon aerosol particles in the lower stratosphere. *Geophysical Research Letters,* **11,** 553–556.

Chughtai, A.R., M.E. Brooks, and D.M. Smith, 1996: Hydration of black carbon. *Journal of Geophysical Research,* **101,** 19505–19514.

CIAP, 1975: *Monograph 2: Propulsion Effluents in the Stratosphere*. Final Report of the Climatic Impact Assessment Program. DOT-TST-75-52, Department of Transportation, Washington, DC, USA, 746 pp.

Considine, D.B., A.R. Douglass, and C.H. Jackman, 1994: Effects of polar stratospheric cloud parameterization on ozone depletion due to stratospheric aircraft in a two-dimensional model. *Journal of Geophysical Research,* **99,** 18879–18894.

Cooke, W.F. and J.J.N. Wilson, 1996: A global black carbon aerosol model. *Journal of Geophysical Research,* **101,** 19395–19409.

Crutzen, P.J., 1976: The possible importance of OCS for the sulfate layer of the stratosphere. *Geophysical Research Letters,* **3,** 73–76.

Cruz, C.N. and S.N. Pandis, 1997: A study of the ability of pure secondary organic aerosol to act as cloud condensation nuclei. *Atmospheric Environment,* **31,** 2205–2214.

Cumpsty, N., 1997: *Jet Propulsion*. Cambridge University Press, Cambridge, United Kingdom, and New York, NY, USA, 281 pp.

Curtius, J., B. Sierau, F. Arnold, R. Baumann, R. Busen, P. Schulte, and U. Schumann, 1998: First direct sulfuric acid detection in the exhaust plume of a jet aircraft in flight. *Geophysical Research Letters,* **25,** 923–926.

Danilin, M.Y., A. Ebel, H. Elbern, and H. Petry, 1994: Evolution of the concentrations of trace species in an aircraft plume: trajectory study. *Journal of Geophysical Research,* **99,** 18951–18972.

Danilin, M.Y., J.M. Rodriguez, M.K.W. Ko, D.K. Weisenstein, R.C. Brown, R.C. Miake-Lye, and M.R. Anderson, 1997: Aerosol particle evolution in an aircraft wake: implications for the high speed civil transport fleet impact on ozone. *Journal of Geophysical Research,* **102,** 21453–21463.

Danilin, M.Y., D.W. Fahey, U. Schumann, M.J. Prather, J.E. Penner, M.K.W. Ko, D.K. Weisenstein, C.H. Jackman, G. Pitari, I. Köhler, R. Sausen, C.J. Weaver, A.R. Douglass, P.S. Connell, D.E. Kinnison, F.J. Dentener, E.L. Fleming, T.K. Berntsen, I.S.A. Isaksen, J.M. Haywood, and B. Kärcher, 1998: Aviation fuel tracer simulation: model intercomparison and implications. *Geophysical Research Letters,* **25,** 3947–3950.

DeGrand, J.Q., A.M. Carleton, and P.J. Lamb, 1990: A mid-season climatology of jet condensation trails from high-resolution satellite data. In: *Proceedings of the Seventh Conference on Atmospheric Radiation, July 23–27, 1990, San Francisco, CA*. American Meteorological Society, Boston, MA, USA, 309–311.

Del Negro, L.A., D.W. Fahey, S.G. Donnelly, R.S. Gao, E.R. Keim, R.C. Wamsley, E.L. Woodbridge, J.E. Dye, D. Baumgardner, B.W. Gandrud, J.C. Wilson, H.H. Jonsson, M. Loewenstein, J.R. Podolske, C.R. Webster, R.D. May, D.R. Worsnop, A. Tabazadeh, M.A. Tolbert, K.K. Kelly, and K.R. Chan, 1997: Evaluating the role of NAT, NAD, and liquid $H_2SO_4/H_2O/HNO_3$ solutions in Antarctic polar stratospheric cloud aerosol: observations and implications. *Journal of Geophysical Research,* **102,** 13255–13282.

DeMott, P.J., 1990: An explanatory study of ice nucleation by soot aerosols. *Journal of Applied Meteorology,* **19,** 1072–1079.

DeMott, P.J, D.C. Rogers, and S.M. Kreidenweis, 1997: The susceptibility of ice formation in upper tropospheric clouds to insoluble aerosol components. *Journal of Geophysical Research,* **102,** 19575–19584.

DeMott, P.J., D.C. Rogers, S.M. Kreidenweis, Y. Chen, C.H. Twohy, D. Baumgardner, A.J. Heymsfield, and K.R. Chan, 1998: The role of heterogeneous freezing nucleation in upper tropospheric clouds: inferences from SUCCESS. *Geophysical Research Letters,* **25,** 1387–1390.

Detwiler, A., 1983: Effects of artificial and natural cirrus clouds on temperatures near the ground. *Journal of Weather Modification,* **15,** 45–55.

Detwiler, A. and R. Pratt, 1984: Clear-air seeding: opportunities and strategies. *Journal of Weather Modification,* **16,** 46–60.

Dibb, J.E., R.W. Talbot, and M.B. Loomis, 1998: Tropospheric sulfate distribution during SUCCESS: contributions from jet exhaust and surface sources. *Geophysical Research Letters,* **25,** 1375–1378.

Diehl, J. and S.K. Mitra, 1998: A laboratory study of the effects of a kerosene burner exhaust on ice nucleation and the evaporation rate of ice crystals. *Atmospheric Environment,* **32,** 3145–3151.

Döpelheuer, A., 1997: *Berechnung der Produkte unvollständiger Verbrennung aus Luftfahrttriebwerken*. IB-325-09-97, Deutsche Zentrum für Luft- und Raumfahrt, Cologne, Germany, 38 pp.

Dowling, D.R. and L.F. Radke, 1990: A summary of physical properties of cirrus clouds. *Journal of Applied Meteorology,* **29,** 970–978.

Duda, D.P. and J.D. Spinhirne, 1996: Split-window retrieval of particle size and optical depth in contrails located above horizontally inhomogeneous ice clouds. *Geophysical Research Letters,* **23,** 3711–3714.

Duda, D.P., J.D. Spinhirne, and W.D. Hart, 1998: Retrieval of contrail microphysical properties during SUCCESS by the split-window method. *Geophysical Research Letters,* **25,** 1149–1152.

Dürbeck, T. and T. Gerz, 1996: Dispersion of aircraft exhausts in the free atmosphere. *Journal of Geophysical Research,* **101,** 26007–26015.

Ebert, E.E. and J.A. Curry, 1992: A parameterization of ice cloud optical properties for climate models. *Journal of Geophysical Research,* **97,** 3831–3836.

Ellingson, R.G. and Y. Fouquart, 1990: *The Intercomparison of Radiation Codes in Climate Models*. WCRP-39, WMO/TD Report no. 371, World Meteorological Organization, Geneva, Switzerland, 49 pp.

Fabian, P. and B. Kärcher, 1997: The impact of aviation upon the atmosphere: an assessment of present knowledge, uncertainties, and research needs. *Physics and Chemistry of the Earth,* **22,** 503–598.

Fahey, D.W., S.R. Kawa, E.L. Woodbridge, P. Tin, J.C. Wilson, H.H. Jonsson, J.E. Dye, D. Baumgardner, S. Borrmann, D.W. Toohey, L.M. Avallone, M.H. Proffitt, J. Margitan, M. Loewenstein, J.R. Podolske, R.J. Salawitch, S.C. Wofsy, M.K.W. Ko, D.E. Anderson, M.R. Schoeberl, and K.R. Chan, 1993: *In situ* measurements constraining the role of sulphate aerosols in mid-latitude ozone depletion. *Nature,* **363,** 509–514.

Fahey, D.W., E.R. Keim, K.A. Boering, C.A. Brock, J.C. Wilson, S. Anthony, T.F. Hanisco, P.O. Wennberg, R.C. Miake-Lye, R.J. Salawitch, N. Louisnard, E.L. Woodbridge, R.S. Gao, S.G. Donnelly, R. Wamsley, L.A. DelNegro, B.C. Daube, S.C. Wofsy, C.R. Webster, R.D. May, K.K. Kelly, M. Lowenstein, J.R. Podolske, and K.R. Chan, 1995a: Emission measurements of the Concorde supersonic aircraft in the lower stratosphere. *Science,* **270,** 70–74.

Fahey, D.W., E.R. Keim, E.L. Woodbridge, R.S. Gao, K.A. Boering, B.C. Daube, S.C. Wofsy, R.P. Lohmann, E.J. Hintsa, A.E. Dessler, C.R. Webster, R.D. May, C.A. Brock, J.C. Wilson, R.C. Miake-Lye, R.C. Brown, J.M. Rodriguez, M. Lowenstein, M.H. Proffitt, R.M. Stimpfle, S.W. Bowen, and K.R. Chan, 1995b: *In situ* observations in aircraft exhaust plumes in the lower stratosphere at mid-latitudes. *Journal of Geophysical Research,* **100,** 3065–3074.

Fairbrother, D.H., D.J.D. Sullivan, and H.S. Johnston, 1997: Global thermodynamical atmospheric modeling: search for new heterogeneous reactions. *Journal of Physical Chemistry,* **101,** 7350–7358.

Feichter, J., E. Kjellström, H. Rodhe, F. Dentener, J. Lelieveld, and G.-J. Roelofs. 1996: Simulation of the tropospheric sulfur cycle in a global climate model. *Atmospheric Environment,* **30,** 1693–1708.

Fordyce, J.S. and D.W. Sheibley, 1975: Estimate of contribution of jet aircraft operation to trace element concentration at or near airports. *Journal of the Air Pollution Control Association,* **25,** 721–724.

Fortuin, J.P.F., R. van Dorland, W.M.F. Wauben, and H. Kelder, 1995: Greenhouse effects of aircraft emissions as calculated by a radiative transfer model. *Annales Geophysicae,* **13,** 413–418.

Fowler, L.D., D.A. Randall, and S.A. Rutledge, 1996: Liquid and ice cloud microphysics in the CSU general circulation model. Part I: Model description and microphysical processes. *Journal of Climate,* **9,** 489–529.

Frankel, D., K.N. Liou, S.C. Ou, D.P. Wylie, and P. Menzel, 1997: Observations of cirrus cloud extent and their impacts to climate. In: *Proceedings, Ninth Conference on Atmospheric Radiation, February 2–7, 1997, Long Beach, CA.* American Meteorological Society, Boston, MA, USA, Vol. 13.1, pp. 414–417.

Frenzel, A. and F. Arnold, 1994: Sulfuric acid cluster ion formation by jet engines: implications for sulfuric acid formation and nucleation. In: *Impact of Aircraft Emissions upon the Atmosphere* [Schumann, U. and D. Wurzel, (eds.)]. Proceedings of an international scientific colloquium, 18–20 April 1994, Cologne, Germany. DLR-Mitteilung 94-06, Deutsches Zentrum für Luft- und Raumfahrt, Oberpfaffenhoffen and Cologne, Germany, pp. 106–112.

Freudenthaler, V., F. Homburg, and H. Jäger, 1995: Contrail observations by ground-based scanning lidar: cross-sectional growth. *Geophysical Research Letters,* **22,** 3501–3504.

Freudenthaler, V., F. Homburg, and H. Jäger, 1996: Optical parameters of contrails from lidar measurements: linear depolarization. *Geophysical Research Letters,* **23,** 3715–3718.

Friedl, R.R. (ed.), 1997: *Atmospheric Effects of Subsonic Aircraft: Interim Assessment Report of the Advanced Subsonic Technology Program.* NASA Reference Publication 1400, National Aeronautics and Space Administration, Goddard Space Flight Center, Greenbelt, MD, USA, 168 pp.

Fu, Q. and K.N. Liou, 1993: Parameterization of the radiative properties of cirrus clouds. *Journal of Atmospheric Sciences,* **50,** 2008–2025.

Gao, R.S., B. Kärcher, E.R. Keim, and D.W. Fahey, 1998: Constraining the heterogeneous loss of O_3 on soot particles with observations in jet engine exhaust plumes. *Geophysical Research Letters,* **25,** 3323–3326.

Gayet, J.-F., G. Febvre, G. Brogniez, H. Chepfer, W. Renger, and P. Wendling, 1996: Microphysical and optical properties of cirrus and contrails: cloud field study on 13 October 1989. *Journal of Atmospheric Sciences,* **53,** 126–138.

Gayet, J.-F., F. Auriol, S. Oshchepkov, F. Schröder, C. Duroure, G. Febvre, J.-F. Fournol, O. Crépel, P. Personne, and D. Daugereon, 1998: *In situ* measurements of the scattering phase function of stratocumulus, contrails and cirrus. *Geophysical Research Letters,* **25,** 971–974.

Gerz, T., T. Dürbeck, and P. Konopka, 1998: Transport and effective diffusion of aircraft emissions. *Journal of Geophysical Research,* **103,** 25905–25913.

Gettelman, A., 1998: The evolution of aircraft emissions in the stratosphere. *Geophysical Research Letters,* **25,** 2129–2132.

Gierens, K., 1996: Numerical simulations of persistent contrails. *Journal of Atmospheric Sciences,* **53,** 3333–3348.

Gierens, K. and U. Schumann, 1996: Colors of contrails from fuels with different sulfur contents. *Journal of Geophysical Research,* **101,** 16731–16736.

Gierens, K. and J. Ström, 1998: A numerical study of aircraft wake induced ice cloud formation. *Journal of Atmospheric Sciences,* **55,** 3253–3263.

Gierens, K., U. Schumann, H.G.J. Smit, M. Helten, and G. Zangl, 1997: Determination of humidity and temperature fluctuations based on MOZAIC data and parameterisation of persistent contrail coverage for general circulation models. *Annales Geophysicae,* **15,** 1057–1066.

Gierens, K., R. Sausen, and U. Schumann, 1998: A diagnostic study of the global distribution of contrails. Part II: Future air traffic scenarios. *Theoretical and Applied Climatology,* (in press).

Gierens, K., U. Schumann, M. Helten, H. Smit, and A. Marenco, 1999: A distribution law for relative humidity in the upper troposphere and lower stratosphere derived from three years of MOZAIC measurements. *Annales Geophysicae,* (in press).

Gleitsmann, G. and R. Zellner, 1998a: The effects of ambient temperature and relative humidity on particle formation in the jet regime of commercial aircrafts: a modelling study. *Atmospheric Environment,* **32,** 3079–3087.

Gleitsmann, G. and R. Zellner, 1998b: A modelling study of the formation of cloud condensation nuclei in the jet regime of aircraft plumes. *Journal of Geophysical Research,* **103,** 19543–19556.

Goldberg, E.D., 1985: *Black Carbon in the Environment.* Wiley-Interscience, New York, NY, USA, 198 pp.

Goodman, J., R.F. Pueschel, E.J. Jensen, S. Verma, G.V. Ferry, S.D. Howard, S.A. Kinne, and D. Baumgardner, 1998: Shape and size of contrail ice particles. *Geophysical Research Letters,* **25,** 1327–1330.

Grassl, H., 1970: Determination of cloud drop size distributions from spectral transmission measurements. *Beiträge zur Physik der Atmosphäre,* **43,** 255–284.

Grassl, H., 1990: Possible climatic effects of contrails and additional water vapour. In: *Air Traffic and the Environment—Background, Tendencies, and Potential Global Atmospheric Effects* [Schumann, U. (ed.)]. Springer-Verlag, Heidelberg, Germany, pp. 124–137.

Hagen, D.E., M.B. Trueblood, and P.D. Whitefield, 1992: A field sampling of jet exhaust aerosols. *Particle Science Technology,* **10,** 53–63.

Hagen, D.E., P. Whitefield, J. Paladino, M. Trueblood, and H. Lilenfeld, 1998: Particulate sizing and emission indices for a jet engine exhaust sampled at cruise. *Geophysical Research Letters,* **25,** 1681–1684.

Hahn, C.J., S.G. Warren, and J. London, 1994: *Climatological Data for Clouds Over the Globe from Surface Observations, 1982–1991: The Total Cloud Edition.* Report no. NDP026A, Carbon Dioxide Information Analysis Center, Oak Ridge National Laboratory, Oak Ridge, TN, USA, 42 pp. [Also available from Data Support Section, National Center for Atmospheric Research, Boulder, CO, USA.]

Hahn, C. J., S.G. Warren, and J. London, 1995: The effect of moonlight on observation of cloud cover at night, and application to cloud climatology. *Journal of Climate,* **8,** 1429–1446.

Hahn, C. J., S.G. Warren, and J. London, 1996: *Edited Synoptic Cloud Reports from Ships and Land Stations over the Globe, 1982–1991.* Report no. NDP026B, Carbon Dioxide Information Analysis Center, Oak Ridge National Laboratory, Oak Ridge, TN, USA, 45 pp.

Halpert, M.S. and G.D. Bell, 1997: Climate assessment for 1996. *Bulletin of the American Meteorological Society,* **78,** S1–S49.

Hamill, P., E.J. Jensen, P.B. Russell, and J.J. Bauman, 1997: The life cycle of stratospheric aerosol particles. *Bulletin of the American Meteorological Society,* **78,** 1395–1410.

Hanisco, T.F., P.O. Wennberg, R.C. Cohen, J.G. Anderson, D.W. Fahey, E.R. Keim, R.S. Gao, R.C. Wamsley, S.G. Donnelly, L.A. DelNegro, R.S. Salawitch, K.K. Kelly, and M.H. Proffitt, 1997: The role of HO_x in super- and subsonic aircraft exhaust plumes. *Geophysical Research Letters,* **24,** 65–68.

Hannegan, B., S. Olsen, M. Prather, X. Zhu, D. Rind, and J. Lerner, 1998: The dry stratosphere: a limit on cometary influx. *Geophysical Research Letters,* **25,** 1649–1652.

Hansen, J.E., M. Sato, and R. Ruedy, 1995: Long-term changes in diurnal temperature range: implications about mechanisms of global climate change. *Atmospheric Research,* **37,** 175–209.

Hansen, J., R. Ruedy, M. Sato, and R. Reynolds, 1996: Global surface air temperature in 1995: return to pre-Pinatubo level. *Geophysical Research Letters,* **23,** 1665–1668.

Hansen, J., M. Sato, and R. Ruedy, 1997: Radiative forcing and climate response. *Journal of Geophysical Research,* **102,** 6831–6864.

Hasselmann, K., 1997: Are we seeing global warming? *Science,* **276,** 914–915.

Hauf, T. and R. Alheit, 1997: Transport of pollutants by gravitational settling of ice crystals. In: *Pollutants from Air Traffic – Results of Atmospheric Research 1992–1997* [Schumann, U., A. Chlond, A. Ebel, B. Kärcher, H. Pak, H. Schlager, A. Schmitt, and P. Wendling (eds.)]. DLR-Mitteilung 97-04, Deutsches Zentrum für Luft- und Raumfahrt, Oberpfaffenhofen and Cologne, Germany, pp. 197–206.

Haywood, J.M. and V. Ramaswamy, 1998: Global sensitivity studies of the direct radiative forcing due to anthropogenic sulfate and black carbon aerosols. *Journal of Geophysical Research,* **103,** 6043–6058.

Helten, M., H. G. J. Smit, W. Sträter, D. Kley, P. Nedelec, M. Zöger, and R. Busen, 1998: Calibration and performance of automatic compact instrumentation for the measurement of relative humidity from passenger aircraft. *Journal of Geophysical Research,* **103,** 25643–25652.

Henderson-Sellers, A., 1989: North American total cloud amount variations this century. *Paleogeography, Paleoclimatology, and Paleoecology,* **75,** 175–194.

Henderson-Sellers, A., 1992: Continental cloudiness changes this century. *Geo Journal,* **27,** 255–262.

Heymsfield, A.J. 1993: Microphysical structures of stratiform and cirrus clouds. In: *Aerosol-Cloud-Climate Interactions* [Hobbs, P.V. (ed.)]. Academic Press, San Diego, CA, USA, pp. 97–121.

Heymsfield, A.J. and L.M. Miloshevich, 1995: Relative humidity and temperature influences on cirrus formation and evolution: observations from wave clouds and FIRE II. *Journal of Atmospheric Sciences,* **52,** 4302–4326.

Heymsfield, A.J., R.P. Lawson, and G.W. Sachse, 1998a: Growth of ice crystals in a precipitating contrail. *Geophysical Research Letters,* **25,** 1335–1338.

Heymsfield, A.J., L.M. Miloshevich, C. Twohy, G. Sachse, and S. Oltmans, 1998b: Upper tropospheric relative humidity observations and implications for cirrus ice nucleation. *Geophysical Research Letters,* **25,** 1343–1346.

Hitchman, M., M. McKay, and C.R. Trepte, 1994: A climatology of stratospheric aerosol. *Journal of Geophysical Research,* **99,** 20689–20700.

Hofmann, D.J., 1990: Increase of the stratospheric background sulfuric acid aerosol mass in the past 10 years. *Science,* **248,** 996–1000.

Hofmann, D.J., 1991: Aircraft sulfur emissions. *Nature,* **349,** 659.

Hofmann, D.J., 1993: Twenty years of balloon-borne tropospheric aerosol measurements at Laramie, Wyoming. *Journal of Geophysical Research,* **98,** 12753–12766.

Hofmann, D.J. and J.M. Rosen, 1978: Balloon observations of a particle layer injected by stratospheric aircraft at 23 km. *Geophysical Research Letters,* **5,** 511–514.

Hofmann, D.J. and S. Solomon, 1989: Ozone destruction through heterogeneous chemistry following the eruption of El Chichon. *Journal of Geophysical Research,* **94,** 5029–5041.

Hofmann, D.J., R.S. Stone, M.E. Wood, T. Deshler, and J.M. Harris, 1998: An analysis of 25 years of balloon-borne aerosol data in search of a signature of the subsonic commercial aircraft fleet. *Geophysical Research Letters,* **25,** 2433–2436.

Höhndorf, F., 1941: *Beitrag zum Problem der Vermeidung von Auspuffwolken hinter Motorflugzeugen.* Forschungsbericht no. 1371, Deutsche Luftforschung, Aerologisches Institut, Deutsche Forschungsanstalt für Segelflug e.V., 15 pp. [Also available from Air Documents Division, T-2, AMC, Wright Field, Ohio, KA, USA, Microfilm no. R 2317 F 834.].

Hoinka, K.P., 1998: Statistics of the global tropopause pressure. *Monthly Weather Review,* **126,** 3303–3325.

Hoinka, K.-P., M.-E. Reinhardt, and W. Metz, 1993: North Atlantic air traffic within the lower stratosphere: cruising times and corresponding emissions. *Journal of Geophysical Research,* **98,** 23113–23131.

Howard, R.P., R.S. Hiers, P.D. Whitefield, D.E. Hagen, J.C. Wormhoudt, R.C. Miake-Lye, and R. Strange, 1996: *Experimental Characterization of Gas Turbine Emissions at Simulated Flight Altitude Conditions.* AEDC-TR-96-3, Arnold Engineering Development Center, National Technical Information Service, Arnold Air Force Base, TN, USA, 159 pp.

Hunter, S.C., 1982: Formation of SO_3 in gas turbines. *Transactions of the ASME Journal of Engineering Power,* **104,** 44–51.

Hurrell, J., 1995: Decadal trends in the North Atlantic oscillation: regional temperatures and precipitation. *Science,* **269,** 676–679.

IPCC, 1996: *Climate Change 1995: The Science of Climate Change. Contribution of Working Group I to the Second Assessment Report of the Intergovernmental Panel on Climate Change* [Houghton, J.T., L.G. Meira Filho, B.A. Callander, N. Harris, A. Kattenberg, and K. Maskell (eds.)]. Cambridge University Press, Cambridge, United Kingdom and New York, NY, USA, 572 pp.

Jackman, C.H., E.L. Fleming, S. Chandra, D.B. Considine, and J.E. Rosenfield, 1996: Past, present, and future modeled ozone trends with comparisons to observed trends. *Journal of Geophysical Research,* **101,** 28753–28767.

Jacob, D.J. and M.R. Hoffmann, 1983: A dynamic model for the production of H^+, NO^{3-}, and SO_4^{2-} in urban smog. *Journal of Geophysical Research,* **88,** 6611–6621.

Jäger, H. and D. Hofmann, 1991: Mid-latitude lidar backscatter to mass, area, and extinction conversion model based on *in situ* aerosol measurements from 1980 to 1997. *Applied Optics,* **30,** 127–138.

Jäger, H., V. Freudenthaler, and F. Homburg, 1998: Remote sensing of optical depth of aerosols and clouds cover related to air traffic. *Atmospheric Environment,* **32,** 3123–3127.

Jensen, E.J. and O.B. Toon, 1992: The potential effects of volcanic aerosols on cirrus cloud microphysics. *Geophysical Research Letters,* **19,** 1759–1762.

Jensen, E.J. and O.B. Toon, 1994: Ice nucleation in the upper troposphere: sensitivity to aerosol number density, temperature, and cooling rate. *Geophysical Research Letters,* **21,** 2019–2022.

Jensen, E.J. and O.B. Toon, 1997: The potential impact of soot particles from aircraft exhaust on cirrus clouds. *Geophysical Research Letters,* **24,** 249–252.

Jensen, E.J., S. Kinne, and O.B. Toon, 1994a: Tropical cirrus cloud radiative forcing: sensitivity studies. *Geophysical Research Letters,* **21,** 2023–2026.

Jensen, E.J., O.B. Toon, D.L. Westphal, S. Kinne, and A.J. Heymsfield, 1994b: Microphysical modeling of cirrus. 1. Comparison with 1986 FIRE IFO measurements. *Journal of Geophysical Research,* **99,** 10421–10442.

Jensen, E.J., O.B. Toon, S. Kinne, G.W. Sachse, B.E. Anderson, K.R. Chan, C.H. Twohy, B. Gandrud, A. Heymsfield, and R.C. Miake-Lye, 1998a: Environmental conditions required for contrail formation and persistence. *Journal of Geophysical Research,* **103,** 3929–3936.

Jensen, E.J., O.B. Toon, R.F. Pueschel, J. Goodman, G.W. Sachse, B.E. Anderson, K.R. Chan, D. Baumgardner, and R.C. Miake-Lye, 1998b: Ice crystal nucleation and growth in contrails forming at low ambient temperatures. *Geophysical Research Letters,* **25,** 1371–1374.

Jensen, E.J., O.B. Toon, A. Tabazadeh, G.W. Sachse, B.E. Anderson, K.R. Chan, C.W. Twohy, B. Gandrud, S.M. Aulenbach, A.J. Heymsfield, J. Hallett, and B. Gary, 1998c: Ice nucleation processes in upper tropospheric wave-clouds observed during SUCCESS. *Geophysical Research Letters,* **25,** 1363–1366.

Jensen, E.J., A.S. Ackerman, D.E. Stevens, O.B. Toon, and P. Minnis, 1998d: Spreading and growth of contrails in a sheared environment. *Journal of Geophysical Research,* **103,** 31557–31567.

Joseph, J.H., Z. Levin, Y. Mekler, G. Ohring, and J. Otterman, 1975: Study of contrails observed from the ERST 1 satellite imagery. *Journal of Geophysical Research,* **80,** 366–372.

Kapala, A., H. Mächel, and H. Flohn, 1998: Behaviour of the centres of action above the Atlantic since 1881. Part II: Associations with regional climate anomalies. *International Journal of Climatology,* **18,** 23–36.

Kärcher, B., 1996: Aircraft-generated aerosols and visible contrails. *Geophysical Research Letters,* **23,** 1933–1936.

Kärcher, B., 1997: Heterogeneous chemistry in aircraft wakes: constraints for uptake coefficients. *Journal of Geophysical Research,* **102,** 19119–19135.

Kärcher, B., 1998a: Physicochemistry of aircraft-generated liquid aerosols, soot, and ice particles. 1. Model description. *Journal of Geophysical Research,* **103,** 17111–17128.

Kärcher, B., 1998b: On the potential importance of sulfur-induced activation of soot particles in nascent jet aircraft exhaust plumes. *Atmospheric Research,* **46,** 293–305.

Kärcher, B. and D.W. Fahey, 1997: The role of sulfur emissions in volatile particle formation in jet aircraft exhaust plumes. *Geophysical Research Letters,* **24,** 389–392.

Kärcher, B., T. Peter, and R. Ottmann, 1995: Contrail formation: homogeneous nucleation of H_2SO_4/H_2O droplets. *Geophysical Research Letters,* **22,** 1501–1504.

Kärcher, B., M.M. Hirschberg, and P. Fabian, 1996a: Small-scale chemical evolution of aircraft exhaust species at cruising altitude. *Journal of Geophysical Research,* **101,** 15169–15190.

Kärcher, B., T. Peter, U.M. Biermann, and U. Schumann, 1996b: The initial composition of jet condensation trails. *Journal of Atmospheric Sciences,* **53,** 3066–3083.

Kärcher, B., R. Busen, A. Petzold, F.P. Schröder, U. Schumann, and E.J. Jensen, 1998a: Physicochemistry of aircraft-generated liquid aerosols, soot, and ice particles. 2. Comparison with observations and sensitivity studies. *Journal of Geophysical Research,* **103,** 17129–17148.

Kärcher, B., F. Yu, F.P. Schröder, and R.P. Turco, 1998b: Ultrafine aerosol particles in aircraft plumes: analysis of growth mechanisms. *Geophysical Research Letters,* **25,** 2793–2796.

Karl, T.R., G. Kukla, and J. Gavin, 1984: Decreasing diurnal temperature range in the United States and Canada from 1941 through 1980. *Journal of Climate and Applied Meteorology,* **23,** 1489–1504.

Karl, T.R., P.D. Jones, R.W. Knight, G. Kukla, N. Plummer, V. Razuvayev, K.P. Gallo, J. Lindseay, R.J. Charlson, and T.C. Peterson, 1993: A new perspective on recent global warming: asymmetric trends of daily maximum and minimum temperature. *Bulletin of the American Meteorological Society,* **74,** 1007–1023.

Kästner, M., K.T. Kriebel, R. Meerkötter, W. Renger, G.H. Ruppersberg, and P. Wendling, 1993: Comparison of cirrus height and optical depth derived from satellite and aircraft measurements. *Monthly Weather Review,* **121,** 2708–2717.

Katz, J.L., F.C. Wen, T. McLaughlin, R.J. Reusch, and R. Partch, 1977: Nucleation on photoexcited molecules. *Science,* **196,** 1203–1205.

Keil, D.G., R.J. Gill, D.B. Olson, and H.F. Calcote, 1984: Ion concentration in premixed acetylene-oxygen flames near soot threshold. In: *The Chemistry of Combustion Processes* [Sloane, T.M. (ed.)]. American Chemical Society, Washington, DC, USA, pp. 33–43.

Kent, G.S., P.H. Wang, M.P. McCormick, and K.M. Skeens, 1995: Multiyear Stratospheric Aerosol and Gas Experiment II measurements of upper tropospheric aerosol characteristics. *Journal of Geophysical Research,* **100,** 13875–13899.

Kent, G.S., C.R. Trepte, and P.L. Lucker, 1998: Long-term Stratospheric Aerosol and Gas Experiment I and II measurements of upper tropospheric aerosol extinction. *Journal of Geophysical Research,* **103,** 28863–28874.

King, M.D., Y.J. Kaufman, W.P. Menzel, and D. Tanre, 1992: Remote sensing of cloud, aerosol, and water vapor properties from the moderate resolution imaging spectrometer (MODIS). *IEEE Transactions on Geoscience and Remote Sensing,* **30,** 2–27.

Kinne, S., and K.-N. Liou, 1989: The effects of the nonsphericity and size distribution of ice crystals on the radiative properties of cirrus clouds. *Atmospheric Research,* **24,** 273–284.

Kinne, S., T.P. Ackerman, M. Shiobara, A. Uchiyama, A.J. Heymsfield, L. Miloshevich, J. Wendell, E.W. Eloranta, C. Purgold, and R.W. Bergstrom, 1997: Cirrus cloud radiative and microphysical properties from ground observations and *in situ* measurements during FIRE 1991 and their application to exhibit problems in cirrus cloud radiative transfer modeling. *Journal of Atmospheric Science,* **54,** 2320–2344.

Kinnison, D.E., K.E. Grant, P.S. Connell, D.A. Rotman, and D.J. Wuebbles, 1994: The chemical and radiative effects of the Mt. Pinatubo eruption. *Journal of Geophysical Research,* **99,** 25705–25731.

Kjellström, E., J. Feichter, R. Sausen, and R. Hein, 1998: The contribution of aircraft emissions to the atmospheric sulfur budget. *Atmospheric Environment,* (in press). [Also available as Report no. CM-93, Department of Meteorology, University of Stockholm, Sweden.]

Klein, S.A. and D.L. Hartmann, 1993: Spurious changes in the ISCCP data set. *Geophysical Research Letters,* **20,** 455–458.

Knollenberg, R.G., 1972: Measurements of the growth of ice budget in a persisting contrail. *Journal of Atmospheric Sciences,* **29,** 1367–1374.

Kolb, C.E., J.T. Jayne, D.R. Worsnop, M.J. Molina, R.F. Meads, and A.A. Viggiano, 1994: Gas phase reaction of sulfur trioxide with water vapor. *Journal of the American Chemical Society,* **116,** 10314–10315.

Konopka, P. and W. Vogelsberger, 1997: Köhler equation for finite systems: a simple estimation of possible condensation mechanisms in aircraft contrails. *Journal of Geophysical Research,* **102,** 16057–16064.

Konrad, T.G. and J.C. Howard, 1974: Multiple contrail streamers observed by radar. *Journal of Applied Meteorology,* **13,** 563–572.

Kotzick, R., U. Panne, and R. Niessner, 1997: Changes in condensation properties of ultrafine carbon particles subjected to oxidation by ozone. *Journal of Aerosol Science,* **28,** 725–735.

Kuhn, P.M., 1970: Airborne observations of contrail effects on the thermal radiation budget. *Journal of Atmospheric Sciences,* **27,** 937–942.

Laaksonen, A., J. Hienola, M. Kulmala, and F. Arnold, 1997: Supercooled cirrus cloud formation modified by nitric acid perturbation of the upper troposphere. *Geophysical Research Letters,* **24,** 3009–3012.

Lacis, A.A. and M.I. Mishchenko, 1995: Climate forcing, climate sensitivity, and climate response: A radiative modeling perspective of atmospheric aerosols. In: *Aerosol Forcing of Climate* [Charlson, R.J. and J. Heintzenberg (eds.)]. J. Wiley, Chichester, United Kingdom, pp. 11–42.

Lacis, A., J. Hansen, and M. Sato, 1992: Climate forcing by stratospheric aerosols. *Geophysical Research Letters,* **19,** 1607–1610.

Langner, J. and H. Rodhe, 1991: A global three-dimensional model of the tropospheric sulfur cycle. *Journal of Atmospheric Chemistry,* **13,** 225–263.

Lary, D.J., A.M. Lee, R. Toumi, M. Newchurch, M. Pierre, and J.B. Renard, 1997: Carbon aerosols and atmospheric photochemistry. *Journal of Geophysical Research,* **102,** 3671–3682.

Lawson, R.P., A.J. Heymsfield, S.M. Aulenbach, and T.L. Jensen, 1998: Shapes, sizes and light scattering properties of ice crystals in cirrus and a persistent contrail during SUCCESS. *Geophysical Research Letters,* **25,** 1331–1334.

Lee, T.F., 1989: Jet contrail identification using the AVHRR infrared split window. *Journal of Applied Meteorology,* **28,** 993–995.

Lewellen, D.C. and W.S. Lewellen, 1996: Large eddy simulations of the vortex-pair breakup in aircraft wakes. *AIAA Journal,* **34,** 2337–2345.

Liepert, B.G., 1997: Recent changes in solar radiation under cloudy conditions. *International Journal of Climatology,* **17,** 1581–1593.

Liepert, B., P. Fabian, and H. Grassl, 1994: Solar radiation in Germany—observed trends and an assessment of their causes. Part I: Regional approach. *Beiträge zur Physik der Atmosphäre,* **67,** 15–29.

Liou, K., 1986: Influence of cirrus clouds on weather and climate processes: a global perspective. *Monthly Weather Review,* **114,** 1167–1199.

Liou, K.-N., S.C. Ou, and G. Koenig, 1990: An investigation of the climatic effect of contrail cirrus. In: *Air Traffic and the Environment: Background, Tendencies, and Potential Global Atmospheric Effects* [Schumann, U. (ed.)]. Springer-Verlag, Berlin, Germany, pp. 154–169.

Liousse, C., J.E. Penner, C. Chuang, J.J. Walton, H. Eddleman, and H. Cachier, 1996: A global three-dimensional model study of carbonaceous aerosols. *Journal of Geophysical Research,* **101,** 19411–19432.

Lohmann, U. and E. Roeckner, 1995: Influence of cirrus cloud radiative forcing on climate and climate sensitivity in a general circulation model. *Journal of Geophysical Research,* **100,** 16305–16323.

Lovejoy, E.R., D.R. Hanson, and L.G. Huey, 1996: Kinetics and products of the gas phase reaction of SO_3 with water. *Journal of Physical Chemistry,* **100,** 19911–19916.

Ludlam, F.H, 1980: *Clouds and Storms*. The Pennsylvania State University Press, University Park, PA, USA.

Lukachko, S.P., I.A. Waitz, R.C. Miake-Lye, R.C. Brown, and M.R. Anderson, 1998: Production of sulfate aerosol precursors in the turbine and exhaust nozzle of an aircraft engine. *Journal of Geophysical Research,* **103,** 16159–16174.

Mächel, H., A. Kapala, and H. Flohn, 1998: Behaviour of the centres of action above the Atlantic since 1881. Part I: Characteristics of seasonal and interannual variability. *International Journal of Climatology,* **18,** 1–22.

Mannstein, H., 1997: Contrail observations from space using NOAA-AVHRR data. In: *Impact of Aircraft upon the Atmosphere*. Proceedings of an international scientific colloquium, 15–18 October 1996, Paris, France, Office National d'Etudes et de Recherches Aerospatiales, Chatillon, France, Vol. II, pp. 427–431.

Mannstein, H., R. Meyer, and P. Wendling, 1999: Operational detection of contrails from NOAA-AVHRR-data. *International Journal of Remote Sensing*. (in press).

Mazin, I.P., 1996: Aircraft condensation trails. *Izvestiya, Atmospheric, and Oceanic Physics,* **32,** 1–13.

McClatchey, R.A.M., R.W. Fenn, J.E.A. Selby, F.E. Volz, and J.S. Garing, 1972: *Optical Properties of the Atmosphere*. AFCRL-72-0497, Air Force Cambridge Research Laboratory, Bedford, MA, USA, 3rd ed., 113 pp.

Meerkötter, R., U. Schumann, D.R. Doelling, P. Minnis, T. Nakajima, and Y. Tsushima, 1999: Radiative forcing by contrails. *Annales Geophysicae,* (in press).

Miake-Lye, R.C., M. Martinez-Sanchez, R.C. Brown, and C.E. Kolb, 1993: Plume and wake dynamics, mixing and chemistry behind an HSCT aircraft. *Journal of Aircraft,* **30,** 467–479.

Miake-Lye, R.C., R.C. Brown, M.R. Anderson, and C.E. Kolb, 1994: Calculation of condensation and chemistry in an aircraft contrail. In: *Impact of Emissions from Aircraft and Spacecraft upon the Atmosphere* [Schumann, U. and D. Wurzel (eds.)]. Proceedings of an international scientific colloquium, 18–20 April 1994, Cologne, Germany. DLR-Mitteilung 94-06, Deutsches Zentrum für Luft- und Raumfahrt, Oberpfaffenhofen and Cologne, Germany, pp. 274–279.

Miake-Lye, R.C., B.E. Anderson, W.R. Cofer, H.A. Wallio, G.D. Nowicki, J.O. Ballenthin, D.E. Hunton, W.B. Knighton, T.M. Miller, J.V. Seeley, and A.A. Viggiano, 1998: SO_x oxidation and volatile aerosol in aircraft exhaust plumes depend on fuel sulfur content. *Geophysical Research Letters,* **25,** 1677–1680.

Minnis, P., E.F. Harrison, L.L. Stowe, G.G. Gibson, F.M. Denn, D.R. Doelling, and W.L. Smith, Jr., 1993: Radiative climate forcing by the Mount Pinatubo eruption. *Science,* **259,** 1411–1415.

Minnis, P., J.K. Ayers, and S.P. Weaver, 1997: *Surface-Based Observations of Contrail Occurrence Frequency Over the U.S., April 1993–April 1994.* NASA Reference Publication 1404, National Aeronautics and Space Administration, Hampton, VA, USA, 79 pp.

Minnis, P., D.F. Young, D.P. Garber, L. Nguyen, W.L. Smith, Jr., and R. Palikonda, 1998a: Transformation of contrails into cirrus during SUCCESS. *Geophysical Research Letters,* **25,** 1157–1160.

Minnis, P., U. Schumann, D.R. Doelhing, J.K. Ayers, R. Palikonda, L. Nguyen, D.F. Young, and K.M. Gierens, 1998b: Contrails: another factor in climate change? *Science,* (under revision).

Minnis, P., D.P. Garber, D.F. Young, R.F. Arduini, and Y. Takano, 1998c: Parameterizations of reflectance and effective emittance for satellite remote sensing of cloud properties. *Journal of Atmospheric Science,* **55,** 3313–3339.

Minnis, P., U. Schumann, D.R. Doelling, K.M. Gierens, and D.W. Fahey, 1999: Global distribution of contrail radiative forcing. *Geophysical Research Letters,* (in press).

Mirabel, P. and J.L. Katz, 1974: Binary homogeneous nucleation as a mechanism for the formation of aerosols. *Journal of Chemical Physics,* **60,** 1138–1144.

Murcray, W.B., 1970: On the possibility of weather modification by aircraft contrails. *Monthly Weather Review,* **98,** 745–748.

Murphy, D.M., K.K. Kelly, A.F. Tuck, and M.H. Proffitt, 1990: Ice saturation at the tropopause observed from the ER-2 aircraft. *Geophysical Research Letters,* **17,** 353–356.

Nakajima, T. and M. Tanaka, 1986: Matrix formulations for the transfer of solar radiation in a plane-parallel scattering atmosphere. *Journal of Quantum Spectroscopic Radiation Transfer,* **35,** 13–21.

Nakajima, T., and M. Tanaka, 1988: Algorithms for radiative intensity calculations in moderately thick atmospheres using a truncation approximation. *Journal of Quantum Spectroscopic Radiation Transfer,* **40,** 51–69.

Oltmans, S.J. and D.J. Hofmann, 1995: Increase in lower-stratospheric water vapour at mid-latitude Northern Hemisphere site from 1981 to 1994. *Nature,* **374,** 146–149.

Ovarlez, J., H. Ovarlez, R.M. Philippe, and E. Landais, 1997: Water vapor measurements during the POLINAT campaigns. In: *Pollution from Aircraft Emissions in the North Atlantic Flight Corridor (POLINAT)* [Schumann, U. (ed.)]. EUR-16978-EN, Office for Publications of European Communities, Brussels, Belgium, pp. 70–81.

Paladino, J., P. Whitefield, D. Hagen, A.R. Hopkins, and M. Trueblood, 1998: Particle concentrations characterization for jet engine emissions under cruise conditions. *Geophysical Research Letters,* **25,** 1697–1700.

Parker, D.E., M. Gordon, D.P.N. Cullum, D.M.H. Sexton, C.K. Folland, and N. Rayner, 1997: A new global gridded radiosonde temperature data base and recent temperature trends. *Geophysical Research Letters,* **24,** 1499–1502.

Penner, J.E., C.S. Atherton, J. Dignon, S.J. Ghan, J.J. Walton, and S. Hameed, 1991: Tropospheric nitrogen: a three-dimensional study of sources, distribution, and deposition. *Journal of Geophysical Research,* **96,** 959–990.

Penner, J.E., R.E. Dickinson, and C.A. O'Neil, 1992: Effects of aerosol from biomass burning on the global radiation budget. *Science,* **256,** 1432–1434.

Penner, J.E., C.E. Atherton, and T. Graedel, 1994: Global emissions and models of photochemically active compounds. In: *Global Atmospheric Biospheric Chemistry* [Prinn, R.G. (ed.)]. Plenum, New York, NY, USA, pp. 223–248.

Penner, J.E., 1995: Carbonaceous aerosols influencing atmospheric radiation: black and organic carbon. In: *Aerosol Forcing of Climate* [Charlson, R.J. and J. Heintzenberg (eds.)]. J. Wiley, Chichester, United Kingdom, pp. 91–108.

Peter, T., 1997: Microphysics and heterogeneous chemistry of polar stratospheric clouds. *Annual Review of Physical Chemistry,* **48,** 785–822.

Peter, T., C. Brühl, and P.J. Crutzen, 1991: Increase in the PSC-formation probability caused by high-flying aircraft. *Geophysical Research Letters,* **18,** 1465–1468.

Petzold, A. and F.P. Schröder, 1998: Jet engine exhaust aerosol characterization. *Aerosol Science Technology,* **28,** 62–76. Correction in *Aerosol Science Technology,* **29,** 355–356.

Petzold, A., R. Busen, F.P. Schröder, R. Baumann, M. Kuhn, J. Ström, D.E. Hagen, P.D. Whitefield, D. Baumgardner, F. Arnold, S. Borrmann, and U. Schumann, 1997: Near field measurements on contrail properties from fuels with different sulfur content. *Journal of Geophysical Research,* **102,** 29867–29881.

Petzold, A., J. Ström, S. Ohlsson, and F.P. Schröder, 1998: Elemental composition and morphology of ice-crystal residual particles in cirrus clouds and contrails. *Atmospheric Research,* **49,** 21–34.

Petzold, A., J. Ström, F.P. Schröder, and B. Kärcher, 1999: Carbonaceous aerosol in jet engine exhaust: emission characteristics and implications for heterogeneous chemistry. *Atmospheric Environment,* (in press).

Pham, M., J.-F. Müller, G.P. Brasseur, C. Granier, and G. Mégie, 1996: A 3-D model study of the global sulfur cycle: contributions of anthropogenic and biogenic sources. *Atmospheric Environment,* **30,** 1815–1822.

Pitari, G., 1993: A numerical study of the possible perturbation of stratospheric dynamics due to Pinatubo aerosols: implications for tracer transport. *Journal of Atmospheric Sciences,* **50,** 2443–2461.

Pitari, G., V. Rizzi, L. Ricciardulli, and G. Visconti, 1993: HSCT impact: the role of sulfate, NAT, and ice aerosols studied with a 2-D model including aerosol physics. *Journal of Geophysical Research,* **98,** 23141–23164.

Plantico, M.S., T.R. Karl, G. Kukla, and J. Gavin, 1990: Is recent climate change across the United States related to rising levels of anthropogenic greenhouse gases? *Journal of Geophysical Research,* **95,** 16617–16637.

Plass, G.N., G.W. Kattawar, and F.E. Catchings, 1973: Matrix-operator theory of radiative transfer. *Applied Optics,* **12,** 314–329.

Platt, C.M.R., 1981: The effect of cirrus of varying optical depth on the extraterrestrial net radiative flux. *Quarterly Journal of the Royal Meteorological Society,* **107,** 671–678.

Platt, C.M.R., 1997: A parameterization of the visible extinction coefficient of ice clouds in terms of ice water content. *Journal of Atmospheric Sciences,* **54,** 2083–2098.

Podzimek, J., D.E. Hagen, and E. Robb, 1995: Large aerosol particles in cirrus type clouds. *Atmospheric Research,* **38,** 263–282.

Ponater, M., S. Brinkop, R. Sausen, and U. Schumann, 1996: Simulating the global atmospheric response to aircraft water vapour emissions and contrails: a first approach using a GCM. *Annales Geophysicae,* **14,** 941–960.

Poole, L.R. and M.C. Pitts, 1994: Polar stratospheric cloud climatology based on Stratospheric Aerosol Measurement II observations from 1978 to 1989. *Journal of Geophysical Research,* **99,** 13083–13089.

Prather, M. and D.J. Jacob, 1997: A persistent imbalance in HO_x and NO_x photochemistry of the upper troposphere driven by deep tropical convection. *Geophysical Research Letters,* **24,** 3189–3192.

Pruppacher, H.R., 1995: A new look at homogeneous ice nucleation in supercooled water drops. *Journal of Atmospheric Sciences,* **52,** 1924–1933.

Pruppacher, H.R. and J.D. Klett, 1997: *Microphysics of Clouds and Precipitation.* Kluwer, Dordrecht, The Netherlands, 954 pp.

Pueschel, R.F., 1996: Stratospheric aerosols: formation, properties, effects. *Journal of Aerosol Science,* **27,** 383–402.

Pueschel, R.F., D.F. Blake, K.G. Snetsinger, A.D.A. Hansen, S. Verma, and K. Kato, 1992: Black carbon (soot) aerosol in the lower stratosphere and upper troposphere. *Geophysical Research Letters,* **19,** 1659–1662.

Pueschel, R.F., K.A. Boering, S. Verma, S.D. Howard, G.V. Ferry, J. Goodman, D.A. Allen, and P. Hamill, 1997: Soot aerosol in the lower stratosphere: pole-to-pole variability and contribution by aircraft. *Journal of Geophysical Research,* **102,** 13113–13118.

Pueschel, R.F., S. Verma, G.V. Ferry, S.D. Howard, S. Vay, S.A. Kinne, J. Goodman, and A.W. Strawa, 1998: Sulfuric acid and soot particle formation in aircraft exhaust. *Geophysical Research Letters,* **25,** 1685–1588.

Quackenbush, T.R., M.E. Teske, and C.E. Polymeropoulos, 1994: A model for assessing fuel jettisoning effects. *Atmospheric Environment,* **28,** 2751–2759.

Rahmes, T.F., A.H. Omar, and D.J. Wuebbles, 1998: Atmospheric distributions of soot particles by current and future aircraft fleets and resulting radiative forcing on climate. *Journal of Geophysical Research,* **103,** 31657–31667.

Ramaswamy, V., M.D. Schwartzkopf, and W.J. Randel, 1996: Fingerprint of ozone depletion in the spatial and temporal pattern of recent lower-stratospheric cooling. *Nature,* **382,** 616–618.

Raschke, E., P. Flamant, Y. Fouquart, P. Hignett, H. Isaka, P.R. Jonas, H. Sundqvist, and P. Wendling, 1998: Cloud-radiation studies during the European Cloud and Radiation Experiment (EUCREX). *Surveys in Geophysics,* **19,** 89–138.

Rebetez, M. and M. Beniston, 1998: Changes in sunshine duration are correlated with changes in daily temperature range this century: an analysis of Swiss climatology data. *Geophysical Research Letters,* **25,** 3611–3613.

Reiner, T. and F. Arnold, 1993: Laboratory flow reactor measurements of the reaction $SO_3 + H_2O + M \rightarrow H_2SO_4 + M$: implications for gaseous H_2SO_4 and aerosol formation. *Geophysical Research Letters,* **20,** 2659–2662.

Rickey, J.E., 1995: *The Effect of Altitude Conditions on the Particle Emissions of a J85-GE-5L Turbojet Engine*. NASA-TM-106669, National Aeronautics and Space Administration, Lewis Research Center, Washington, DC, USA, 52 pp.

Roeckner, E., L. Bengtsson, J. Feichter, J. Lelieveld, and H. Rodhe, 1998: Transient climate change simulations with a coupled atmosphere-ocean GCM including the tropospheric sulfur cycle. Report no. 266, Max-Planck-Institut für Meteorologie, Hamburg, Germany, July 1998, 48 pp.

Rogaski, C.A., D.M. Golden, and L.R. Williams, 1997: Reactive uptake and hydration experiments on amorphous carbon treated with NO_2, SO_2, HNO_2 and H_2SO_4. *Geophysical Research Letters,* **24,** 381–384.

Rogers, D.C., P. DeMott, S.M. Kreidenweis, and Y. Chen, 1998: Measurements of ice-nucleating aerosols during SUCCESS. *Geophysical Research Letters,* **25,** 1383–1386.

Rosen, J.M., N.T. Kjome, and J.B. Liley, 1997: Tropospheric aerosol backscatter at a mid-latitude site in the Northern and Southern Hemisphere. *Journal of Geophysical Research,* **102,** 21329–21339.

Rossow, W.B. and R.A. Schiffer, 1991: ISCCP cloud data products. *Bulletin of the American Meteorological Society,* **72,** 2–20.

Russell, P.B., S.A. Kinne, and R.W. Bergstrom, 1997: Aerosol climate effects: local radiative forcing and column closure experiments. *Journal of Geophysical Research,* **102,** 9397–9407.

Sassen, K., 1992: Evidence for liquid-phase cirrus cloud formation from volcanic aerosols: climatic implications. *Science,* **257,** 516–519.

Sassen, K., 1997: Contrail-cirrus and their potential for regional climate change. *Bulletin of the American Meteorological Society,* **78,** 1885–1903.

Sassen, K., D.O. Starr, G.G. Mace, M.R. Poellot, S.H. Melfi, W.L. Eberhard, J.D. Spinhirne, E.W. Eloranta, D.E. Hagen, and J. Hallett, 1995: The 5–6 December 1991 FIRE IFO II jet stream cirrus case study: possible influences of volcanic aerosols. *Journal of Atmospheric Sciences,* **52,** 97–123.

Sato, M., J.E. Hansen, M.P. McCormick, and J.B. Pollack, 1993: Stratospheric aerosol optical depths, 1850–1990. *Journal of Geophysical Research,* **98,** 22987–22994.

Sausen, R., and I. Koehler, 1994: Simulating the global transport of nitrogen oxides emissions from aircraft. *Annales Geophysicae,* **12,** 394–402.

Sausen, R., K. Gierens, M. Ponater, and U. Schumann, 1998: A diagnostic study of the global distribution of contrails. Part I: Present day climate. *Theoretical and Applied Climatology,* **61,** 127–141.

Saxena, P., L.M. Hildemann, P.H. McMurry, and J.H. Seinfeld, 1995: Organics alter hygroscopic behavior of atmospheric particles. *Journal of Geophysical Research,* **100,** 18755–18770.

Schlager, H., P. Schulte, H. Ziereis, F. Arnold, J. Ovarlez, P. van Velthoven, and U. Schumann, 1996: Airborne observations of large scale accumulations of air traffic emissions in the North Atlantic flight corridor within a stagnant anticyclone. In: *Impact of Aircraft Emissions upon the Atmosphere*. Proceedings of a scientific colloquium, 15–18 October 1996, Paris, France. Office National d'Etudes et de Recherches Aerospatiales, Chatillon, France, Vol. 1, pp. 247–252.

Schlager, H., P. Konopka, P. Schulte, U. Schumann, H. Ziereis, F. Arnold, M. Klemm, D.E. Hagen, and P.D. Whitefield, 1997: *In situ* observations of air-traffic emission signatures in the North Atlantic flight corridor. *Journal of Geophysical Research,* **102,** 10739–10750.

Schmidt, E., 1941: Die Entstehung von Eisnebel aus den Auspuffgasen von Flugmotoren. In: *Schriften der Deutschen Akademie der Luftfahrtforschung*. Verlag R. Oldenbourg, Munich and Berlin, Germany, Vol. 44, pp. 1–15.

Schmitt, A. and B. Brunner, 1997: Emissions from aviation and their development over time. In: *Pollutants from Air Traffic – Results of Atmospheric Research 1992–1997* [Schumann, U., A. Chlond, A. Ebel, B. Kärcher, H. Pak, H. Schlager, A. Schmitt, and P. Wendling (eds.)]. DLR-Mitteilung 97-04, Deutsches Zentrum für Luft- und Raumfahrt, Cologne, Germany, pp. 37–52.

Schröder, F. and J. Ström, 1997: Aircraft measurements of submicrometer aerosol particles (> 7 nm) in the mid-latitude free troposphere and tropopause region. *Atmospheric Research,* **44,** 333–356.

Schröder, F.P., B. Kärcher, A. Petzold, R. Baumann, R. Busen, C. Hoell, and U. Schumann, 1998a: Ultrafine aerosol particles in aircraft plumes: *in situ* observations. *Geophysical Research Letters,* **25,** 2789–2792.

Schröder, F., B. Kärcher, C. Duroure, J. Ström, A. Petzold, J.-F. Gayet, B. Strauss, and P. Wendling, 1998b: On the transition of contrails into cirrus clouds. *Journal of Atmospheric Sciences,* (submitted).

Schoeberl, M.R., C.H. Jackman, and J.E. Rosenfield, 1998: A Lagrangian estimate of aircraft effluent lifetime. *Journal of Geophysical Research,* **103,** 10817–10825.

Schulte, P., H. Schlager, H. Ziereis, U. Schumann, S.L. Baughcum, and F. Deidewig, 1997: NO_x emission indices of subsonic long-range jet aircraft at cruise altitude: *in situ* measurements and predictions. *Journal of Geophysical Research,* **102,** 21431–21442.

Schulz, J., 1998: On the effect of cloud inhomogeneity on area-averaged radiative properties of contrails. *Geophysical Research Letters,* **25,** 1427–1430.

Schumann, U., 1994: On the effect of emissions from aircraft engines on the state of the atmosphere. *Annales Geophysicae,* **12,** 365–384.

Schumann, U., 1996a: On conditions for contrail formation from aircraft exhausts. *Meteorologische Zeitschrift,* **5,** 4–23.

Schumann, U. (ed.), 1996b: *Pollution from Aircraft Emissions in the North Atlantic Flight Corridor (POLINAT)*. Air Pollution Research Report 58, Report EUR-16978-EN, Office for Official Publications of the European Communities, Luxembourg, 303 pp.

Schumann, U. and P. Wendling, 1990: Determination of contrails from satellite data and observational results. In: *Air Traffic and the Environment—Background, Tendencies, and Potential Global Atmospheric Effects* [Schumann, U. (ed.)]. Springer-Verlag, Heidelberg, Germany, pp. 138–153.

Schumann, U., P. Konopka, R. Baumann, R. Busen, T. Gerz, H. Schlager, P. Schulte, and H. Volkert, 1995: Estimate of diffusion parameters of aircraft exhaust plumes near the tropopause from nitric oxide and turbulence measurements. *Journal of Geophysical Research,* **100,** 14147–14162.

Schumann, U., J. Ström, R. Busen, R. Baumann, K. Gierens, M. Krautstrunk, F.P. Schröder, and J. Stingl, 1996: *In situ* observations of particles in jet aircraft exhausts and contrails for different sulfur containing fuels. *Journal of Geophysical Research,* **101,** 6853–6869.

Schumann, U., F. Arnold, B. Droste-Franke, T. Dürbeck, C. Feigl, F. Flatoy, I.J. Ford, D.E. Hagen, G.D. Hayman, A.R. Hopkins, O. Hov, H. Huntrieser, I.S.A. Isaksen, C.E. Johnson, J.E. Jonson, H. Kelder, G. Kirchner, M. Klemm, I. Köhler, P. Konopka, A. Kraabol, H. Ovarlez, J. Overlez, J. Paladino, R. Sausen, H. Schlager, J. Schneider, P. Schulte, D.S. Stevenson, F. Stordal, H. Teitelbaum, P. van Velthoven, W. Wauben, P.D. Whitefield, and H. Ziereis, 1997: Pollution from aircraft emission in the North Atlantic flight corridor—overview on the results of the POLINAT project. In: *Impact of Aircraft upon the Atmosphere*. Proceedings of an international scientific colloquium, 15–18 October 1996, Paris, France. Office National d'Etudes et de Recherches Aerospatiales, Chatillon, France, Vol. I, pp. 63–68.

Schumann, U., H. Schlager, F. Arnold, R. Baumann, P. Haschberger, and O. Klemm, 1998: Dilution of aircraft exhaust plumes at cruise altitudes. *Atmospheric Environment,* **32,** 3097–3103.

Schwartz, S.E., 1996: The whitehouse effect—shortwave radiative forcing of climate by anthropogenic aerosols: an overview. *Journal of Aerosol Science,* **27,** 359–382.

Sheridan, P.J., C.A. Brock, and J.C. Wilson, 1994: Aerosol particles in the upper troposphere and lower stratosphere: elemental composition and morphology of individual particles in northern midlatitudes. *Geophysical Research Letters,* **21,** 2587–2590.

Slemr, F., H. Giehl, J. Slemr, R. Busen, P. Haschberger, and P. Schulte, 1998: In-flight measurements of aircraft non-methane hydrocarbon emission indices. *Geophysical Research Letters,* **25,** 321–324.

Solomon, S., S. Borrmann, R.R. Garcia, R. Portmann, L. Thomason, L.R. Poole, D. Winker, and M.P. McCormick, 1997: Heterogeneous chlorine chemistry in the tropopause region. *Journal of Geophysical Research,* **102,** 21411–21429.

Spicer, C.W., M.W. Holdren, D.L. Smith, D.P. Hughes, and M.D. Smith, 1992: Chemical composition of exhaust from aircraft turbine engines. *Journal of Engineering and Gas Turbine Power,* **114,** 111–115.

Spicer, C.W., M.W. Holdren, R.M. Riggin, and T.F. Lyon, 1994: Chemical composition and photochemical reactivity of exhaust from aircraft turbine engines. *Annales Geophysicae,* **12,** 944–955.

Spinhirne, J.D., W.D. Hart, and D.P. Duda, 1998: Evolution of the morphology and microphysics of contrail cirrus from airborne remote sensing. *Geophysical Research Letters,* **25,** 1153–1156.

Spiro, P.A., D.J. Jacob, and J.A. Logan, 1992: Global inventory of sulfate emissions with 1° x 1° resolution. *Journal of Geophysical Research,* **97,** 6023–6036.

Starr, D.O. and S.K. Cox, 1985: Cirrus clouds. Part I: A cirrus cloud model. *Journal of Atmospheric Sciences,* **42,** 2663–2681.

Staylor, W.F. and A.C. Wilber, 1990: Global surface albedo from ERBE data. In: *Proceedings of the Seventh Conference on Atmospheric Radiation, San Francisco, CA, July 23–27, 1990.* American Meteorological Society, Boston, MA, USA, pp. 231–236.

Steele, H.M. and P. Hamill, 1981: Effects of temperature and humidity on the growth and optical properties of sulfuric acid-water droplets in the stratosphere. *Journal of Atmospheric Sciences,* **12,** 517–523.

Steinbrecht, W., H. Claude, U. Köhler, and K.P. Hoinka, 1998: Correlations between tropopause height and total ozone: implications for long-term changes. *Journal of Geophysical Research,* **103,** 19183–19192.

Stephens, G.L. and P.J. Webster, 1981: Clouds and climate: sensitivity of simple systems. *Journal of Atmospheric Sciences,* **38,** 235–247.

Stockwell, W.R. and J.G. Calvert, 1983: The mechanism of the HO-SO_2 reaction. *Atmospheric Environment,* **17,** 2231–2235.

Stolarski, R.S., S.L. Baughcum, W.H. Brune, A.R. Douglass, D.W. Fahey, R.R. Friedl, S.C. Liu, R.A. Plumb, L.R. Poole, H.L. Wesoky, and D.R. Worsnop, 1995: *1995 Scientific Assessment of the Atmospheric Effects of Stratospheric Aircraft.* NASA Reference Publication 1381, National Aeronautics and Space Administration, Washington, DC, USA, 110 pp.

Strauss, B., R. Meerkötter, B. Wissinger, P. Wendling, and M. Hess, 1997: On the regional climatic impact of contrails: microphysical and radiative properties of contrails and natural cirrus clouds. *Annales Geophysicae,* **15,** 1457–1467.

Ström, J. and J. Heintzenberg, 1994: Water vapor, condensed water and crystal concentration in orographically influenced cirrus clouds. *Journal of Atmospheric Sciences,* **51,** 2368–2383.

Ström, J., B. Strauss, T. Anderson, F. Schröder, J. Heintzenberg, and P. Wendling, 1997: *In situ* observations of the microphysical properties of young cirrus clouds. *Journal of Atmospheric Sciences,* **54,** 2542–2553.

Ström, J. and S. Ohlsson, 1998: *In situ* measurements of enhanced crystal number densities in cirrus clouds caused by aircraft exhaust. *Journal of Geophysical Research,* **103,** 11355–11361.

Sundqvist, H., 1993: Inclusion of ice phase of hydrometeors in cloud parameterizations for mesoscale and large-scale models. *Beiträge zur Physik der Atmosphäre,* **66,** 137–147.

Tabazadeh, A., E.J. Jensen, and O.B. Toon, 1997: A model description for cirrus nucleation from homogeneous freezing of sulfate aerosols. *Journal of Geophysical Research,* **102,** 23845–23850.

Talbot, R.W., J.E. Dibb, and M.B. Loomis, 1998: Influence of vertical transport on free tropospheric aerosols over the central USA in springtime. *Geophysical Research Letters,* **25,** 1367–1370.

Taleb, D.E., R. McGraw, and P. Mirabel, 1997: Time lag effects on the binary homogeneous nucleation of aerosols in the wake of an aircraft. *Journal of Geophysical Research,* **102,** 12885–12890.

Tett, S.F.B., J.F.B. Mitchell, D.E. Parker, and M.R. Allen, 1996: Human influence on the atmospheric vertical temperature structure: detection and observations. *Science,* **274,** 1170–1173.

Thomason, L.W., G.S. Kent, C.R. Trepte, and L.R. Poole, 1997a: A comparison of the stratospheric aerosol background periods of 1979 and 1989–1991. *Journal of Geophysical Research,* **102,** 3611–3616.

Thomason, L.W., L.R. Poole, and T. Deshler, 1997b: A global climatology of stratospheric aerosol surface area density deduced from Stratospheric Aerosol and Gas Experiment II measurements: 1984–1994. *Journal of Geophysical Research,* **102,** 8967–8976.

Thuburn, J. and G.C. Craig, 1997: GCM tests of theories for the height of the tropopause. *Journal of Atmospheric Sciences,* **54,** 869–882.

Timbal, B., J.-F. Mahfouf, J.-F. Royer, U. Cubasch, and J.M. Murphy, 1997: Comparison between doubled CO_2 time-slice and coupled experiments. *Journal of Climate,* **10,** 1463–1469.

Tie, X., G.P. Brasseur, C. Granier, A. deRudder, and N. Larsen, 1996: Model study of polar stratospheric clouds and their effect on stratospheric ozone. 2: Model results. *Journal of Geophysical Research,* **101,** 12575–12584.

Travis, D.J. and S.A. Chagnon, 1997: Evidence of jet contrail influences on regional-scale diurnal temperature range. *Journal of Weather Modification,* **29,** 7–83.

Tremmel, H.G., H. Schlager, P. Konopka, P. Schulte, F. Arnold, M. Klemm, and B. Droste-Franke, 1998: Observations and model calculations of jet aircraft exhaust products at cruise altitude and inferred initial OH emissions. *Journal of Geophysical Research,* **103,** 10803–10816.

Trepte, C.R., R.E. Viega, and M.P. McCormick, 1993: The poleward dispersal of Mount Pinatubo volcanic aerosol. *Journal of Geophysical Research,* **98,** 18563–18573.

Twohy, C.H. and B.W. Gandrud, 1998: Electron microscope analysis of residual particles from aircraft contrails. *Geophysical Research Letters,* **25,** 1359–1362.

Twomey, S., 1977: *Atmospheric Aerosols.* Elsevier Press, Amsterdam, The Netherlands, 293 pp.

Vandersee, W., 1997: Strahlungsmeßreihe am MOHp. *Promet,* **26(1/2),** 8–16.

Wahl, C., M. Kapernaum, P. Wiesen, J. Kleffmann, and R. Kurtenbach, 1997: Measurements of trace species in the exhaust of a reverse flow combustor. In: *Impact of Aircraft upon the Atmosphere.* Proceedings of an international scientific colloquium, 15–18 October 1996, Paris, France. Office National d'Etudes et de Recherches Aerospatiales, Chatillon, France, Vol. I, pp. 107–112.

Wallace, J.M., Y. Zhang, and J.A. Renwick, 1995: Dynamic contribution to hemispheric mean temperature trends. *Science,* **270,** 780–783.

Wang, P.-H., P. Minnis, and G.K. Yue; 1995: Extinction coefficient (1 μm) properties of high-altitude clouds from solar occultation measurements (1985–1990): evidence of volcanic aerosol effect. *Journal of Geophysical Research,* **100,** 3181–3199.

Wang, P.-H., P. Minnis, M.P. McCormick, G.S. Kent, and K.M. Skeens, 1996: A 6-year climatology of cloud occurrence frequency from SAGE II observations (1985–1990). *Journal of Geophysical Research,* **101,** 29407–29429.

Warneck, P., 1988: *Chemistry of the Natural Atmosphere.* Academic Press, San Diego, CA, USA, 757 pp.

Warren, S.G., C.J. Hahn, J. London, R.M. Chervin, and R.L. Jenne, 1986: *Global Distribution of Total Cloud Cover and Cloud Type Amounts over Land.* NCAR Technical Note TN-273+STR, National Center for Atmospheric Research, Boulder, CO, USA, 29 pp.

Warren, S.G., C.J. Hahn, J. London, R.M. Chervin, and R.L. Jenne, 1988: *Global Distribution of Total Cloud Cover and Cloud Type Amounts over Ocean.* NCAR Technical Note NCAR/TN-317+STR, National Center for Atmospheric Research, Boulder, CO, USA, 42 pp.

Watson, R.T., L.G. Meira Filho, E. Sanhuenza, and A. Janetos, 1992: Greenhouse gases: sources and sinks. In: *Climate Change 1992: The Supplemental Report to the IPCC Scientific Assessment.* Prepared by IPCC Working Group I [Houghton, J.T., B.T. Callander, and S.K. Varney (eds.)] and WMO/UNEP. Cambridge University Press, Cambridge, United Kingdom and New York, NY, USA, 23–46.

Wauben, W.M.F., P.F.J. van Velthoven, and H. Kelder, 1997: A 3-D CTM study of changes in atmospheric ozone due to aircraft NO_x emissions. *Atmospheric Environment,* **31,** 1819–1836.

Weaver, C.J., A.R. Douglass, and D.B. Considine, 1996: A 5-year simulation of supersonic aircraft emission transport using a 3-D model. *Journal of Geophysical Research,* **101,** 20975–20984.

Weber, G.-R., 1990: Spatial and temporal variation of sunshine in the Federal Republic of Germany. *Theoretical and Applied Climatology,* **41,** 1–9.

Weickmann, H., 1945: Formen und Bildung atmosphärischer Eiskristalle. *Beiträge zur Physik der Atmosphäre,* **28,** 12–52.

Weisenstein, D.K., M.K.W. Ko, J.M. Rodriguez, and N.D. Sze, 1991: Impact of heterogeneous chemistry on model-calculated ozone change due to HSCT aircraft. *Geophysical Research Letters,* **18,** 1991–1994.

Weisenstein, D.K., M.K.W. Ko, N.D. Sze, and J.M. Rodriguez, 1996: Potential impact of SO_2 emissions from stratospheric aircraft on ozone. *Geophysical Research Letters,* **23,** 161–164.

Weisenstein, D.K., G.K. Yue, M.K.W. Ko, N.D. Sze, J.M. Rodriguez, and C.J. Scott, 1997: A two-dimensional model of sulfur species and aerosol. *Journal of Geophysical Research,* **102,** 13019–13035.

Weisenstein, D.K., M.K.W. Ko, I.G. Dyominov, G. Pitari, L. Ricciardulli, G. Visconti, and S. Bekki, 1998: The effects of sulfur emissions from HSCT aircraft: a 2-D model intercomparison. *Journal of Geophysical Research,* **103,** 1527–1547.

Westphal, D.L., S. Kinne, P. Pilewskie, J.M. Alvarez, P. Minnis, D.F. Young, S.G. Benjamin, W.L. Eberhard, R.A. Kropfli, S.Y. Matrosov, J.B. Snider, T.A. Uttal, A.J. Heymsfield, G.G. Mace, S.H. Melfi, D.O. Starr, and J.J. Soden, 1996: Initialization and validation of a simulation of cirrus using FIRE-II data. *Journal of Atmospheric Sciences,* **53,** 3397–3429.

Whitefield, P.D., M.B. Trueblood, and D.E. Hagen, 1993: Size and hydration characteristics of laboratory simulated jet engine combustion aerosols. *Particle Science Technology,* **11,** 25–36.

Wilson, J.C., H.H. Jonsson, C.A. Brock, D.W. Toohey, L.M. Avallone, D. Baumgardner, J.E. Dye, L.R. Poole, D.C. Woods, R.J. DeCoursey, M. Osborn, M.C. Pitts, K.K. Kelly, K.R. Chan, G.V. Ferry, M. Loewenstein, J.R. Podolske, and A. Weaver, 1993: *In situ* observations of aerosol and chlorine monoxide after the 1991 eruption of Mount Pinatubo: effect of reactions on sulfate aerosol. *Science,* **261,** 1140–1143.

Winkler, P., L. Gantner, and U. Köhler, 1997: Hat sich wegen der langfristigen Ozonabnahme die UV-Strahlung erhöht? In: *Deutscher Wetterdienst,* Offenbach am Main, Germany, Vol. 49, 37 pp.

WMO, 1986: *A Preliminary Cloudless Standard Atmosphere for Radiation Computation.* WMO/TD Report no. 24, World Climate Research Programme, World Meteorological Organization, Geneva, Switzerland, 45 pp.

WMO, 1995: *Scientific Assessment of Ozone Depletion: 1994.* World Meteorological Organization, Geneva, Switzerland, 536 pp.

Wolf, M.E. and G.M. Hidy, 1997: Aerosols and climate: anthropogenic emissions and trends for 50 years. *Journal of Geophysical Research,* **102,** 11113–11121.

Wulff, A. and J. Hourmouziadis, 1997: Technology review of aeroengine pollutant emissions. *Aerospace Science Technology,* **1,** 557–572.

Wylie, D.P. and W.P. Menzel, 1999: Eight years of high cloud statistics using HIRS. *Journal of Climate,* **12,** 170–184.

Wyser, K. and J. Ström, 1998: A possible change in cloud radiative forcing due to aircraft exhaust. *Geophysical Research Letters,* **25,** 1673–1676.

Wyslouzil, B.E., K.L. Carleton, D.M. Sonnenfroh, and W.T. Rawlins, 1994: Observation of hydration of single, modified carbon aerosols. *Geophysical Research Letters,* **21,** 2107–2110.

Yamato, M. and A. Ono, 1989: Chemical and physical properties of stratospheric aerosol particles in the vicinity of tropopause folding. *Journal of the Meteorological Society of Japan,* **67,** 147–165.

Yu, F. and R.P. Turco, 1997: The role of ions in the formation and evolution of particles in aircraft plumes. *Geophysical Research Letters,* **24,** 1927–1930.

Yu, F. and R.P. Turco, 1998a: The formation and evolution of aerosols in stratospheric aircraft plumes: numerical simulations and comparisons with observations. *Journal of Geophysical Research,* **103,** 25915–25934.

Yu, F. and R.P. Turco, 1998b: Contrail formation and impacts on aerosol properties in aircraft plumes: effects of fuel sulfur content. *Geophysical Research Letters,* **25,** 313–316.

Yu, F., R.P. Turco, B. Kärcher, and F.P. Schröder, 1998: On the mechanisms controlling the formation and properties of volatile particles in aircraft wakes. *Geophysical Research Letters,* **25,** 3839–3842.

Yue, G.K., L.R. Poole, P.-H. Wang, and E.W. Chiou, 1994: Stratospheric aerosol acidity, density, and refractive index deduced from SAGE II and NMC temperature data. *Journal of Geophysical Research,* **99,** 3727–3738.

Zhang, R., M.-T. Leu, and L.F. Keyser, 1996: Heterogeneous chemistry of HONO on liquid sulfuric acid: a new mechanism of chlorine activation on stratospheric sulfate aerosols. *Journal of Physical Chemistry,* **100,** 339–345.

Zhao, J. and R.P. Turco, 1995: Nucleation simulations in the wake of a jet aircraft in stratospheric flight. *Journal of Aerosol Science,* **26,** 779–795.